NICKEL-63 MICROIRRADIATORS AND APPLICATIONS

A Thesis
Presented to
The Academic Faculty

by

Jennifer L. Steeb

In Partial Fulfillment
of the Requirements for the Degree
Doctor of Philosophy in the
School of Chemistry and Biochemistry

Georgia Institute of Technology
August 2010

NICKEL-63 MICROIRRADIATORS AND APPLICATIONS

Approved by:

Dr. Jiří Janata, Advisor
School of Chemistry and Biochemistry
Georgia Institute of Technology

Dr. Mira Josowicz
School of Chemistry and Biochemistry
Georgia Institute of Technology

Dr. Lawrence Bottomley
School of Chemistry and Biochemistry
Georgia Institute of Technology

Dr. Chris Wang
College of Engineering
Georgia Institute of Technology

Dr. Facundo Fernandez
School of Chemistry and Biochemistry
Georgia Institute of Technology

Date Approved: June 29, 2010

To Mom and Dad, thanks.

ACKNOWLEDGEMENTS

There are so many people involved within this thesis project itself and in helping me get to this stage in my life that it would take pages to thank everyone. Thanks must first be given to Prof. Art Janata and Dr. Mira Josowicz. One of the most important things said to me by Art was "This isn't my thesis project, I got my degree long ago." As simple as this may sound, this really was an important realization, and from there I have been given the creative freedom to begin separate projects within my thesis that I am grateful for. It is rare that advisors such as Art are available almost on a daily basis to go over data or just questions in general, and this has been a tremendous help through the entire thesis project. Mira as well has been a wonderful coworker, advisor, and friend throughout this entire process, and without her in the lab somedays would be impossible. She has been such a positive role model for me not only as a scientist but as practically a family member, and I am extremely grateful to both in helping me throughout this thesis process.

Secondly, its been a pleasure to have interacted on a regular basis with all of my committee members, such as Prof. Chris Wang, Prof. Facundo Fernandez, Prof. Larry Bottomley, Prof. Art Janata, and of course Dr. Mira Josowicz. It's been a pleasure to not only collaborate on research projects but to be sincerely interested in my research. Thanks as well must be give to the Medical College of Georgia, with Dr. Dynan, Dr. Kuhne, and Zhen Cao. Without their help, some of this project would be impossible. Since my research involves working with radioactive materials, a special thanks must be given to the Office of Radiation Safety at Georgia Tech. Thanks must be given to Nazia

Zakir, who allowed our research group to resume research with radioactive materials, and without her this thesis would not have been completed. I would also like to give thanks to Jeremiah Sauber and Gary Spichiger for their help in aiding me with my research. And I would also like to thank Christina Tabor, who not only has been my friend, but a wonderful coworker and help in all matters I have ever come to her with. A special thanks goes to all the building managers at Georgia Tech. I have become friends with many of the maintenance staff and custodial staff throughout working here, and they too have been an enormous help as well. Financially, I have been graciously funded by the Georgia Research Alliance and the Nuclear Forensics Graduate Fellowship from the Department of Defense/Departement of Homeland Security. Without their generous funding none of this research could have been possible.

Besides academic support, friends have supported me in good and in tough times. I'd like to give thanks to my current and former group members Dr. George Yu, Ryan Cantor, Alex Jonke, Ryan West, KC Vavra, and Roya Kalantari. It is safe to say that not only have I worked with you, but became good friends with all of you as well. Of course, friends within my class have also been of great help. Thanks to all of my graduate girlfriends for organizing special get togethers. I would like to also thank Anthony and Cortney for being great roommates and friends. And a special thanks to Irene, who not only has brought miss Leela into the world, but has been my best friend ever since we discovered we lived in the same part of Florida. I have been the silly sister you never wanted and it's been a great four years because of it.

Last but not least, the people who have financed me, listened to me yell, scream and cry to get to where I am today deserve the most thanks. Thanks to my boyfriend

Mike, who has been an enormous help in transitioning from graduate student to a career. You have always listened to me whine and complain without saying a word, and buy my dinner on top of that and for this I will be eternally grateful. Thanks as well to my grandparents, who in their generosity left funds to get me through graduate school as well as my undergraduate education. My greatest thanks must be given to my parents for raising me correctly, pushing me to be the best I could be, fixing my car when I decide to drive like a mad woman, cleaning my entire apartment whenever they came to visit, repainting my apartment when I decide to paint it purple, sending me money when I decided braves tickets were more important than food, sacrificing your lives for me and my brother, and in general listening to my annoying antics. Without the both of you, none of this would have been possible.

TABLE OF CONTENTS

LIST OF TABLES

LIST OF FIGURES

SUMMARY

In this thesis, manufacturing of microirradiators, electrodeposition of radioactive elements such as Ni-63, and applications of these radioactive sources are discussed. Ni-63 has a half life of 100 years and an average low energy beta electron of 17 keV, ideal for low dose low linear energy transfer (LET) research. The main focus of the research is on the novel Ni-63 microirradiator. It contains a small amount of total activity of radiation but a large flux, allowing the user to safely handle the microirradiator without extensive shielding.

This thesis is divided into nine chapters. Properties of microirradiators and various competing radioactive sources are compared in the introduction (chapter 1). Detailed description of manufacturing Ni-63 microirradiator using the microelectrode as the starting point is outlined in chapter 2. The microelectrode is a 25 μm in diameter Pt disk sealed in a pulled 1 mm diameter borosilicate capillary tube, as a protruding wire or recessed disk microelectrode. The electrochemically active surface area of each is verified by cyclic voltammetry. Electrodeposition of nickel with a detailed description of formulation of the electrochemical bath in a cold "non-radioactive setting" was optimized by using parameters as defined by pourbaix diagrams, radioactive electroplating of Ni-63, and incorporation of safety regulations into electrodeposition.

Calibration and characterization of the Ni-63 microirradiators as protruding wire and recessed disk microirradiators is presented in chapter 3. Diagrams of the estimated flux and calibration curves comparing the amount of Ni-63 deposited versus activity in disintegrations per minute are found here. Estimations of the dose that irradiated objects

can receive from the microirradiator in air, water, and tissue are calculated using the calculations shown in this chapter.

In chapters 4 through 6, applications of the Ni-63 microirradiators and wire sources are presented. Chapter 4 provides a radiobiological application of the recessed disk microirradiator and a modified flush microirradiator with osteosarcoma cancer cells. Cells were irradiated with two sources, with activies of 1 and 2000 Bq. Real time observations of DNA double strand breaks were observed. A novel benchtop detection system for the microirradiators is presented in chapter 5. Ni-63 is most commonly measured by liquid scintillation counters, which are expensive and not easily accessible within a benchtop setting. A developed solid state plastic scintillation device allows the microirradiators to be measured within a manufactured cavity of the plastic scintillation crystal. Precise measurements of the activity of the tip of the microirradiator were observed and compared against liquid scintillation. Results show liquid scintillation measurements overestimates the amount of radiation coming from the recessed disk. A novel 10 μCi Ni-63 electrochemically deposited wire acting as an ambient chemical ionization source for pharmaceutical tablets in mass spectrometry is in chapter 6. Typically, larger radioactive sources (15 mCi) of Ni-63 have been used in an ambient ionization scenario. However, custom electrochemically depositing Ni-63 onto a copper wire lowers the total activity by three orders of magnitude, allowing safe handling of the radioactive source. Additionally, this is the first application of using Ni-63 to ionize in atmosphere pharmaceutical tablets, leading to a possible field portable device.

In the last chapters, chapters 7 through 8, previous microirradiator experiments and future work are summarized. Chapter 7 illustrates the prototype of the

electrochemically deposited microirradiator, the Te-125 microirradiator. In conjunction with Oak Ridge National Laboratory, Te-125m is a low dose x-ray emitting element determined to be the best first prototype of an electrochemically deposited microirradiator. Manufacturing, characterization, and experiments that were not successful leading to the development of the Ni-63 microirradiator are discussed. In chapter 8, future work is entailed in continuing on with this thesis project. The work presented in the thesis is concluded in chapter 9.

Overall, this thesis has developed a new type of radiation research involving small total activity sources that deliver a large flux. It demonstrates a novel opportunity for using radioactive sources and provides valuable information regarding their implementation to future radioactive sources using electrochemically deposited radioisotopes on microirradiators or other shaped sources. Safety is always a priority in dealing with radioactive materials, and in some instances has hindered research expanding this field.

CHAPTER 1

INTRODUCTION

1.1 General

The main objective of this thesis is the microirradiator, which is a microelectrode with a radioactive element deposited onto the end. A microelectrode is an electrochemical tool using a 25 μm and under 1 micron diameter conducting wire (Pt, Au, C) encapsulated in glass. Instead of using this as an electroanalytical device, the microirradiator's main purpose is to deliver high flux density of ionizing radiation while allowing the user to encounter only a minimal amount of radiation. It is transformed into a radiation delivery tool by depositing a radioisotope onto its electroactive surface area (4.9×10^{-6} cm^2).[1] This allows for a small amount of total activity but for a high flux density (electrons (β)/cm^2) due to the small surface area. This allows the microirradiator to be used in various experiments by introducing a low activity from an open source that can be handled safely in the laboratory.

1.2 Sealed vs. Open Source

A sealed source is defined as a radioactive source that has been sealed within an outer container and tested to ensure that the active materials cannot escape the container. Various types of sealed sources are used for calibration and research, anywhere from a button source to irradiators used in large facilities.[2] Specific categories are held for each sealed source, ranging from sources that can deliver a lethal dose with close exposure in minutes (industrial irradiators) to sealed sources that are unlikely to cause harm (x-ray

fluorescence generators). Especially in the case of irradiators and electron beams, mostly used in research type applications are one of the most dangerous kind (Category 5). These irradiators need to be housed in separate buildings with extensive shielding, controlled access and other safety procedures. Electron beams also require high vacuum to prevent scattering of the electrons in air and have mica windows underneath specimens to be irradiated to ensure delivery of radiation. [3]

The advantage of our microirradiator is that it is an open source. An open source in contrast to a sealed source is not in an external container, allowing the source to interact with the adjacent areas where it is located. These types of sources are extensively used in biology and medical applications, where radiation is commonly used as radiolabeled tracers and/or radiation delivered therapy (prostate seeds).[4] An important issue when dealing with open sources is contamination with radioactivity. In contrast, the microirradiator has a low activity for an open source. This advantage has opened the door for using low activity sources in various bench applications in-situ.[1, 5]

1.3 Alpha, Beta, Gamma Radiation

Within open and sealed sources different types of radiation can be housed. The three main types of radiation are alpha, beta, and gamma rays. Alpha particles are a He nucleus ejected from the atom. In general the equation for alpha decay is

$$ {}^{A}_{Z}X \rightarrow {}^{A-4}_{Z-2}Y + {}^{4}_{2}He \quad (1) $$

Where X is the parent nuclide and Y is the daughter nuclide. Heavy and proton rich nuclei are the most common alpha emitters, where the elements typically above Polonium (Z=84) are almost exclusively alpha emitters.[4] Concerning alpha particle

interaction with humans, alphas are the most dangerous particle internally, and the least harmful externally. This is due to the fact that alphas are high linear energy transfer (LET) radiation. LET is defined as the amount of energy deposited within a material per unit distance. An alpha particle release all of its energy within 50-70 microns of dead skin layer, rendering the particle harmless transdermally. However, internally there is no protective dead skin cell layer, and alpha particles wreak havoc on the living cells because of this.

Gamma decay is a high energy photon emission (150 keV-GeV) from a nucleus transition from the excited state to the ground state. Gamma rays are also most commonly accompanying other modes of radioactive decay such as in transition to other elements. Gamma photons are not as dangerous externally because of their low LET, however in high enough doses they are dangerous externally. Beta particles are the ejection of an electron (or positron) from the nucleus of an atom. In general the equation for beta emission is

$$ {}^{A}_{Z}X \rightarrow {}^{A}_{Z+1}Y + \beta^{-} + \bar{\nu}_{e} \quad (2) $$

Where X is the parent nuclei, Y is the daughter nuclei, and $\bar{\nu}$ is the antineutrino. Beta particles are unique because they do not emit monoenergetic energies such as alpha and gamma emitters.[4] Because of the ejection of the antineutrino in following Fermi's golden rule, a spectrum of energy levels is released dependent upon how much interaction the electron and antineutrino had before passing the outer electron shell boundaries. This leads to a broad energy spectrum with an E_{max} representing the endpoint of the distribution. Beta is a low LET emitter. Beta particles are not as dangerous as alpha internally, and not as dangerous as gamma externally. Because of this, Beta particles are

not as heavily studied in radiation studies because of the lack of pure beta emitting materials and the need for an electron gun or large scale irradiators for research if electron studies are required.

1.4 Microbeams vs. Microirradiators

Irradiators and microbeams have long been used in the field of radiobiology for the study of the "bystander effect" and the study of the mechanism of double strand DNA (dsDNA) breaks. Commonly, these experiments are run in sequences such as by using a microbeam, running experiments, fixing cells, and then recording the observations. These irradiators and microbeams typically involve a large collimated radioactive source (such as Cs-137) with shielding to form a microbeam. Alternatively, x-ray and electron beams are used, where monoenergetic electron beams are under vacuum. Samples must then be placed under a sheath of mica to form the boundary layer between atmosphere and vacuum when they are irradiated. The drawback of using microbeams and macroirradiators are that real short-time experiments are not possible to conduct due to the physical space separation of the beam and biological facilities. In other words, large amounts of radiation are not allowed in standard biological laboratories for safety reasons. In contrast, the microirradiator enables to use a microscope and to observe the experiment in situ, while irradiation experiments are taking place. Furthermore, many research experiments cannot be done because of the health and safety concerns with working with large amounts of radiation. Microbeams have been available since the 90's, but the field of radiobiology much is to be gained with real time observations and data collection whilst radiation is being applied. [3, 6, 7]

1.5 Ni-63

Ni-63 was chosen as the element to be used in the microirradiator throughout this thesis due to its low energy beta emission with a maximum energy of 67 keV, average 18 keV. Ni-63 decays to stable Cu-63 by pure beta emission with a 100 year half life, as shown below in the equation.

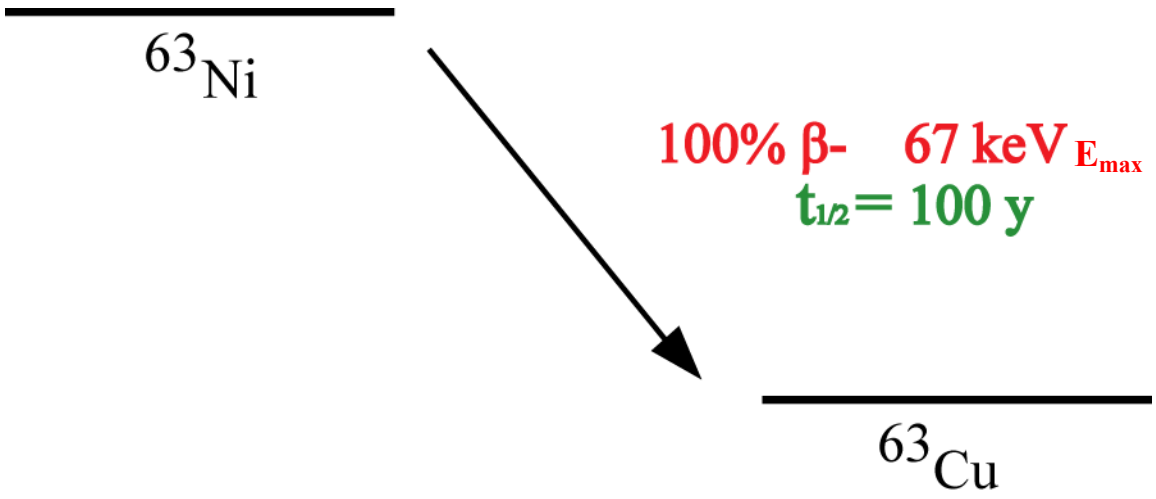

Figure 1. Decay Scheme of Ni-63

Ni-63 is most commonly used in electron capture detectors, where halogenated organics, nitro and amine groups are particularly suitable for this mode of detection.[8] In these instances, Ni-63 comes in a foil, with an activity from 10-15 mCi. This radioisotope is only available as a $NiCl_2$ salt, where nickel forms a strong and stable electrochemical deposit, with formal potential E= -.259 V vs. the standard hydrogen electrode potential (SHE).[9] Because of these reasons, Ni-63 was the element of choice for all of the microirradiators manufactured in this project.

1.6 Tritium Microirradiator

Previously, our research group had developed a tritium irradiator incorporating tritiated sodium propionate within a polyaniline (PANI) film on a microelectrode. Tritium has the unique capability of being incorporated into any compound with hydrogens. Therefore, a microirradiator can be made from a molecule with radiolabeled hydrogen instead of an electrochemically deposited metal. However, from this prototype, we learned that the use of tritiated ions presented serious handling and regulatory problems. Moreover, the PANI film was not stable enough for repetitive use. We also learned that an electrochemical metallic deposition would be easier and more reliable for deposition strength and stability.[10]

CHAPTER 2

EXPERIMENTAL

2.1 General

This chapter is dedicated to the detailed description of manufacturing and electrodepositing onto microirradiators. To start, a microirradiator is a microelectrode with a radioactive metal electrodeposited onto its electroactive surface. Specific microelectrodes, including the recessed disk microelectrode and the microcylinder electrodes are outlined below. Since the microirradiator uses a microelectrode as the tool for radiation delivery, specific microelectrodes are manufactured to optimize the flux delivered to the source at hand. In electrochemistry in general, the most popular microelectrode used is the radial disk microelectrode, in which a micron sized electroactive surface is flush to the glass. The microirradiator differs from general electrochemistry tools due to the shape of the microelectrode enhancing the delivery of radiation by shielding or projecting radiation to the sample. In this chapter a detailed description of the fabrication of microelectrodes, specific microelectrodes used, and electrodeposition techniques of Ni-63 will be discussed.

2.2 Fabrication of Microelectrodes

Microelectrodes can be defined as an electrode in which the electroactive area is less than or equal to 25 microns.[11] These are common tools used in the field of electrochemistry to quantify oxidation and reduction potentials, diffusion coefficients, and electron transfer to name a few. To manufacture a microelectrode, typically glass is

melted around the electroactive surface to ensure proper sealing and to prevent the outer solution from coming into contact with the inner wires of the microelectrode. There are several methods involving melting the glass around the electrochemical surface, including by hand or by a glass puller. Glass pullers are preferred due to minimizing the glass surrounding the microelectrode surface, in turn minimizing surface imperfections and/or adsorption of undesired compounds by conducting experiments in solution. Types of pullers that can be used are either vertical or horizontal, in which the glass containing the platinum wire is sealed within by melting and pulling simultaneously. The amount of glass and or the amount of pulling done can be controlled by the instrument. Common glass used to make microelectrodes are capillary tubes made of either borosilicate or lead glass. Depending upon the application, 1 mm outer diameter capillary tubes are most commonly used throughout the literature for pulled microelectrodes. For the application of the microirradiator, minimal glass is ideal due to the main use in cells 20 μm in diameter and the minimization of radioactive materials adsorbed onto the glass.

The electroactive surface can involve various conducting materials, such as gold, platinum, silver, and carbon fiber. Metals that are unreactive are most desirable for experimentation within solution, and the noble metals with the highest overpotential such as gold and platinum are most commonly used in electrochemical microelectrode research.[11] Once the electroactive surface material has been sealed within glass, a contact, usually involving metallic epoxy is made between the microelectrode and the external contact and is ready for electrochemical experiments.

A three electrode cell is a basic electrochemical setup to study oxidation and reduction. Within the scope of this thesis, many methods from the field of

electrochemistry are used and will be explained further below. A three electrode electrochemical cell consists of a working, auxillary, and reference electrode.[11, 12]

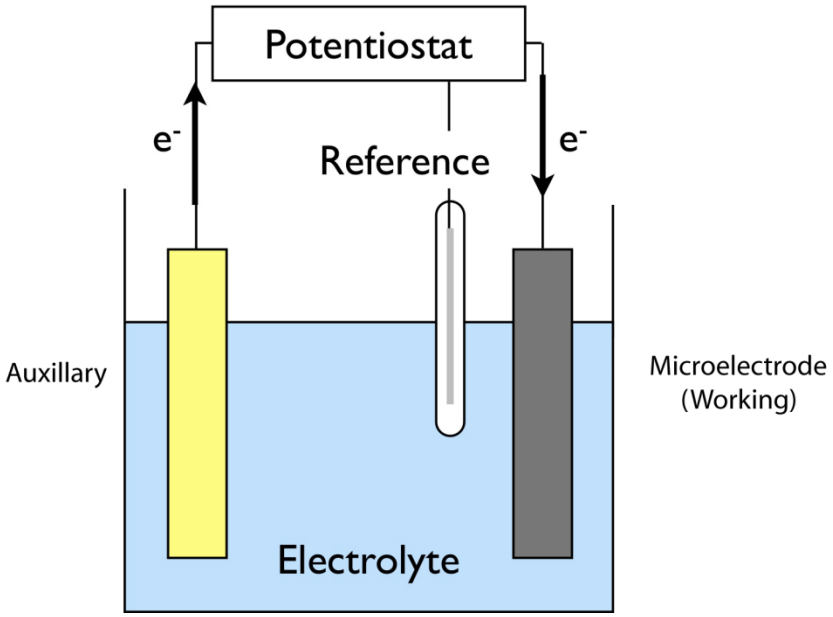

Figure 2. Diagram of three electrode cell.[13]

The working electrode is the microelectrode, the auxillary electrode is a Pt wire (1 mm diameter, 3 mm in length) and the reference electrode is a Ag/AgCl reference manufactured in house. Within the electrochemical cell, an electrically conducting solution contacts all three electrodes, forming the complete cell. A potentiostat is used to control the current between the auxillary and working electrode, where the working electrode's potential is controlled in respect to the reference electrode.

In electrochemistry, oxidation and reduction can be monitored using the three electrode cell by cyclic voltammetry, which is a measurement involving a potentiodynamic change in time while monitoring the current.[1] The electrode potential ramps in time, and is defined as the scan rate (V/s). Diffusion to the surface of the

working electrode can also be determined from cyclic voltammetry. This is governed by the Cottrell equation, where

$$i = \frac{nFAC_j\sqrt{D}}{\sqrt{\pi t}} \quad (3)$$

i is current in amps, n is electrons transferred in the reaction, F is faraday's constant, A is area of the electrode in cm^2, Cj is the initial concentration of solution in mol/cm^3, D is diffusion coefficient in cm^2/s, and t is time.[11] According to this equation, the current will decrease as time increases. For a planar electrode, in which diffusion to the electrode is limited by current, a decrease due to mass transport will occur (Fig.4,5). However, in the case of disk microelectrodes used throughout this thesis, the diffusion layer expands spherically in time, leading to the equation modification of

$$i = 4nFAcD \quad (4)$$

Where 4 is a constant, n is the number of electrons transferred in the reaction, F is Faraday's constant, A is area of the electrode in cm^2, c is the initial concentration of solution in mol/cm^3, D is diffusion coefficient in cm^2/s, and a is the radius of the disk.[11, 14, 15] These equations allow the determination of the surface area of an electrode using current. This equation more specifically is used for the microirradiators to determine whether the area has changed or has been modified by calculating the amount of current passed.

All electrochemical characterizations of microelectrodes before and after etching utilized a Princeton Applied Research Potentiostat/Galvanostat 273 A. The potentiostat was interfaced to a PC computer, and all voltammetric data was acquired through CView and CWare v 2.8d electrochemical software programs (Scribner Associates, Inc).

2.2.1 Fabrication and Characterization of Recessed Disk Microelectrode

Fabrication of the recessed disk microelectrode began by sealing platinum wire in 0.5 cm bore diameter borosilicate glass capillaries (Sutter Instruments, CA). A 3 cm piece of the 25 μm Pt wire was threaded through the capillary and flame sealed at the end for stability. Each sealed capillary was pulled in a glass electrode pulling apparatus (Narshige model pp-880, Japan) at 800 ºC with a pull length of 3 cm. The end of the pulled Pt wire in glass was then polished with varying grades of sand paper and alumina polish (9- 1 μm diameter, Buehler Scientific, Inc.) producing a smooth disk. Copper wire with silver epoxy (Epotek Scientific, Inc.) was used for the contact. Finally, the microelectrodes were sonicated in water for 10 minutes, and heated at 150 ºC for 15 minutes. An optical micrograph can be seen in Figure 3 below.

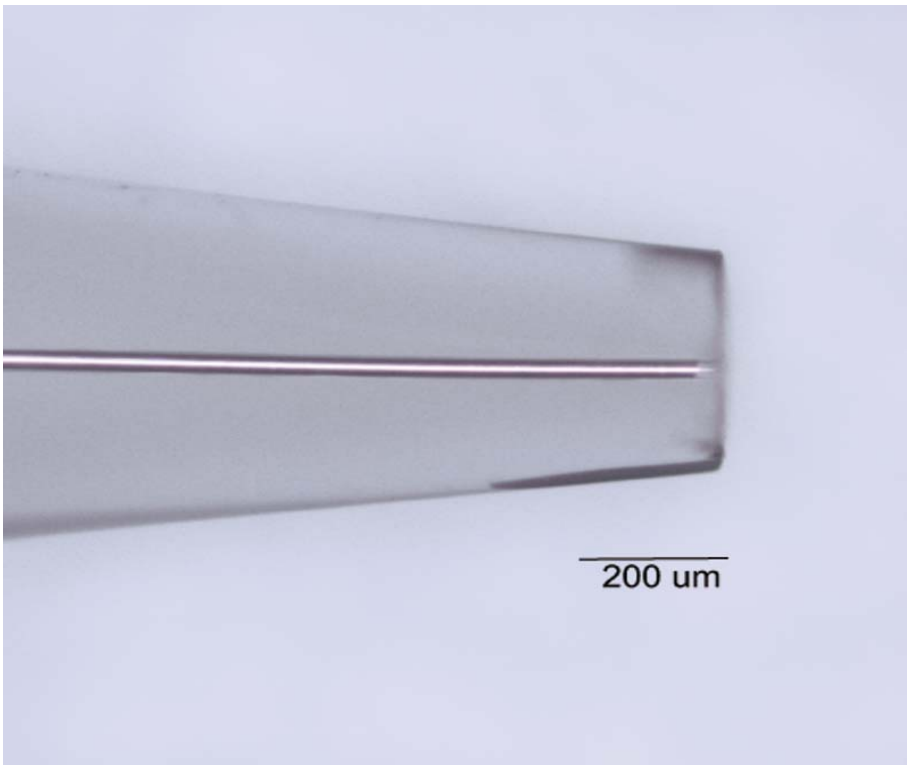

Figure 3. Top view micrograph of recessed disk microelectrode.[1]

The contacted microelectrodes were then cycled in 2.5 mM Ferrocene (Fc) (Acros Organics, 99%), 0.1 M tetrabutylammonium perchlorate (TBAP) (Alfa Aesar, electrochemical grade) in acetonitirle (CH3CN) (Acros Organics, ACS grade) at 20 mV s^{-1}, to verify the electrochemical preparation. After ensuring electrical contact, each electrode was placed in saturated $NaNO_2$ (Alfa Aesar, ACS reagent grade) solution and etched for 20 seconds at -9 V vs Pt auxillary, Ag/AgCl (1 M KCl).[17] This procedure enables a channel depth of approximately 30 to 40 μm of Platinum within the electrode, with deeper channels attained at longer etching times. The recessed disk electrodes were then sonicated in water and acetonitrile, respectively.

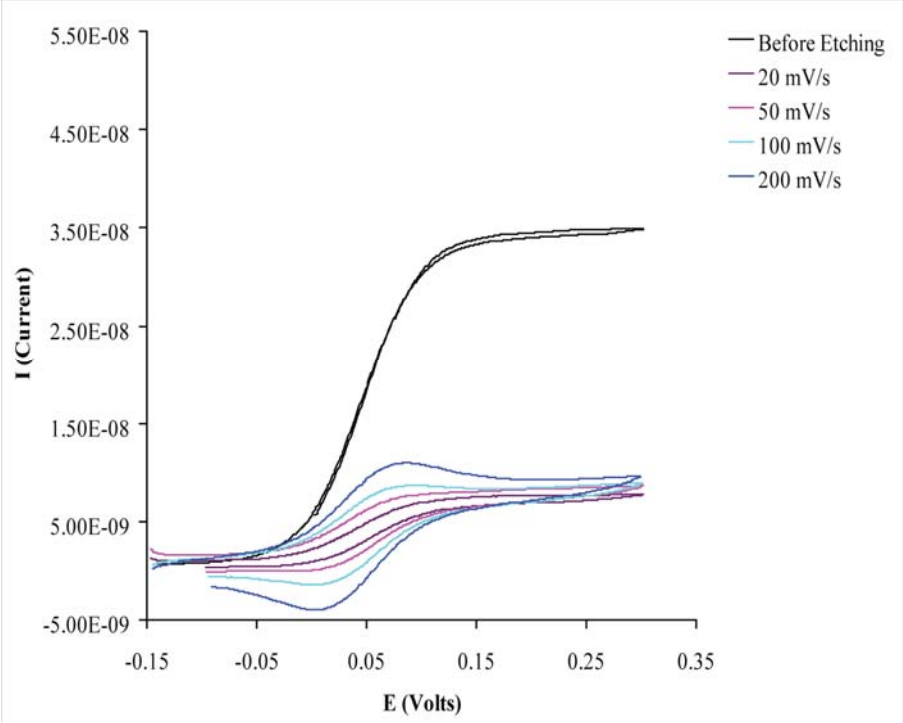

Figure 4. Voltammetric responses of 25 μm recessed disk microelectrode before and after electrochemical etch recorded in CH_3CN / 2.5 mM Fc, 0.1 M TBAP vs Ag / 0.1 M $AgNO_3$ with scan rates of 20, 50, 100 and 200 mV s^{-1}.

In order to ensure that the etching back of the Pt disk took place, the electrodes were cycled again in 2.5 mM Fc solution at varying scan rates from 20-200 mV s^{-1} as previously described. Figure 6 shows a drop in current after etching back the Pt in the glass. Furthermore, at faster scan rates, the CVs showed characteristic planar diffusion properties, which is a result of the analyte being confined to the channel during cycling. This behavior is typical for a recessed disk microelectrode.[14-17]

2.2.2 Protruding Wire Microelectrodes.

Fabrication began by sealing 25 μm Pt /Ir wire (90:10) in 0.5 cm bore diameter borosilicate glass capillaries (Sutter Instruments, CA). The sealed Pt wire in glass electrodes were pulled, contacted, and heated following the same procedure as described above. An optical micrograph is shown in Figure 5 below.

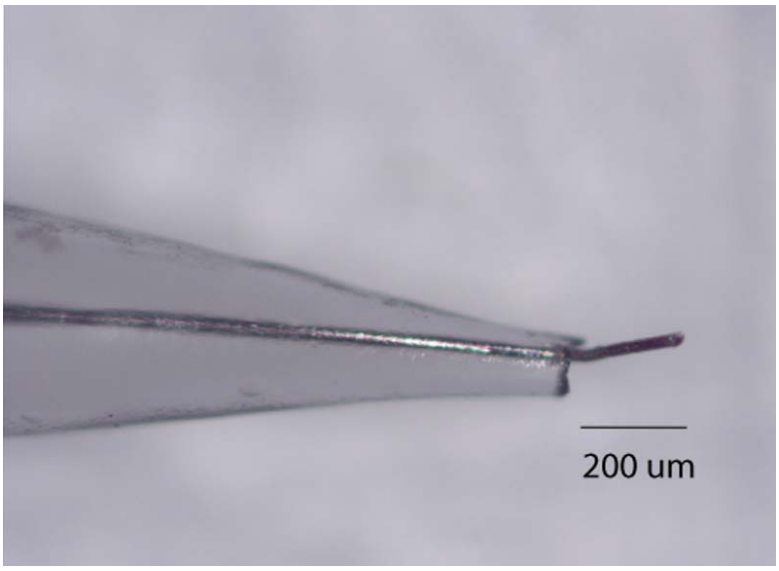

Figure 5. Top view micrograph of protruding wire microelectrode.

The tip of the pulled Pt/Ir wire in glass (approximately 500 μm), was dipped into conc. HF in a hood by dipping the electrode into the bath until barely touching the surface to remove the glass surrounding the Pt/Ir wire tip. Caution must be taken in using HF, as it is extremely dangerous to work with. After etching, each were rinsed thoroughly with water and acetonitrile. This procedure removed approximately 500 – 800 μm of the glass. The exposed wire was then trimmed to approximately 200 μm in length. Following the same procedures described above, CVs and optical micrographs (Figure 4 and 5, respectively) were taken to ensure the electrochemical contact, the length and the shape of wire of each microirradiator. As shown in Figure 5, the CVs of the protruding wire microirradiator shows microcylinder voltammetry characteristics, with the radial diffusion component dominating at slower scan rates (> 20 mV s^{-1}).[16, 18] At higher scan rates (< 20 mV s-1), the planar diffusion down the length of the cylinder dominates

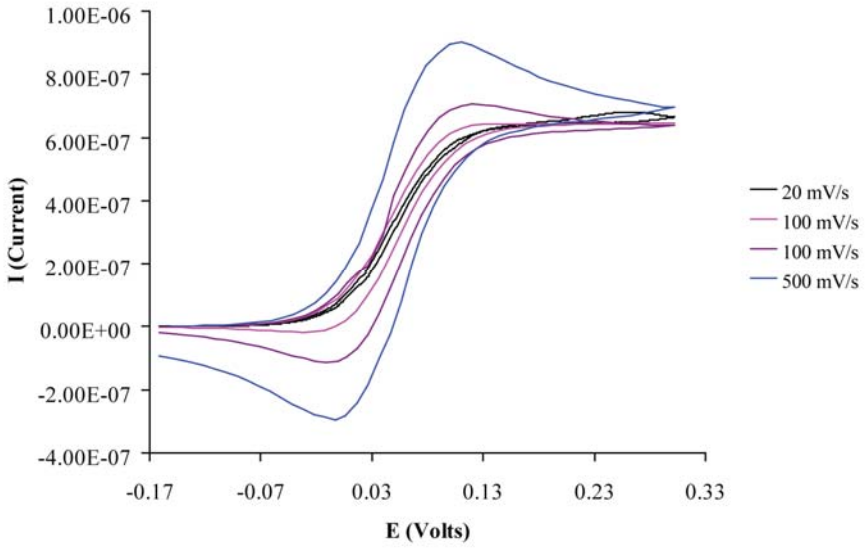

Figure 6. Voltammetric responses of 25 μm diameter, 200 μm length protruding wire microelectrode with scan rates from 20-500 mV s^{-1} were recorded in CH_3CN / 2.5 mM Fc, 0.1 M TBAP vs Ag / 0.1 M $AgNO_3$.

2.3 Nickel Electroplating

2.3.1 Watt's bath

The most common type of chemical bath used to electrodeposit Ni is the Watt's bath.[19 20] Typically, the Watts bath is composed of SO_4^{2-} anions in the form of $NiSO_4$ for strength, Cl^- anions as $NiCl_2$ for plasticity, and H_3BO_3 to inhibit hydrogen evolution at far negative potentials.[19, 21] Since the radioactive source is a standard $^{63}NiCl_2$ in 0.9 M HCl, a non-radioactive ("cold") Ni standard, was made to test the current efficiency and deposition techniques of both types of microirradiators. The addition of 25 mg of $NiCl_2$ and 30 mg of K_2SO_4 to a 5 mL, 6 μCi NIST Ni-63 source provided the best current efficiency needed for a strong nickel metal deposit. K_2SO_4 was added in equal concentrations of a cold carrier of $NiCl_2$ to get a minimum concentration possible for an effective deposition. Other modified Watts bath have been reported[22, 23] but to our knowledge, this is a new method of preparing Ni-63 for electrochemical deposition. Electrochemical deposition thus provides stability of the Ni-63 needed to deliver the radiation doses to the target without flaking off into the rest of the sample.[24]

2.3.2 Pourbaix diagram

A pourbaix diagram (Fig. 7) illustrates the type of nickel deposited at varying pH and potentials. The horizontal lines "a" and "b" represent the potentials and pH that hydrogen and oxygen are evolved along with the deposit desired, respectively., It was experimentally determined at a pH of 4 and a deposition potential of - 0.775 V, that the lowest amount of hydrogen evolution was taking place.

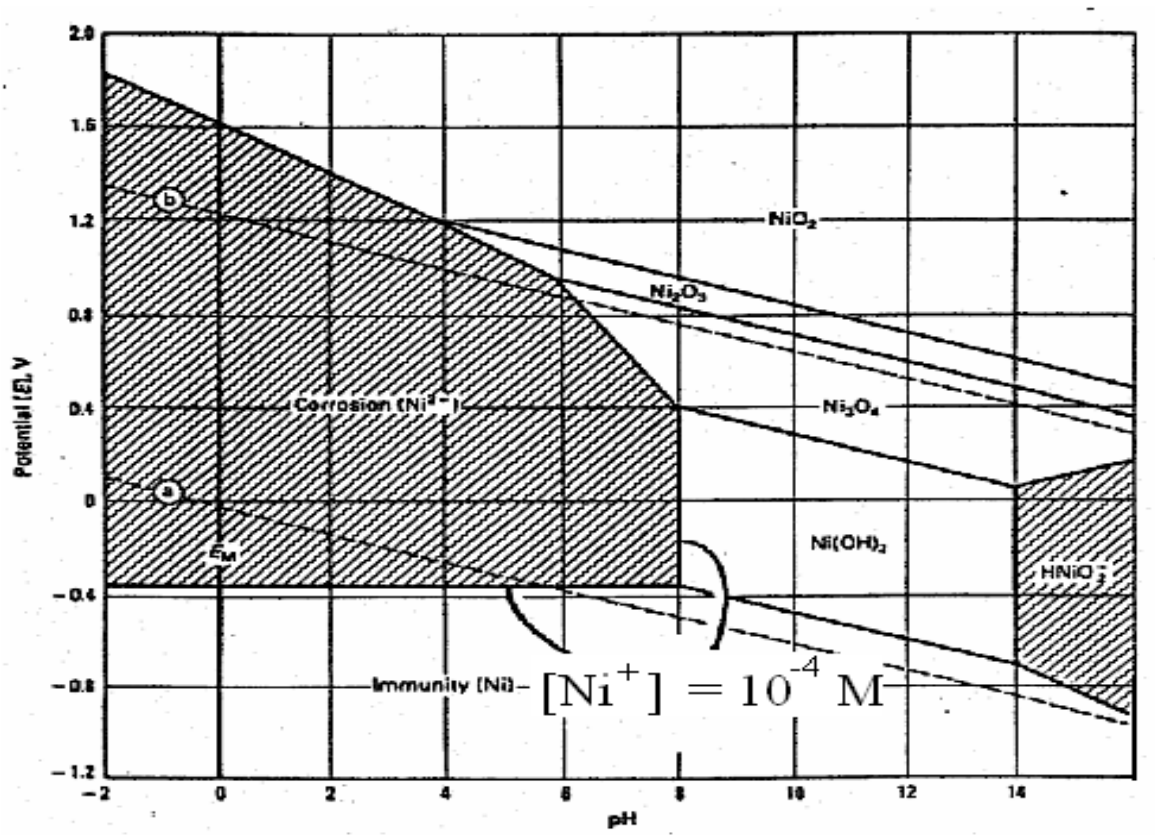

Figure 7. Pourbaix diagram of the different forms of Ni depositions in aqueous medium according to voltage applied and pH.[25]

A linear sweep is similar to cyclic voltammetry except for only completing a half a cycle in either the oxidation or reduction potentials. The graph below represents a platinum 25 μm microelectrode swept at 10 mV/s from 0 to -1 V vs. Ag/AgCl, 1 M KCl in a cold non radioactive nickel solution as discussed in Section 2.2.1. As seen below, the graph is constant until slightly after -.8 V is reached, and sharply decreases in current, representing hydrogen evolution. Deposition at a potential slightly more positive of this value is the optimal one due to the elimination of hydrogen evolution.

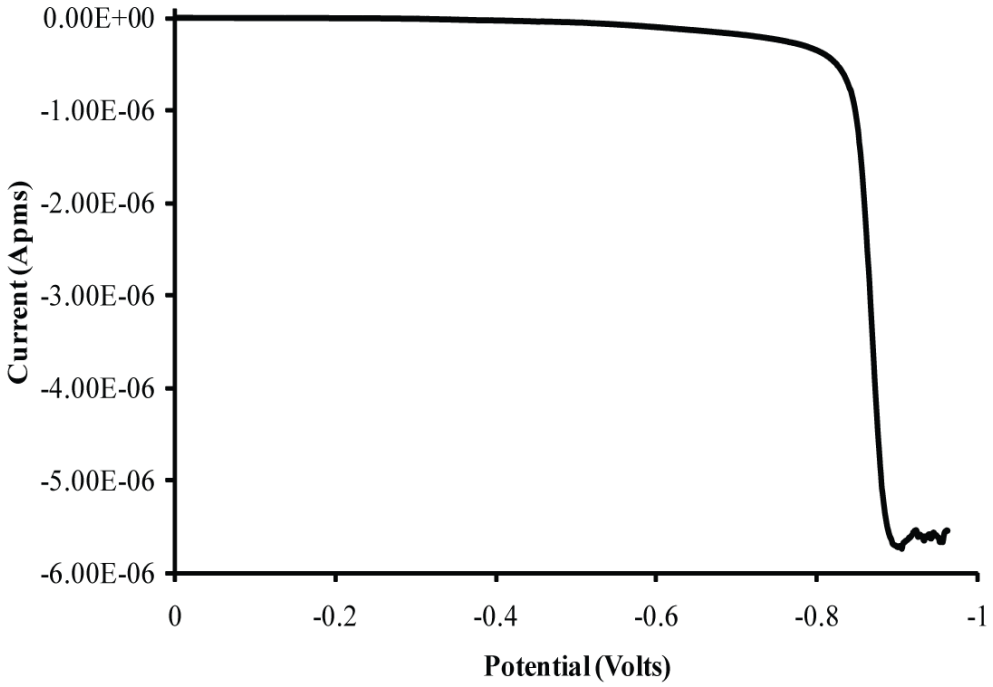

Figure 8. Linear Sweep Voltammetry of cold Ni in pseudo watts bath solution on a Pt 25 µm recessed disk microelectrode vs. Ag/AgCl in 1 M KCl. Sweep rate 50 mV/s.

2.3.3 Development of plating procedure for Ni-63

To electroplate Ni-63, the electrochemical conditions are identical, however precautions need to be taken in order to prevent contamination and to ensure safety to the researcher. All experiments need to be separated into a "hot bench" and a "cold bench", in which all materials that need to interact with the hot material be done in a separate area (e.g. fume hood), and any materials that don't directly need to come into contact with the radioactive solution be away from the hot area (e.g. bench outside the fume hood).

In the hot area, liquid radioactive sources need to be transferred to a fume hood to minimize contamination. Additionally, a special electrochemical cell to minimize incidental splashing of the radioactive electrochemical solution must be within the fume hood. An example of this cell is shown below.

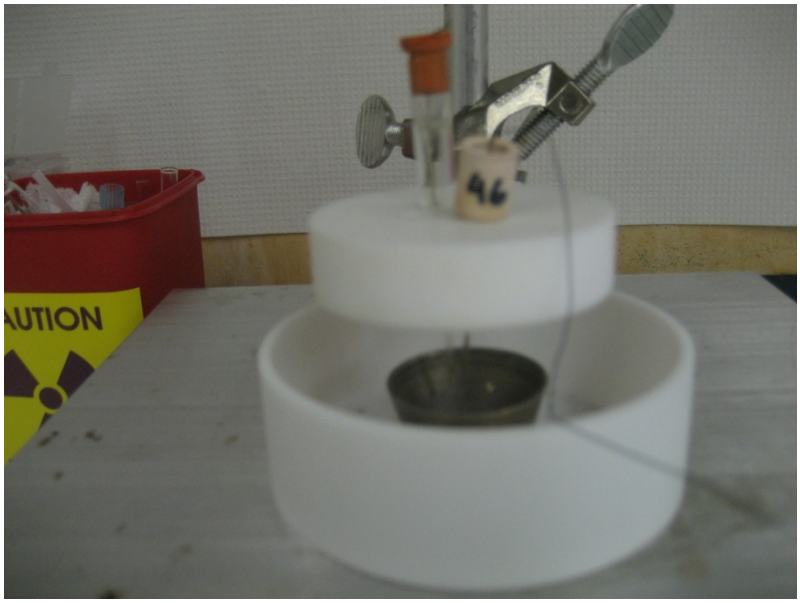

Figure 9. Picture of radioelectrochemical cell.

An example of a radiological electrochemical cell is shown in Figure 9, in which the bottom of the white Teflon container is a containment vessel for the counter electrode, which is the Ni metallic cup in the center. It is conveniently also the housing the Ni-63 solution during electrodeposition. A Teflon holder suspended above holds the working and reference electrodes in place during deposition. Extra care must be taken after electrochemical deposition of all sources to prevent Ni-63 contaminated in or outside the hood. Since Ni-63 is a low beta energy emitter, it is not detectable by a regular Geiger Muller counter and must be detected by liquid scintillation.[2] This entails smears being taken weekly to ensure the safety of everyone that comes in contact with this solution.

2.3.4 Plating Ni-63 on microelectrodes

Throughout this entire thesis, this procedure is common throughout for making all of the liquid electrochemical sources, radioactive or non-radioactive. Various radioactive sources were purchased with different activities. **A**: The 6 μCi Ni-63 stock solution used in chapter 3 was purchased from NIST (National Institute of Standard and Technology) as 5 mL of a solution of $^{63}NiCl_2$ in 0.9 M HCl, 2.22 MBq total activity. **B**: The solution used in chapter 3,4,5, and 6 was 50 mCi Ni-63 stock solution purchased from NRD, Inc. as a 5 mL solution of $^{63}NiCl_2$ in .6 M HCl, 1.85 GBq. All electrochemical experiments were performed in a 5 mL nickel cup serving also as the auxillary electrode (Figure 9). Solution was prepared into a pseudo Watt's bath as discussed in (Section 2.2.1). The reference and working electrodes were suspended vertically in the solution, with the entire setup maintained at 60 ºC for optimum deposition efficiency. The pH of the solution plays a significant role within the deposition of nickel, as it dictates the type of nickel deposited according to pH and voltage applied.[20, 21, 26] The pH was maintained by adding drops of 1 M HCl or 1 M H_2SO_4 every half hour, with pH strips to verify the pH has reached 4. To manufacture each type of microirradiator, radioactive metallic Ni must be electrochemically deposited within the channel and on the surface of the recessed Pt disk and protruding Pt wire, respectively.

To deposit Ni onto each microirradiator, both the protruding wire and recessed disk microirradiators were sonicated (generic jewelry cleaning sonicator) in a portion of the Ni-63 electroplating solution for one minute to saturate potential adsorption sites on the glass and to ensure solution is in contact with the electroactive surface. Irradiators were suspended in Ni solution within the counter electrode Ni-cup and held at -0.775 V

vs Ag/AgCl (1 M KCl). From the charge passed during the deposition, the mass (grams) of Ni can be calculated using Faraday's Law, m = QM/nF**,** where m = mass (g), Q = charge, M = molecular weight, n = number of electrons, and F = Faraday's constant.[11] Each microelectrode was sonicated in water for 5 minutes post-electroplating. After plating, the Ni-63 solution was stored in a radiological housing as designated by the radiation safety office. All procedures are identical regardless of the Ni-63 radioactive source used.

Electrochemical characterizations of the deposition of radioactive materials used a portable OMNI 90 Potentiostat interfaced to a PC through a National Instruments NI-DAQ 6008 card. All voltammetric data testing the cold deposition and radioactive deposition of Ni were analyzed through LabVIEW version 8.5.

2.4 Assessment of radioactivity on Ni-63 plated microelectrodes

As mentioned previously, liquid scintillation is the most common detection method for Ni-63.[2, 27] Liquid scintillation runs upon the principle of radiation interacting with a fluor within a solution. A radiation event typically interacts with the solvent first, which in turn radiatively transfers this interaction to the fluor. This interaction with the fluor produces light, which is then detected by a detector, commonly a photomultiplier tube (PMT). The liquid scintillation cocktail is strategically designed to interact with the solvent molecules and then the fluor to prevent quenching of the light emitted from the solvent itself.

The intensity of light produced is directly proportional to the energy of the emitted radiation particle, commonly to be 8-10 photons/keV.[27] A photomultiplier tube's

cathode interacts with the photon and produces an electron via the photoelectric effect. This electron is then amplified within a dynode chain and produces a voltage pulse which is directly proportional to the energy emitted from the radioactive material. Each voltage pulse can be counted as one count per unit time, or also one disintegration event per unit time. The Becquerel is the SI unit of this measurement, defined as one disintegration per second. From these voltage pulses the activity in Bq of the radioactive material can be determined.

All liquid scintillation measurements were taken using a Perkin Elmer Pacard TriCarb 2900TR detector with National Diagnostics LS-275 water soluble liquid scintillation cocktail with the detection efficiency for Ni-63 of 70%. All count rates were corrected for the values measured the background sample. All microirradiators were taped to a liquid scintillation vial in the same configuration to ensure no statistical deviations due to positioning. Considering the quenching by the material of the microirradiator, the background samples were counted in the same manner (with a microirradiator with cold Ni).

2.5 Safety

As the case with any radioactive material, special safety procedures must be followed while working with aqueous Ni-63. These materials cannot be obtained without a license, so the campus office of radiological safety must be contacted to get proper approval. This involves special waste containers for solid and liquid waste, and proper disposal of gloves while working with the materials. Since Ni-63 cannot be detected with

a standard Geiger Muller counter, smears must be taken weekly with liquid scintillation to detect contamination.

Due to the multiple transfers of solution, and the ultimate goal of preventing contamination, all experiments should be done in a fume hood with proper trays. The goal of this is to prevent contamination from liquid transfer out of the hood and spreading to the inside of the hood. Trays can be easily cleaned with specialized radiochemical decontaminants after work has finished to prevent further contamination. While working in the hood, gloves must be doubled and changed frequently. It is assumed that everything in the hood is contaminated until proven otherwise, leading to glove exchanges after each step has been finished to ensure touching other materials does not spread the contamination further around the hood. Specific safety procedures to work safely with radioactive materials are specific to the situation, and must always be followed to ensure the safety of the worker and the general public and environment.

CHAPTER 3

CHARACTERIZATION OF NICKEL-63 MICROIRRADIATORS

3.1 Introduction

Research in radiation biology has significantly advanced over the last 100 years.[28] From the discovery of x-rays by Roentgen in 1895 to the recent exploration of the bystander effect, radioactive sources play an imperative role in understanding the role of ionizing radiation in biological systems.[4, 29] In this field, one of the hot topics today in radiobiology research is the low dose radiation.[30] This subject requires delivery of localized, low doses of radiation to biological targets and subsequent observation of the induced effects. Such studies are aimed at understanding of the real effects of radiation on the large and small biological systems. To probe such questions, radioactive sources in the forms of X-ray, gamma, and proton microbeams and alpha irradiators are used to expose cells and study the effects in time.[3, 7, 31, 32]

As mentioned above, the bystander effect is the phenomenon when nonirradiated cells exhibit response to radiation damage to the neighboring irradiated cells.[33] Currently, types of radiation used in this field are dominated by high linear energy transfer (LET) alpha and neutron particles, and deposit all of their energy within a very short distance of the penetrating material, causing many localized ionization events within a short distance.[28, 33] However, in the low LET field there are several microbeam facilities incorporating low LET electron and soft x-ray microbeams able to target single cells. However, typically these types of radiation sources are costly and involve high absolute levels of activity that require sophisticated shielding to form the targeted beam. Another

problem is that the radioactive source is typically large in relation to the area of the target, and must be shielded and or collimated with multiple optical and magnetic lenses to form a targeted beam microns in diameter. A compact radioactive source would overcome most of these problems.[2, 28]

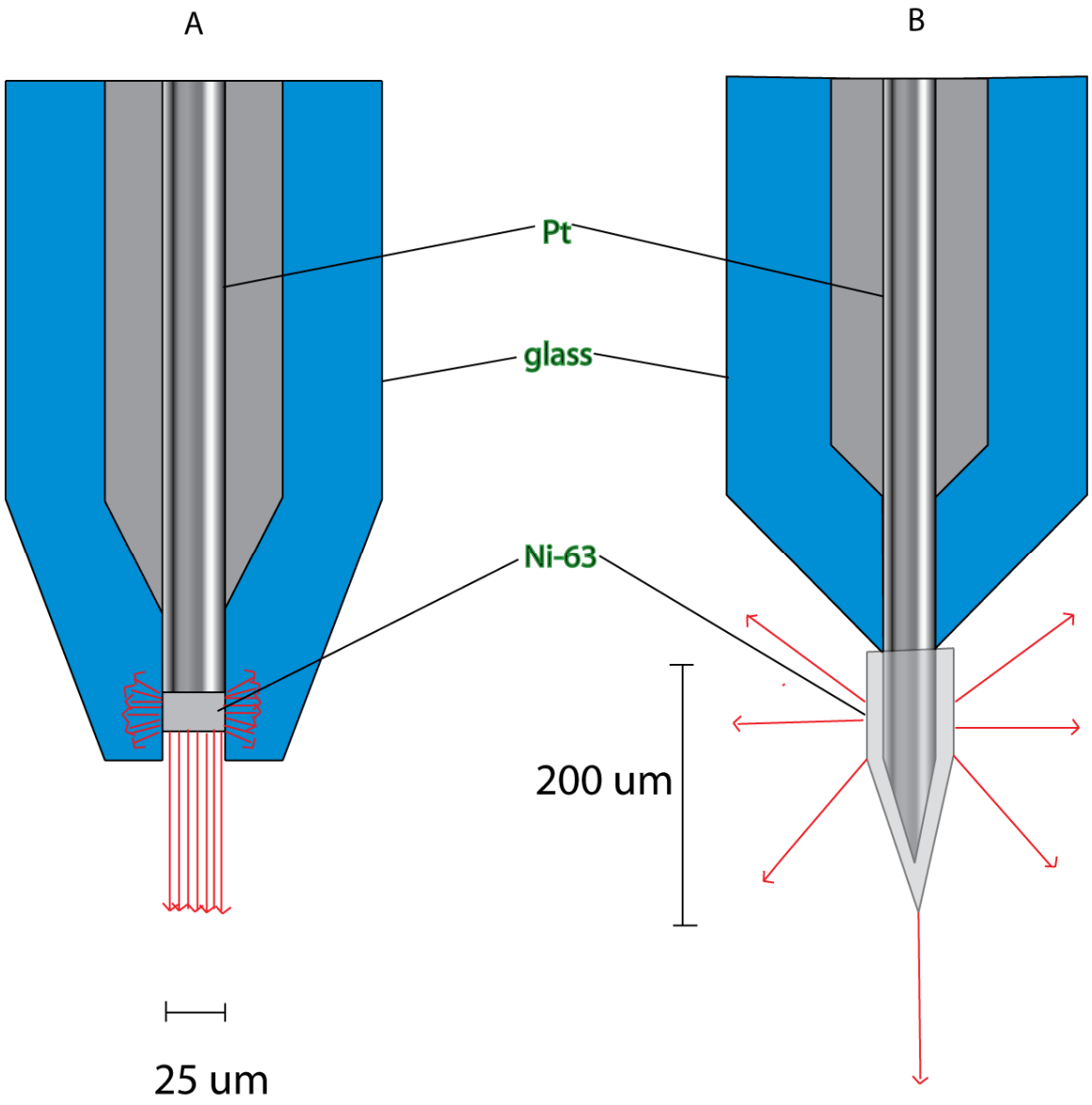

Figure 10. Diagram of projected radiation field from (A) recessed disk and (B) protruding wire microirradiator. The source of Ni (in light grey) is shielded by the glass and Pt wire, creating a collimated beam. The radiation from the protruding wire microirradiator is not shielded by air, but is completely absorbed by the cell when implanted.

In this thesis we report the unique use of modified microelectrodes for fabrication of two different tools that contain small amounts (nanograms) of electrodeposited Ni-63, to a small surface area. This greatly increases the flux density (10^5 β/cm^2) of radiation to cells of diameter (10-30 μm), enabling the targeted cells to receive a high dose. In previous attempts we have developed beta microirradiator incorporating tritium into conducting polymer deposited on microelectrodes.[10] However, due to the volatility of tritium and the instability of the doped polymer layer over time no practical microirradiator has been constructed. Two different devices based on microelectrodes were chosen as the platforms, a recessed disk microelectrode and protruding microcylinder electrode.[11, 14, 15] Since Ni-63 is a pure low energy beta emitter (Emax = 67 keV), it is easily shielded by few microns of glass and other materials8, and can be electrochemically deposited from a Watts bath.[19] Because of the low energy betas of Ni-63, the recessed disk electrode shielded by the surrounding glass yields a built-in collimated beam, with beta electrons being delivered only to the irradiated target.[34] A diagram of both prototypes with respective flux is shown in Figure 10. Additionally, Ni-63 electroplated onto the wire of a microcylinder electrode can be implanted into a cell, leading the cell to absorb total flux of activity from the device. It is important to note that the dose at these amounts of radiation is high on a cellular level, but the dose to operator is minimal. Thus at the distance of 1 cm from the tip the radiation intensity is zero.[34] Therefore, these devices can be used in a bench top laboratory experiments without any risk to the user.

3.2 Results

3.2.1 Electrodeposition of Nickel

In order to verify the amount of deposited Ni, each microelectrode underwent an electrochemical anodic stripping method was applied.[35] Therefore, each microirradiator deposited with cold Ni was transferred to a 1 M NaCl aqueous solution, pH 2 and cycled from -0.3 to 0.8 V at 20 mV s^{-1}.

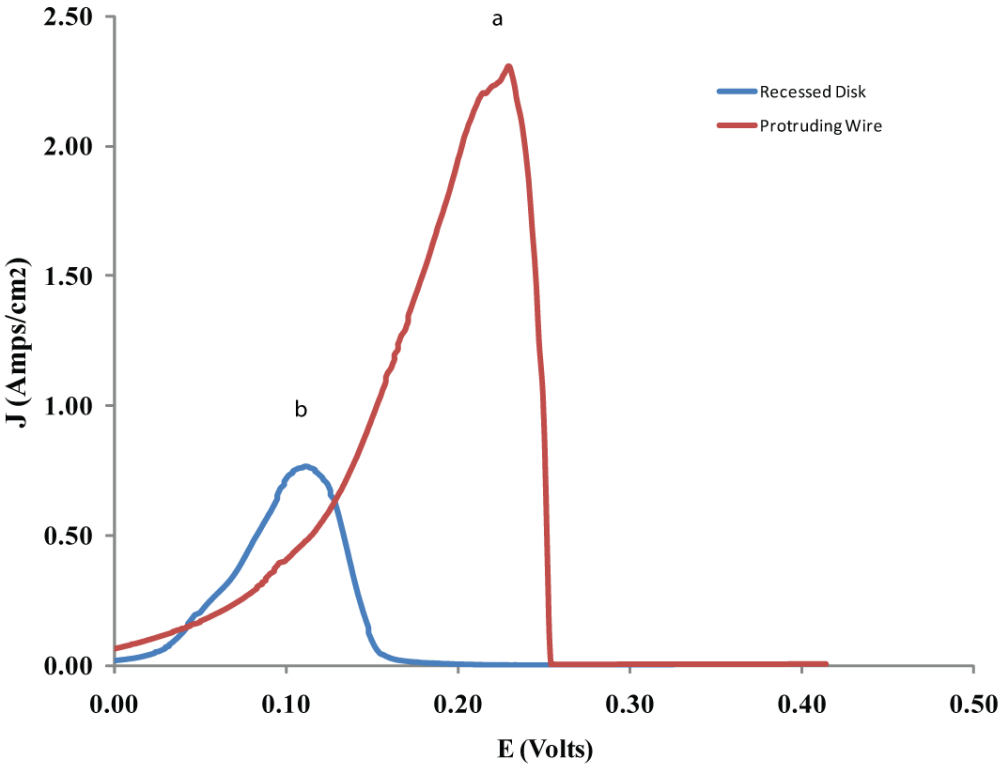

Figure 11. Anodic stripping analysis of Ni (a) protruding wire and (b) recessed disk microirradiators in 1 M NaCl, pH 2 adjusted with HCl, vs Ag/AgCl in 1 M KCl.

As shown in Figure 11, oxidation peaks for both the recessed disk and protruding wire are indicative of Ni oxidation, with a standard potential of 0.259 V vs standard

hydrogen electrode (SHE). The two oxidation peaks having different geometries and peak voltages (Ep) are indicative of the geometry of the electrode and fit well with conventional theory.[11] To calculate the current efficiency, charges from both oxidation stripping peaks and deposition were calculated by Efficiency = $Q_{stripping}/Q_{deposition}$, where Q is charge. This process helps determine how much of the charge passed during deposition is towards Ni deposition versus other competing processes (i.e. reduction of hydrogen).[19] The current efficiency of Ni on both the recessed disk and protruding wire electrodes are high, averaging 85 +/- 5% for each electrode on an OMNI portable potentiostat.

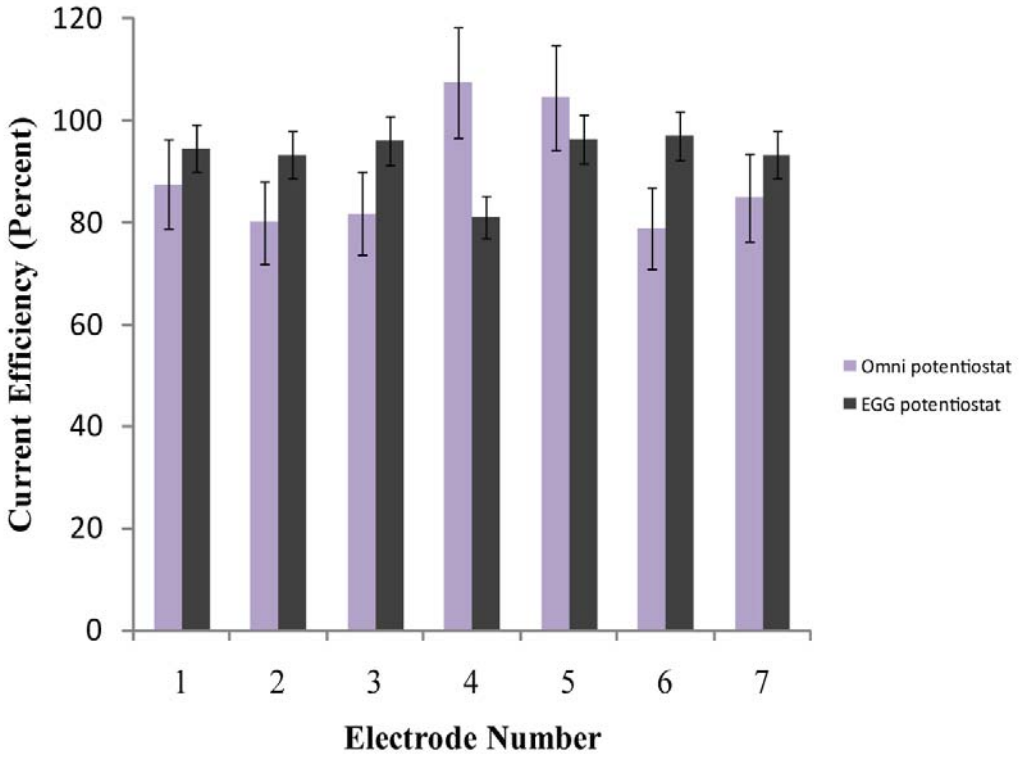

Figure 12. Bar graph of current efficiencies on seven recessed disk microelectrodes tested on a portable Omni potentiostat and a benchtop EGG potentiostat, respectively.

This current efficiency is imperative in determination of the activity of Ni-63 electrochemically deposited and can be correlated with the specific activity of the Ni-63 liquid source.

3.2.2 Liquid Scintillation

Using several trials for measuring activities were taken with 3 recessed disk and protruding wire microirradiators. Counting by liquid scintillation was performed before and after ensuring that no residual radioactive materials were adsorbed on the electrode body after electrochemical deposition and anodic stripping. Each electrode was deposited with different amount of Ni and fastened into a liquid scintillation vial to minimize the optical shielding effects during the liquid scintillation counting. After each measurement, the microirradiator was removed from the cocktail, rinsed and soaked in water for 20 minutes to minimize the effects of the cocktail on the electrochemical stripping.

The exact amount of Ni on each electrode was determined by anodic stripping analysis (Chapter 3) and correlated with the measured activities of Ni-63. As shown in Figure 13 for both the recessed disk and protruding wire microirradiator, activity increases linearly with amount of Ni-63 until leveling off, due to self absorption of the low energy emitting betas.[36] For the recessed disk microirradiator, activity detected by liquid scintillation leveled off at approximately 15 ± 3 disintegrations per minute (dpm) (Fig. 13A), corresponding to 0.25± 0.5 Bq. Taking into consideration that this source is confined to a surface area of 4.9×10^{-6} cm^2, the flux density shown from each recessed disk microirradiator is approximately 5.1×10^4 β/cm^2. Additionally, the activity of the protruding wire microirradiator levels off at approximately 60± 12 dpm (Fig 13B),

corresponding to 1.0 ± 0.2 Bq total activity detected. These higher activity values are achieved because of the larger surface area of the wire versus the recessed disk, enabling more Ni-63 to be deposited across the surface. With this being said, the flux density for each protruding wire electrode shown is approximately 1.1 x 10^4 Bq/cm^2.

Additionally, at the point of deviation from linearity on the graph, the recessed disk and protruding wire electrode clearly show self absorption effects at 10 ng and 200 ng, which correlate to 2.29 and 2.24 μm (ρ= 8.9 g/cm^3) in thickness assuming uniform thickness. This agrees well with self absorption and thickness of deposit values reported in the literature.[37, 38] This once again assumes that each deposit is uniform in morphology and density at 8.9 g/cm^3. Morphology of the deposited layers could ultimately vary the activity data shown.

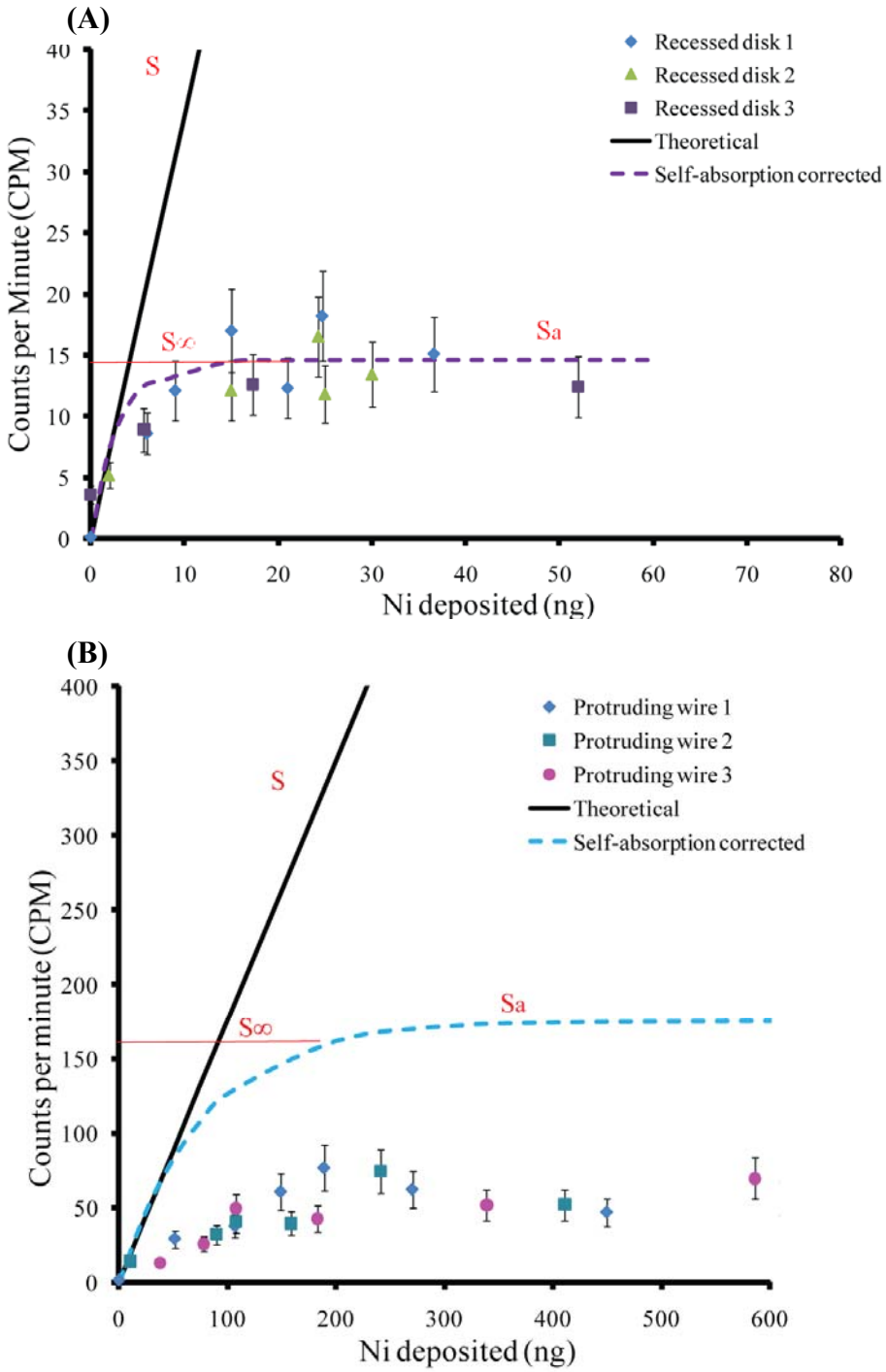

Figure 13: Changes in experimental, theoretical(S), and self-absorption (Sa) corrected activity determined for counts per minute (CPM) versus Ni deposited (ng) at different charges for **(A)** recessed disk and **(B)** protruding wire microirradiators. S∞ is indicative of the saturation range for Sa. Errors in activity values range from (± 20%) with all activity measurements background corrected.

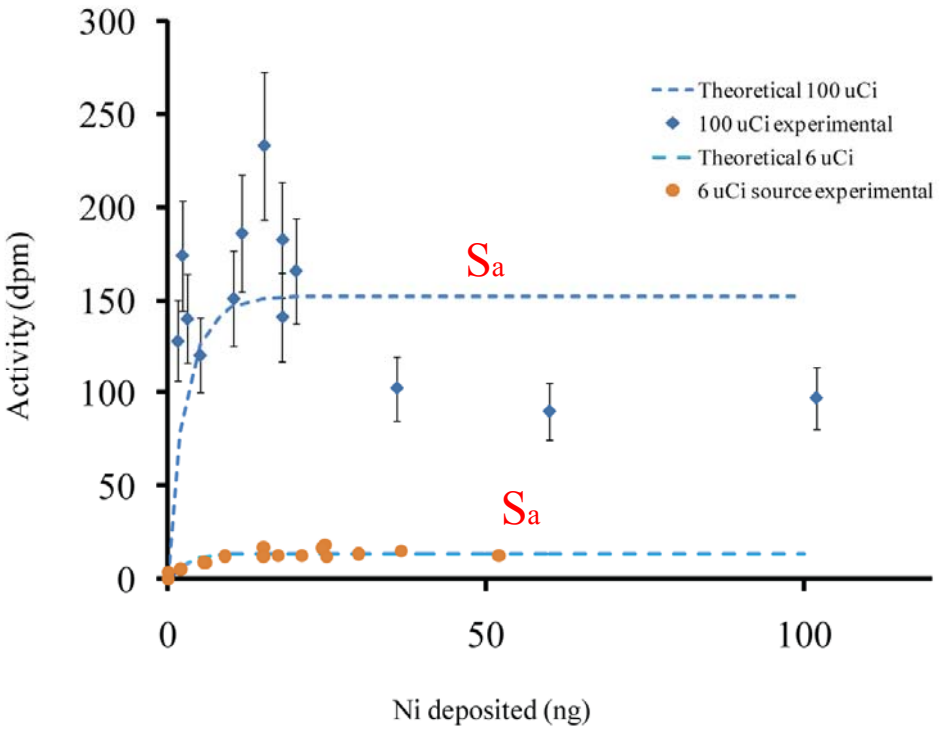

Figure 14. Experimental and self-absorption (Sa) corrected activity of Ni deposited for recessed disk microirradiator. Calibration of 100 uCi source vs. 6 uCi source (shown in Figure 11).

To prove that the theoretical curves shown in Figure 13 can be applied to various concentrations of sources, calibration (data not published) on a recessed disk microelectrode with a 100 uCi Ni-63 were produced (Figure 14). Three recessed disk microirradiators were used in calibration following the exact procedure outlined in Chapter 2 for determination of the amount of Ni deposited and activity measurements. At a maximum, the recessed disk microirradiators saturated at approximately 150 +/- 22.5 dpm, with at larger Ni deposits seeing a drop to approximately 100 +/- 15 dpm. It is unlikely this drop is attributed to anything other than error since the amount of Ni deposited well exceeded the original calibration trials for the recessed disk in Figure 13.

This additional data proves that higher concentration of radioactive sources can follow this exact format by altering the specific activity of the source.

3.2.3 Data Analysis of the Ni-63 Flux

The amount of radiation detected from any point source is defined from the strength of the source, and its geometrical configuration with respect to the object of irradiation.[2] To estimate the total amount of radiation emitted from each device (Bq) and its density, a theoretical calculation of the flux density (β/cm^2) has been done for each type of microirradiator. Since Ni-63 is a low energy beta emitting material, its flux is limited in the fact that there is a maximum beta particles output due to self absorption within the source already at very low thicknesses (microns).[36]

In this hypothetical calculation and for simplicity, a 1 μm deposit of Ni-63 will be used as the thickness of the source. This produces a disk of Ni, 1 μm high, 12.5 μm radius, and a surface area of 4.9×10^{-6} cm^2. If the Ni-63 is a disk source only the surface area of the disk proximal to the irradiated object will be relevant due to the shielding effects of the surrounding glass and of the Pt wire. The ratio of the flux through the exposed proximal surface of the disk to the total surface area activity of the disk source will define the geometry factor f_G , i.e. how much beta radiation is emitted from the proximal surface area (Figure 10) of the nickel disk source.

$$f_G = \frac{S_p}{S_t} = \frac{\pi r^2}{2\pi rh + 2\pi r^2} = \frac{r}{2h + 2r} \quad (5)$$

This equation demonstrates that with increasing amounts of Ni deposited, the height of the disk increases. With increasing height, the radius of the disk source remains the same, causing the shielding factor to decrease with increasing deposits. It is important to note

that for simplicity, (Figure 10) the Ni-63 source has been shown as a disk (r << h), assuming that the non-collimated radiation is completely shielded. To illustrate this, a Ni-63 disk source with r = 12.5 μm, h = 1 μm would have a shielding factor of 46%. Applying the backscattering factor of 1.5 for Pt (equivalent to Au backscattering factor) yields an additional 23% beta flux from the source.[2] With this being said, only about 69% of total beta radiation from the deposited radioisotope would be (ideally) emitted at the proximal end at this height.

To estimate the amount of radiation emitted from the protruding wire microirradiator, the mass of the deposit of Ni on the wire can be similarly calculated by the same method described above, taking into consideration the change in geometry of the wire.[2, 10]The geometrical shape of the Ni source on the wire will be that of a hollow cylinder, with geometry where h = height of deposit, r = radius of internal cylinder (12.5 μm), and R = radius of external cylinder. Taking this into consideration, the surface area of the proximal face (S_{pf}) of the hollow cylinder is exposed to the specimen and the distal face on top of the Pt/Ir wire backscatters into the wire, with the top scattering into the glass . This translates to 50% of beta particles emitted.

$$f_G = \frac{S_{pf}}{S_{hc}} = \frac{2\pi r^2 + 2\pi rh}{2\pi Rh + 2\pi rh + 2(\pi R^2 - \pi r^2)} = 0.5 \qquad (6)$$

Unlike the recessed disk irradiator, the thickness, h, of the Ni deposit on the wire increases proportionally with the radius of the external cylinder, causing the shielding factor be constant. Taking into factor the backscattering coefficient 1.5 for Pt, an additional 25% percent of radiation will be emitted for a total of 75%. However, as mentioned above, the weak energy beta particles are partially attenuated in their specimens, and Ni-63 has an attenuation coefficient of 1.56 mg/cm^2, so there will be a

value of d at an infinite thickness, d_∞, determined from the saturation limits in Figure 12 A and B. As mentioned above, for Ni-63 once again has self-absorption limitations, so for these calculations f_G at infinite thickness must be calculated as well, according to experimental data.

3.2.4 Estimation of the Self-Absorption Factor and Particle Flux

The theoretical activity levels A_t, deposited on each microirradiator, is calculated from the deposited amount of Ni element determined experimentally by electrochemical stripping, and the specific activity of the Ni-63 radioisotope:

$$A_t = mA_{sp} \qquad (8)$$

where A_t is the theoretical activity in Bq or dpm, m is the mass of nickel in grams and A_{sp} is the specific activity of Ni-63 in Bq/g. Because Ni-63 is a pure beta emitter and because each beta decay emits one electron, the electron emission rate (electrons/second) can be calculated as

$$S = f_G m A_{sp} \quad (9)$$

where S is the electron emission rate, m is the mass of nickel in grams, A_{sp} is the specific activity of Ni-63 in Bq/g, and f_G= 0.69 and 0.75 are the geometry factors for the recessed disk and protruding wire, correspondingly. To include self-absorption of the beta particles, the electrons actually emitted from the microirradiator becomes:

$$S_a = S_\infty (1 - e^{-\mu d}) \quad (10)$$

where S_a is self absorption, S_∞ is the "saturated" activity at an infinite thickness of the specimen as determined from Fig. 13, μ is the absorption coefficient for the isotope (Ni =1.56 cm^2/mg), and d is the thickness of the Ni-63 deposit in mg/cm^2.[2, 2, 37, 38]

Figure 13A shows the activity and shielding factors at infinite thickness are taken at 10 ng and 100 ng for the recessed disk and protruding wire, where the saturation of Ni-63 begins. Theoretical levels of the emitted activity are calculated from the mass deposited, times the specific activity in Bq/g (Eq. 9). Taking this into consideration, the recessed disk model (red) fits excellently with experimental data, averaging 14 dpm (0.23 Bq) within ±1% of values shown in Figure 13A. The activity of the protruding wire microirradiator levels off at approximately 60±20 dpm. For the protruding wire model, however, is higher than experimentally observed, but this, we assume, could be due to the fact that the body of the electrode placed in the vial quenched a significant amounts of the photon output, and thus limiting the detector efficiency.[39]

3.2.5 Dose Calculations

Since both microirradiators are going to be utilized in the future for the irradiations of cells, the range of the betas in water and tissue must be addressed. Additionally, estimates of expected dose to the tissue (Gy/min) are essential for future biological work. To calculate dose rate D_β,

$$D_\beta = 5.678x10^{-5}\Phi_\beta \bar{E}\mu e^{-\mu(\rho x)} \quad (11)$$

Where Φ_β is the flux of betas in electrons (β)/cm^2 , E is 1/3 of the maximum energy of the beta particle ($1/3E_{max}$), μ is the absorption coefficient of radionuclide in deposition material (cm^2/g), ρ is density of the deposition material in g/cm^3, and x is thickness in

cm.^{2} Assuming the recessed disk and protruding wire electrodes have activities of 11 and 51 electrons/cm^2 respectively, each flux of beta electrons would be 2.04 and 1 x10^5 β/cm^2. Using each individual flux value, and absorption coefficients in tissue leads to a direct dose of 0.071 and 0.035 Gy/min to individual cells for the recessed disk and protruding wire microirradiator, respectively. This gives the theoretical dose rate of the source of radiation without taking into consideration any shielding absorption from air or any other encountering material.

Table 1. Calculated dose rates at different distances for both microirradiators.

Microirradiator Type	Flux , Φ_β (β/cm^2)	Calculated dose to cell with various attenuation values (Gy/min)			
		0 μm	5 μm	10 μm	20 μm
Protruding wire	1.00×10^5	0.035	0.029	0.024	0.017
Recessed disk	2.04×10^5	0.071	0.059	0.049	0.034

Realistically, both the protruding wire and the recessed disk microirradiators will be mounted at a 45 degree angle, with the tip being placed anywhere between 5-10 μm away from the cells. Modifying Equation 11, the new total dose rate, $D_{\beta,T}$ is

$$D_{\beta,T} = D_\beta e^{-\rho(x)\mu_{\beta,w}} \qquad (12)$$

Where μ_β takes into consideration the shielding effects from the distance the betas have to travel through the extracellular matrix, consisting of mostly water.[2] As shown in Table 1, placement of the microirradiator with respect to the cell is crucial of the dose the cell receives. Additionally, the thickness of each cell is important to maximize DNA damage and hydrolysis within the cell. With a stopping power of 14.9 $MeVcm^2/g$, and an average range of 4.79 μm, thin cells risk the probability of radiation scattering through the cell into surrounding medium. Different distances between the radioactive source and the cell are crucial in dose rate calculations through water, since its limiting distance is approximately 60 μm. Optimally, placing the microirradiator as close to the cell as possible would be the optimal configuration for the application of the highest dose rate.

3.3 Conclusions

This thesis chapter describes two different types of microirradiators that can deliver a small activity but an intense flux of beta electrons to cells for observations of cellular effects. Fabrication and the results electrochemical calibration of two different types of irradiators fit well with conventional electrochemical theory. The deposition of Ni-63 that was developed in laboratory with cold Ni and Ni-63 show a new general electrochemical deposition technique for different radionuclides. The reproducibility of multiple microirradiators of each kind demonstrates the reproducibility of activity levels on each probe in correlation to the amount of Ni-63 deposited.

CHAPTER 4

Ni-63 MICROIRRADIATION SYSTEM FOR OBSERVATION OF DNA DOUBLE-STRAND BREAK RESPONSE

4.1 Introduction

Ionizing radiation affects living tissue in a unique way, by depositing energy along discrete, nanometer-scale tracks. When a track intersects DNA, damage can occur on both DNA strands simultaneously, which may lead to an outright chromosome break. As such, even one such break can cause chronic genetic instability or cancer-associated gene rearrangements. It is thus not surprising that ionizing radiation evokes complex biological defense and repair mechanisms. A central aspect of the radiation response is the self-assembly of nucleoplasmic repair foci, which are characterized by specific histone modifications, accumulation of DNA damage sensing and signal transduction proteins, and assembly of the DNA repair machine proper from pre-existing components. Repair foci begin to appear shortly after irradiation and resolve over the course of several hours [40, 41]

Conventional methods for evoking this radiation response require placing cells or tissues in the proximity of a radiation source. These "off-line" methods require physical transfer of samples from the irradiator to a microscope stage for observation, which precludes observation of early-stage assembly of repair foci in real time. In addition, one of the most common methods for laboratory irradiation requires a high-activity $^{137}CsCl_2$ source. These sources face increasing restrictions because they are perceived as threat to public health and safety in the event of an accident or attack [42]. An inexpensive replacement technology using smaller amounts of isotope would address this concern.

One approach to address the shortcoming of conventional irradiation methods is to position a small radioisotope source in proximity to the sample on a microscope stage. One of the first examples of this approach was the use of a polonium-coated tungsten micro-needle to deliver α-particles to living cells [43]. Recently, Steeb and coworkers described an updated version of the microirradiator concept based on the deposition of isotopes by electroplating on a microelectrode enveloped by a glass capillary [44]. Importantly, the diameter of the microelectrode is on the same order as the size of a mammalian cell. Concentrated deposition of isotope within this small area allows for a high local radiation flux (10^6 to 10^9 β/cm^2) using sub-nanogram amounts of isotope. In addition, the electroplated surface can be recessed within the capillary, which allows the glass walls to act as a collimator for the beam [44]. The concept was implemented using ^{63}Ni, a long-lived, low-energy beta particle emitter. The maximum range of the emissions is only about 66 μm in water or tissue, which allows the user to handle the device without special radiological precautions.

Here we describe the first use of the ^{63}Ni microirradiator in a biological application. We mounted the device in a micromanipulator on the stage of a deconvolution microscope and used it to irradiate cultured human cells. Cells were transfected with expression constructs for fluorescently-tagged 53BP1, a widely used marker for DNA double-strand break repair foci (reviewed in [45, 46]). We collected real-time image data, which enabled quantitative characterization of the appearance, disappearance, and motion of these foci. Initial studies suggest heterogeneous rates of formation and resolution, which could not have been observed using a conventional off-line radiation source.

4.2 Materials and Methods

4.2.1 Microirradiator

The microirradiator was fabricated as described with modifications as indicated below [44]. Briefly, a 25 μm Pt wire was threaded through a 0.5 cm bore diameter borosilicate glass capillary, which was flame-sealed and pulled in a glass electrode pulling apparatus at 800 ºC with a pull length of 3 cm. The end of the pulled Pt wire in glass was polished to produce a smooth disk. After cleaning, the electrode was electrochemically plated using a 50 mCi $^{63}NiCl_2$, (1.6 X 10^{13} Bq/g) source (NRD LLC, Grand Island, NY). This source was transformed into a pseudo Watts bath with the addition of $NiSO_4$ and H_3BO_4 for optimum Ni deposition. The Pt surface was deposited and monitored by constant potential (-0.75 V) until ample charge was passed (10^{-4} C) to indicate ^{63}Ni had plated the surface, extending slightly past the capillary. After ^{63}Ni deposition, a micron layer of Poly(3,4-ethylenedioxythiophene) (PEDOT) was deposited to ensure Ni did not interact with the cellular medium. A 0.1 mM solution of PEDOT was dissolved in 1 mM tetraethylammonium perchlorate (TEAP) in acetonitrile for 20 s at 0.25 V. Total activity of the microirradiator was 2000 Bq, as measured by liquid scintillation counting. The microirradiator was rinsed after each use and stored in a detergent solution.

4.2.2 Reporter plasmid

A PCR-XL-TOPO vector containing the human full-length 53BP1 open reading frame (ORF) (locus accession number BC112161) was purchased from Open Biosystems (Huntsville AL). It was digested with KpnI and XhoI to release the 53BP1 ORF together

with upstream and downstream untranslated regions (UTRs). The recipient vector, pENTR/D-TOPO (Invitrogen, Carlsbad CA) was first modified by insertion of an XhoI/KpnI polylinker, and the 53BP1-encoding fragment was inserted between these two sites. To delete unwanted 5' UTR sequences, a 520 nucleotide N-terminal segment of the 53BP1 ORF was amplified using primers d(GGCGCTCGAGATGGACCCTACTGGAAGT) and d(GGCGCATATGGCACAGTATTTTCC), digested with XhoI and NdeI to create cohesive ends, and substituted for the corresponding XhoI-NdeI fragment in the natural cDNA, resulting in the promoterless pENTR/53BP1 vector. To insert an N-terminal fluorescent tag, the EYFP coding sequence was amplified, together with flanking Kozak consequence sequence, using primers d(GGCGGCGGCCGCGCCACCATGGTGAGCAAGGGCGAGG) and d(GCGCTCGAGCTTGTACAGCTCGTCCATGC). The product was cleaved with NotI and XhoI and inserted between the NotI and XhoI sites of pENTR/53BP1, upstream of and in frame with the 53BP1 ORF. The resulting construct was transferred using phage lambda recombinase into pcDNA-DEST40 (Invitrogen) for mammalian expression under the control of the CMV promoter/enhancer. The full sequence of the expression construct is provided in Supplementary Material.

4.2.3 Cells and electroporation conditions

U2OS 2-6-3 cells [47] were maintained in high glucose DMEM supplemented with GlutaMAX-1 (Invitrogen), 10% fetal bovine serum, 100 U/ml penicillin, 100 µg/ml streptomycin and 0.25 µg/ml Amphotericin B. Electroporation was performed using 3 µg of plasmid DNA and 40 µg of sheared salmon sperm DNA carrier (Ambion, Austin TX)

using a Gene Pulser II (BioRad, Hercules CA). Electoporation was performed in a 0.4 cm cuvette containing 120 µl of culture medium, with settings of 170 V and 975 µF, resulting in a 60-90 ms time constant. Following electroporation, cells were seeded into glass bottom culture dishes (MatTek, Ashland MA) and incubated at 37 ºC to allow protein expression. Irradiation and imaging were performed 24-48 h post-electroporation.

4.2.4 Conventional γ-irradiation and cell imaging

Cells were electroporated with plasmids encoding EYFP-53BP1 and H2B-diHcRed, a nuclear marker [48]. Cells were irradiated using a self-contained ^{137}Cs irradiator (Gammacell 40 Exactor, MDS Nordion, Ottawa ON, Canada) at a dose rate of 0.84 Gy/min, then transferred to the WeatherStation environmental chamber of an Applied Precision Deltavision microscope, where incubation was continued at 37 ºC in a humidified, 5% CO_2 atmosphere. Live cell images were collected using a 60X Plan Achro oil objective beginning 25-30 min post-irradiation. Filter sets were as follows: EYFP, 500 nm excitation/535 nm emission; diHcRed, 572 nm excitation/632 nm emission. Z stacks of 15-24 images were collected using a 0.4 µm step size and deconvoluted using softWoRx software. Projection images were prepared and foci were scored manually. To determine the dose response, regression analysis was performed using SigmaPlot v11.0 software (Systat Software, San Jose CA).

4.2.5 ^{63}Ni microirradiator β-irradiation.

A micromanipulator (World Precision Instruments, Sarasota FL) was mounted inside the Weatherstation environmental chamber of the Applied Precision Deltavision

microscope to facilitate precise positioning of the microirradiator tip. The microirradiator probe was secured in an acrylic electrode holder. Cells were electroporated, incubated 24-48 h, transferred into the environmental chamber, and the microirradiator was positioned directly over a target cell, as determined by observation through the Deltavision optics. Time-lapse exposures were performed, with 15-24 Z-stack sections per timepoint, 0.4 μm section thickness, 0.5 sec exposure time, and auto-focusing in the EYFP channel. Images were deconvoluted, projection images were prepared and foci were scored manually. Foci present prior to irradiation excluded.

To track and quantify individual foci, a region of interest was defined within the projection images, exported in TIF format, and loaded into DeCyder 6.5 software (GE Healthcare, Buckinghamshire UK). Automated spot detection was performed, foci ("spots") were matched across the time-lapse images, and spot volumes were determined and plotted as a function of time.

4.3 Results

4.3.1 Microscope stage-mounted irradiation system

The microirradiator was made by electrochemical deposition of an approximately 1 μm thick layer of ^{63}Ni on a 25 μm-diameter microelectrode wire enveloped in a glass capillary [44]. The configuration of the device used here was similar to the "recessed disk" design reported earlier [44], except that the device was prepared without etching the tip of the microelectrode, allowing ^{63}Ni to be plated directly onto a flush, polished Pt surface. This design change eliminates concern over attenuation of activity due to trapping of medium or debris in the cavity of the "recessed disk" configuration. The isotopic enrichment of the ^{63}Ni was higher, resulting in a more highly active probe surface. In

addition, a polymer PEDOT coating was applied to prevent direct contact between the Ni surface and the cell medium.

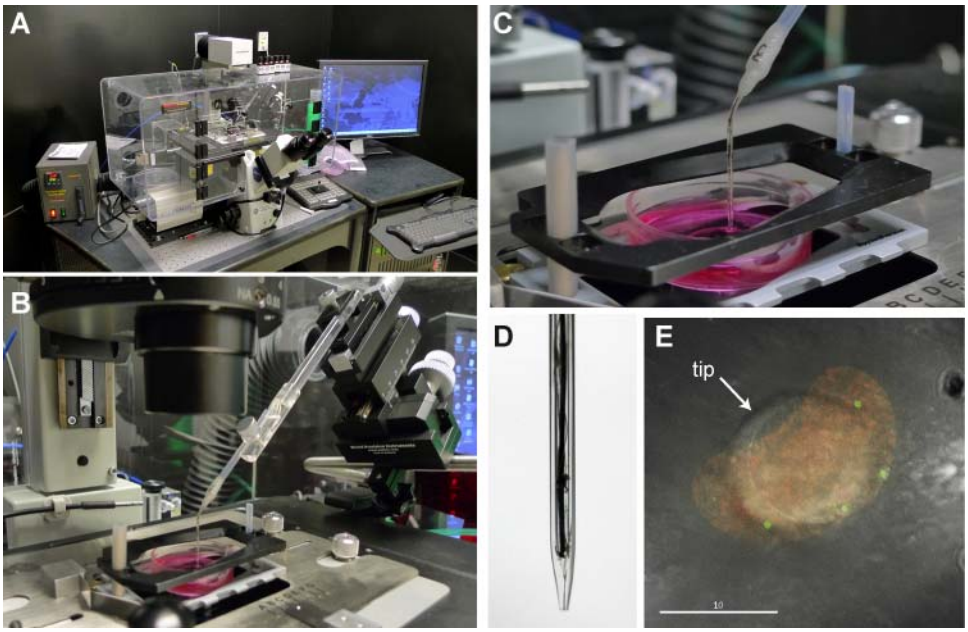

Figure 15. Microscope stage-mounted microirradiation system. **A**. Gross view of microirradiation system. Device is mounted on a micromanipulator housed within a heated, humidified, environmental chamber of the Applied Precision Deltavision microscope. **B.** Close-up view showing attachment of device to micromanipulator. **C.** Detail showing bend in enclosing capillary, which allows positioning of the active surface directly above the target cell. **D.** View of microirradiator tip in dissecting microscope. **E.** Close-up view through Deltavision microscope optics. Cell has been transfected with EYFP-53BP1 and H2B-diHcRed expression plasmids as described in Materials and Methods. Scale bar, 10 microns.

The microirradiator was mounted within the WeatherStation environmental chamber of an Applied Precision Deltavision microscope (Fig. 15A), using a precision micromanipulator with an acrylic electrode holder (Fig. 15B). The micromanipulator allows precise manual adjustment of the position along three orthogonal axes. A bend was introduced in the capillary such that the capillary tip is coaxial with the optical path

(Fig. 15C). A dissecting microscope view showing the flush tip is shown in Fig. 15D. The microirradiator was positioned so that the tip of the capillary was slightly above the target cell and was visible through the microscope optics (Fig. 15E). The plane of the active surface is parallel to the plane of the culture dish.

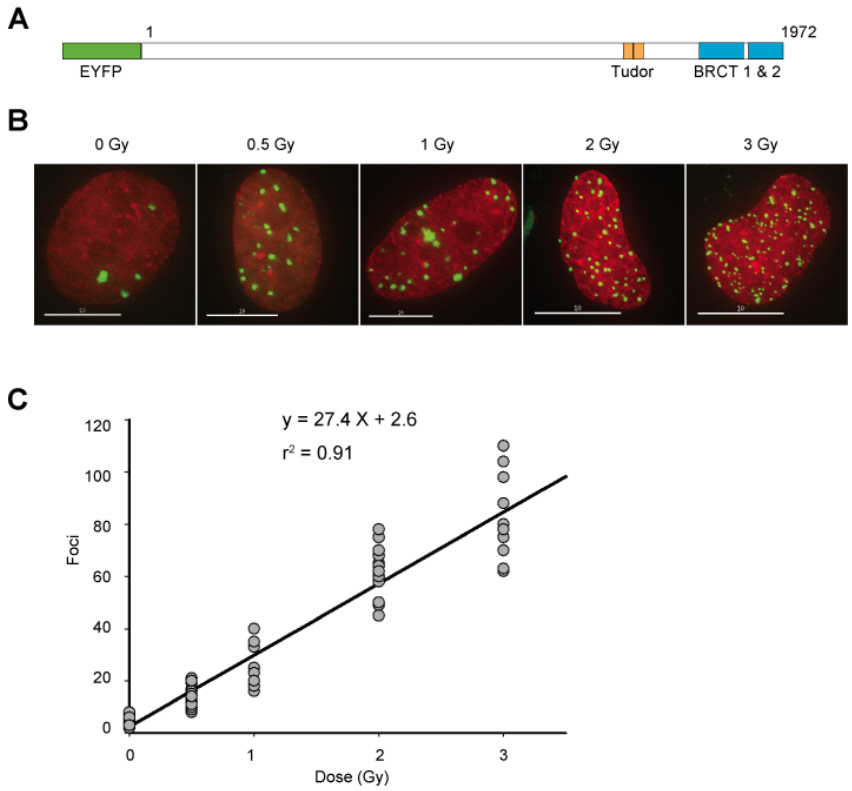

Figure 16. Calibration EYFP-53BP1 reporter system. **A.** EYFP-53BP1 primary structures. EYFP coding sequence is joined to full-length 53 BP1, with Tudor and BRCT domains indicated. EYFP1-53BP coding sequence was inserted into pcDNA-DEST40 (Invitrogen) for expression under control of the CMV promoter. **B.** Dose response to calibrated doses of ^{137}Cs reference radiation. Cells were co-transfected with EYFP-53BP1 WT and H2B-diHcRed. Live-cell images were collected 30 min post-irradiation. **C.** Quantification of dose response. Foci were scored using 8-24 individual nuclei at each dose point, and linear regression was performed to obtain the slope of the dose-response curve.

4.3.2 Calibration of biological reporter system

The EYFP-53BP1 expression construct was as described in Materials and Methods (Fig. 16A). and consists of an intrinsically fluorescent enhanced yellow fluorescent protein domain joined to full-length 53BP1. It is essentially identical to constructs used in previous live-cell imaging studies (for example, [49-51]). The U2OS 2-6-3 recipient cells [47] are derived from the U2OS osteosarcoma cell line, which has been widely used in prior studies of 53BP1 foci formation [50, 52].

To calibrate the number of foci per unit dose of radiation in this system, cells were exposed to 0 to 3 Gy of ^{137}Cs radiation and imaged 25-30 min post-exposure, at which time the response has reached a maximum. H2B-diHcRed [48] was co-expressed as a registration marker [53]. Live cell images were collected (Fig. 16E) and foci were scored manually using 8-24 nuclei for each dose point (Fig. 16F). Regression analysis indicated formation of 27.4 foci per nucleus per Gy. The slope of the 53BP1 dose response curves is 1.4-fold greater than reported in a prior live-cell imaging study [51]. This is consistent with the fact that the hypertriploid U2OS cells contain about 1.5-fold more DNA per nucleus than the quasi-diploid HT1080 cells in the prior study and thus present a larger target for radiation damage.

4.3.3 Real-time observation of microirradiator induced foci formation.

Results of several microirradiator experiments are shown in Fig. 17. Cells were electroporated with EYFP-53BP1 and H2B-diHcRed expression constructs. After 24-48 h, they were transferred to the stage of the Deltavision microscope, where they were maintained in growth medium in a humidified 5% CO_2 atmosphere at 37 ºC. The

microirradiator was positioned above a target cell, and image collection was initiated within 1 min (Fig 17A). Z-stack images were collected at 5 min intervals. The irradiator was withdrawn after the 16 min timepoint, and cells were allowed to recover for a further 46 min. Images were deconvoluted, projections were prepared, and foci were counted manually. Results for three individual cells are presented in Fig. 16. In all three instances, foci appear with no discernible lag and increase to a maximum about 35 minutes after the probe was withdrawn and 50 minutes after the start of the experiment. The absolute number of foci varied between experiments, perhaps reflecting slight differences in the position of the probe. In order to pool the data from the three experiments, we normalized the data to the percent of maximum response in each experiment. We calculated the mean and standard deviation to obtain the data in the rightmost panel of Fig. 17B. The result is a smooth curve showing an increase with approximately linear kinetics until a plateau is reached.

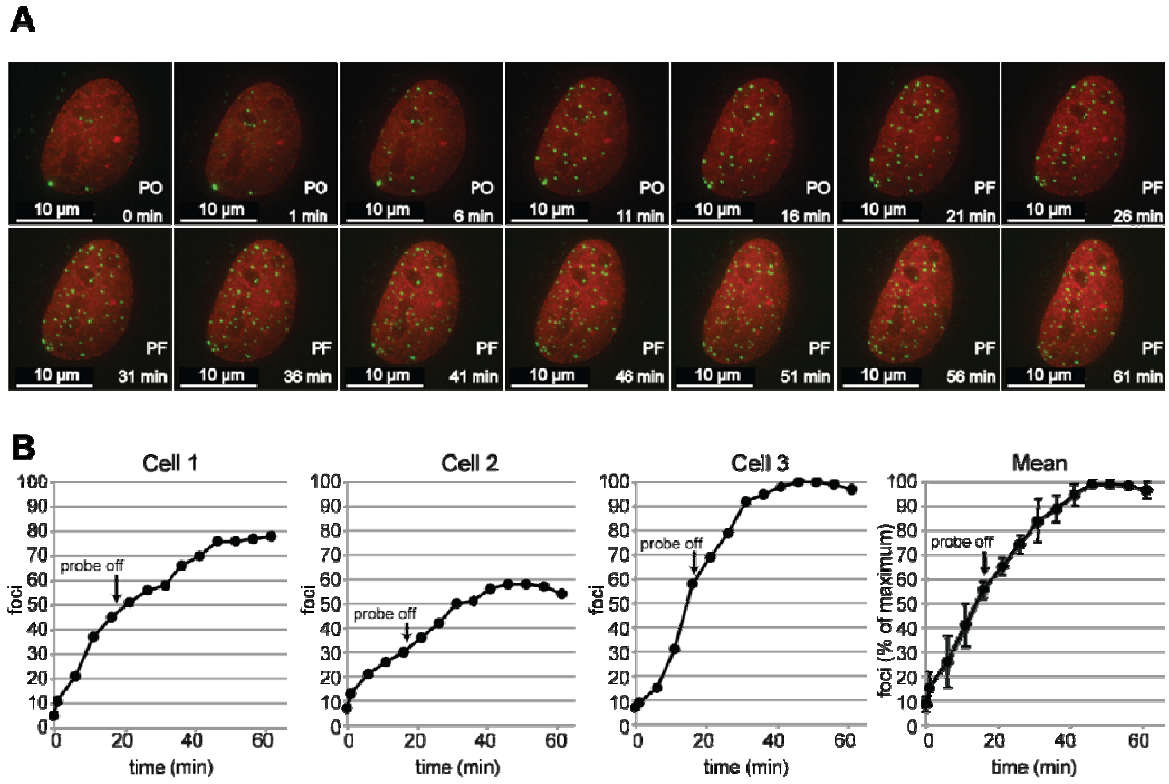

Figure 17. Real-time imaging of microirradiator-induced 53BP1 foci. A. Representative images of same cell collected at indicated time points. Microirradiator was introduced 1 min prior to the first time point and withdrawn after the 16 min. Z-stacks containing 15-24 individual images were collected at each time point and deconvoluted. Projections are shown. PO, probe on; PF, probe off. Quantification of microirradiator-induced foci from three independent experiments. Cell 1 corresponds to images in Panel A. Rightmost panel shows pooled data from the three experiments. Data were normalized to maximum response=100%, averaged, and plotted. Error bars denote standard deviation.

To estimate the radiation dose based on foci numbers to radiation dose, we compared the maximum number of foci attained in each experiment in Fig. 17 to the calibration curves in Fig. 16. No adjustment is required for the different radiation types (γ rays versus β particles) as both are sparsely ionizing, low linear energy transfer (LET), radiation and may be considered as radiobiologically equivalent. The total dose delivered

by the microirradiator in a 16 min exposure was 2.8 Gy, 2.0 Gy, and 3.6 Gy for cells 1, 2, and 3 respectively, with the variability presumably attributable to differences in the positioning of the probes. These doses equate to dose rates range of 0.12 to 0.22 Gy/min. This is about an order of magnitude less than predicted by modeling a source with this activity and geometry (see Appendix), and the reason for the difference is still to be determined.

Although an effort was made to minimize the light exposure during imaging, we were aware of the possibility that phototoxicity might itself result in repair foci formation. We therefore performed a mock irradiation under the same conditions, but without the microirradiator. No time-dependent accumulation of foci was seen above the background present at the beginning of the experiment (Figure 18)

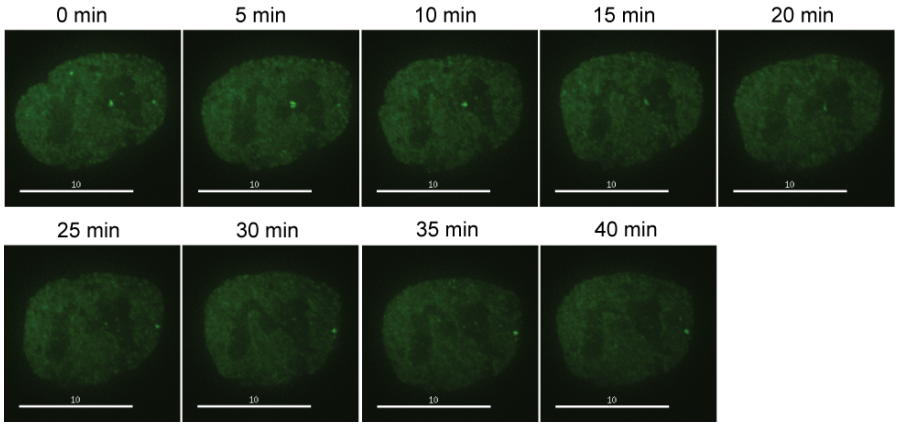

Figure 18. Real time observation of foci in absence of microirradiator

4.3.4 Dynamic behavior of individual foci

The time course in Fig. 17B shows that the time between initial traversal of a radiation track and appearance of foci is variable, as some foci appeared immediately after the onset of irradiation, whereas others did not appear until 30 min after microirradiator was removed. It also follows from inspection of the shape of the curve that the time required for resolution of foci must also be variable. If the foci appeared at variable times post exposure, but all were long-lived (i.e., persistent throughout the experiment), then a plot of foci versus time should be strongly sigmoidal. This was not the case. Instead, the system rapidly approached a steady state, showing a quasilinear response over the first 50 min. To account for this steady state, some of the foci that appear rapidly must also disappear rapidly.

To test this prediction, we tracked the behavior of individual foci over time. Fig. 18A shows the same nuclei as in Fig. 17A, but with expansion of a region of interest. Eighteen foci ("spots") were matched manually across the time series and intensities were quantified as described in Materials and Methods. Fig. 19B shows plots of spot volumes as a function of time. Several patterns are seen in these data. Foci 7, 9, and 11 appear and disappear rapidly, losing at least half their peak intensity within 10 min. Foci 1, 2, 5, 10, 12, and 15 decay with intermediate kinetics, losing half their peak intensity within 15-30 min. Foci 3, 6, 14, 16, 17, and 18 were stable for the duration of the experiment. Foci 4, 8, and 13 showed somewhat irregular behavior. Clearly, it will be of interest to collect longer and finer-grained time series, to analyze larger numbers of foci, and to perform a more computationally intensive analysis using the original three-dimensional imaging data, rather than the two-dimensional projections that were analyzed here. Even this

limited analysis, however, suggests that foci fall into several classes, with some appearing and disappearing rapidly, and others that are stable over the period of observation.

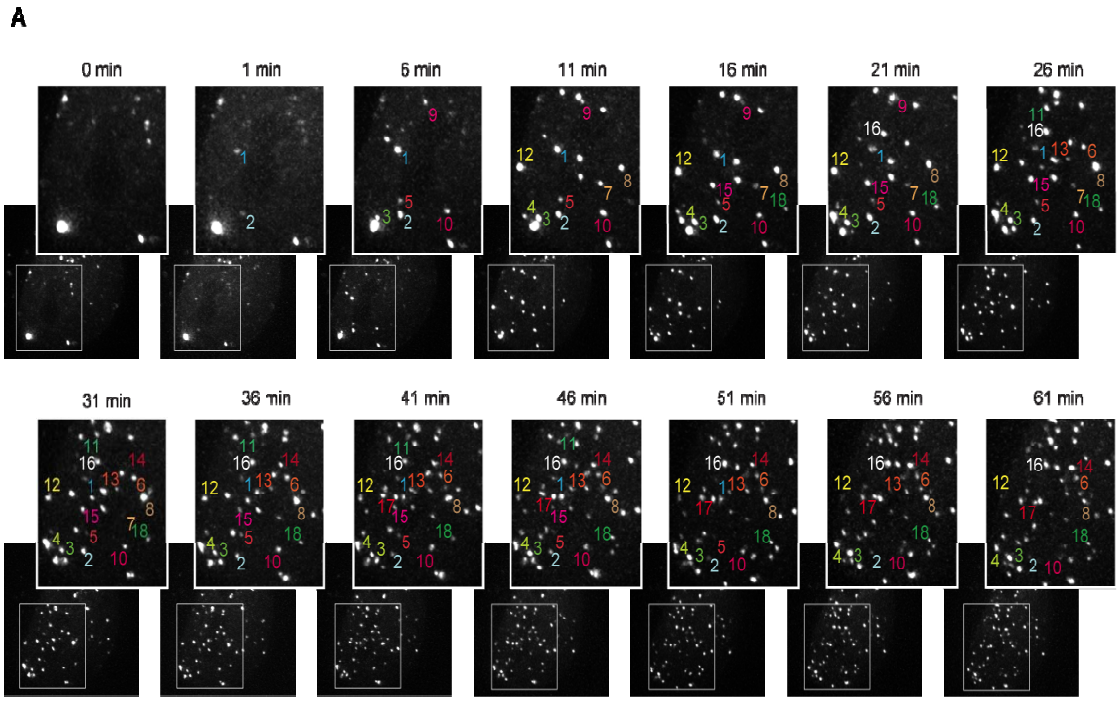

Figure 19A. Tracking of individual 53BP1 foci. Images are from nuclei from Cell 1 in Fig. 16. Inset panels show enlargement of region of interest marked by white rectangle. Eighteen individual foci were identified manually and are marked.

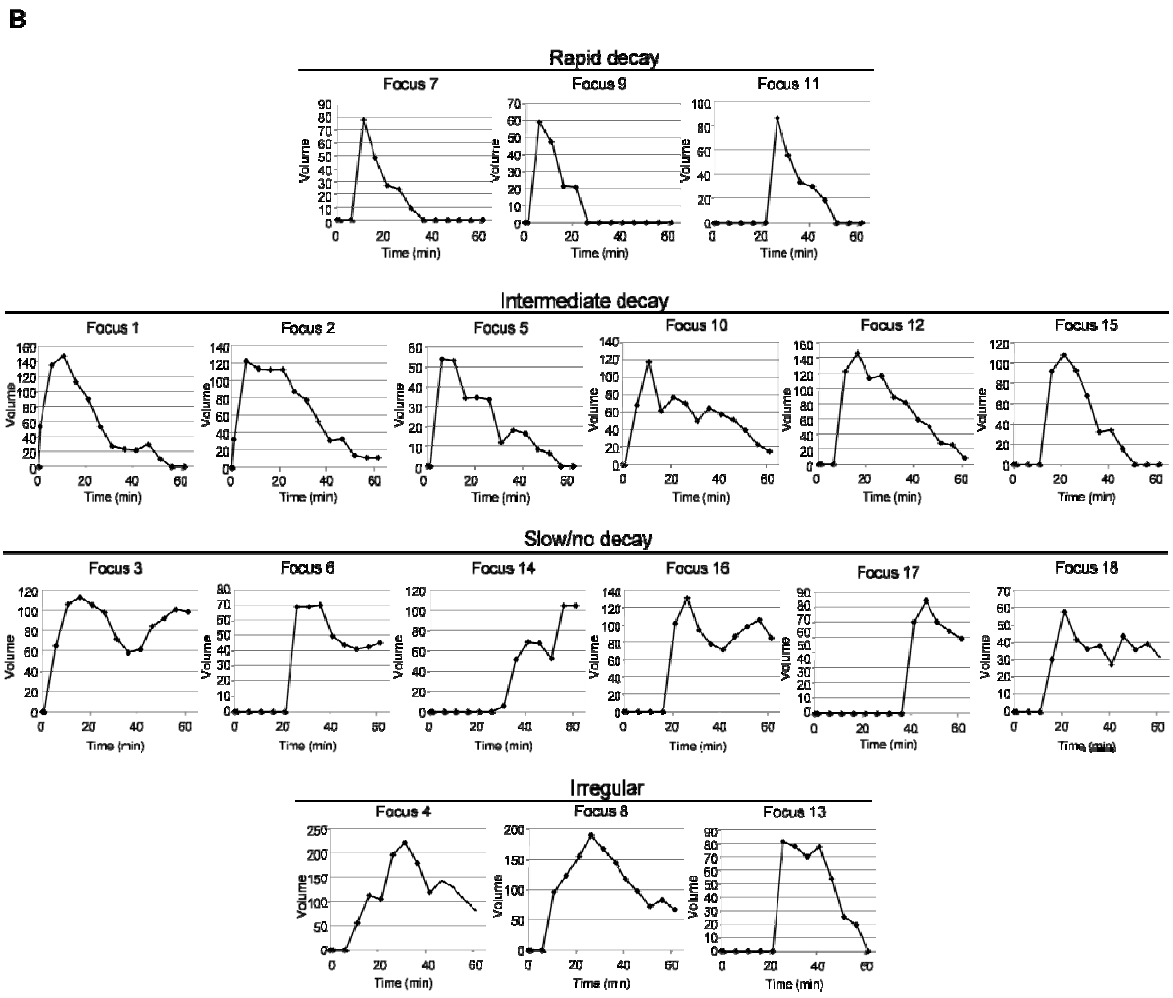

Fig 19B. Quantification of image intensity for individual foci. Image projections were loaded in DeCyder v6.5 (GE Healthcare, Buckinghamshire UK) and automated spot detection was performed. Volumes corresponding to each spot were quantified. Plots show image intensity for individual foci as a function of time. The same arbitrary units are used in all panels. Time is indicated in min

4.4 Discussion

We describe here the first biological application of a novel microirradiator that is designed specifically for compatibility with a standard cell biology laboratory environment. The device is characterized by small physical dimensions, intense radiation flux, and minimal radiological hazards. We demonstrate the use of the device in

experiments to track and characterize the induction of repair foci in irradiated cells. The microirradiator is a potential replacement for a self-contained $^{137}CsCl_2$ irradiator in certain cell and molecular biology research applications, particularly where biological response is measured at the single cell level. The device is made from inexpensive, commercially available materials, and the low total activity mitigates the public health and security concerns that have been raised for high-activity $^{37}CsCl_2$ radiation sources [42].

Because the microirradiator can be mounted directly to a microscope stage, it provides a capability for real-time observation of the early stages of the radiation response. This early response has not been well studied, particularly for sparsely radiation such as gamma rays and x-rays. Preliminary analysis has revealed heterogeneous behavior of repair foci. In particular, there is a class of rapidly resolved foci that would not be apparent in experiments using conventional irradiation methods. The existence of a rapidly resolved subset of foci is significant because it may account for a small, but unexplained, discrepancy between the best estimate of the number of double strand breaks determined by physical methods (approximately 30 DSBs per Gy per diploid genome) [54, 55] and the number of breaks estimated by careful counting 53BP1 foci (approximately 19 DSBs per Gy per diploid genome) [51]. Several explanations for the heterogeneous behavior of repair foci may be contemplated, including heterogeneity in the structure of the radiation-induced DNA breaks and the existence of competing repair or signaling pathways. Potentially, these explanations could be investigated by selective knockdown of individual DNA processing and repair enzymes in the target cells.

We predicted a dose rate for the microirradiator based on modeling as described in [44] [2]. We assumed hemispherical geometry, a 1 μm PEDOT coating and a 10 μm

working distance from the target cell (details in Appendix) to obtain a predicted dose rate of 2.65 Gy/min. Further experimental characterization of the microirradiator beta particle flux and emission spectrum by solid-state scintillation counting is in progress, which will establish the accuracy of the modeling (J.S. and J.J., unpublished). Although the observed dose rate (0.12 to 0.22 Gy/min) falls short of what can theoretically be achieved, it is clearly sufficient for experiments to investigate the biology of the low-dose radiation response.

Particle microbeams provide another means to introduce a targeted radiation dose to samples directly on a microscope stage. More than fifty years ago, Zirkle and Bloom [56] described the use of a Van de Graaf generator and microaperture to deliver an intense proton beam to a 2.5 μm diameter spot within living cells. It is now estimated that there are 30 operational microbeam facilities worldwide [57]. Microbeam facilities have been developed that are capable of delivering precisely targeted heavy particles, electrons, or ultrasoft X-ray photons, with varying degrees of real-time imaging capability (see for example, [58-62]). We view the microirradiator technology as a useful complement to the microbeams. As currently configured, the microirradiator lacks the capabilities for precision targeting and particle counting that are found at the most advanced microbeam facilities. The portability of the microirradiator and its potentially low cost of manufacture provide offsetting advantages, however, for many applications.

In principle, it should be possible to adapt the same electroplating technology to construct analogous microirradiators using other radioisotopes. For example, ^{252}Cf could be used as a source of fission neutrons or ^{241}Am as a source of alpha particles. Both of these isotopes are used industrially and are potentially available for construction of

research microirradiators. The cellular and molecular response to high LET radiation, such as neutrons and alpha particles, has not been as extensively studied as low LET radiation, in part because convenient sources are not available outside the radiation community. Concentrated deposition of isotope on a very small surface in the microirradiator allows experiments to be performed using very small total amount of isotope, mitigating health and safety concerns that pose barriers to access to nuclear materials.

4.5 Previous Experiments

Before the success with the Ni-63 microirradiation system as discussed throughout Chapter 4, there were experiments done that did not work, but led us down the path to achieving results. Originally, we had used a recessed disk microirradiators, as dicussed in Chapters 1 and 2. This microirradiator had an activity of 1 Bq, with an activity flux of 2×10^5 Bq/cm^2.Originally, we had used the configuration of a straight microirradiator, shown below. This irradiator is pointed at a 45 degree angle to the surface of the cells, and experiments commenced using this setup.

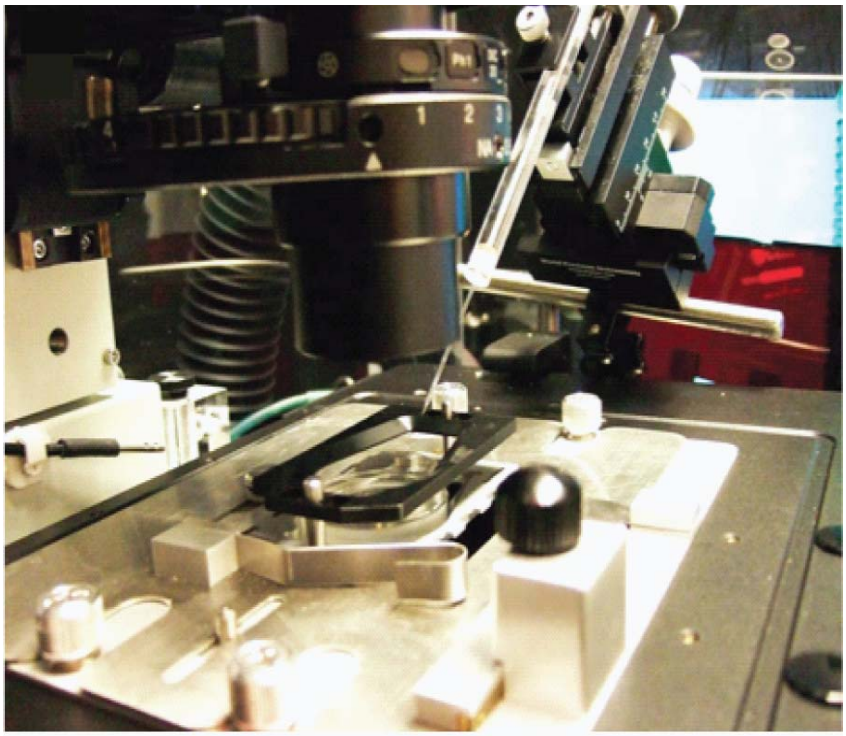

Figure 20. Experimental setup with straight recessed microirradiator.

One of the first experiments completed was with the 1 Bq probe with osteosarcoma cells. As shown in the figure, originally approximately 4 foci were present before the irradiator was places above the cells. Once this was accomplished, the number of foci steadily increased in time until the irradiator was taken off the cell. In comparison to the control, no other extraneous foci are caused by the light of the microscope or other environmental conditions.

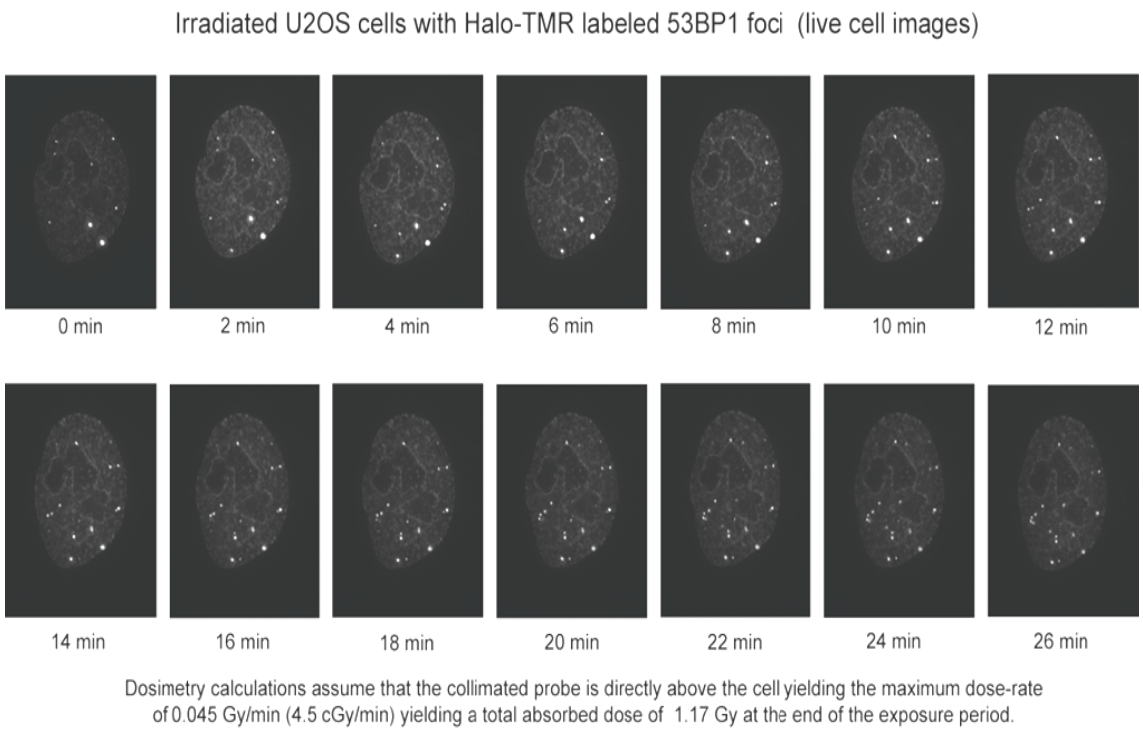

Figure 21. Optical Micrographs of the nucleus of one osteosarcoma cell in time undergoing irradiation.

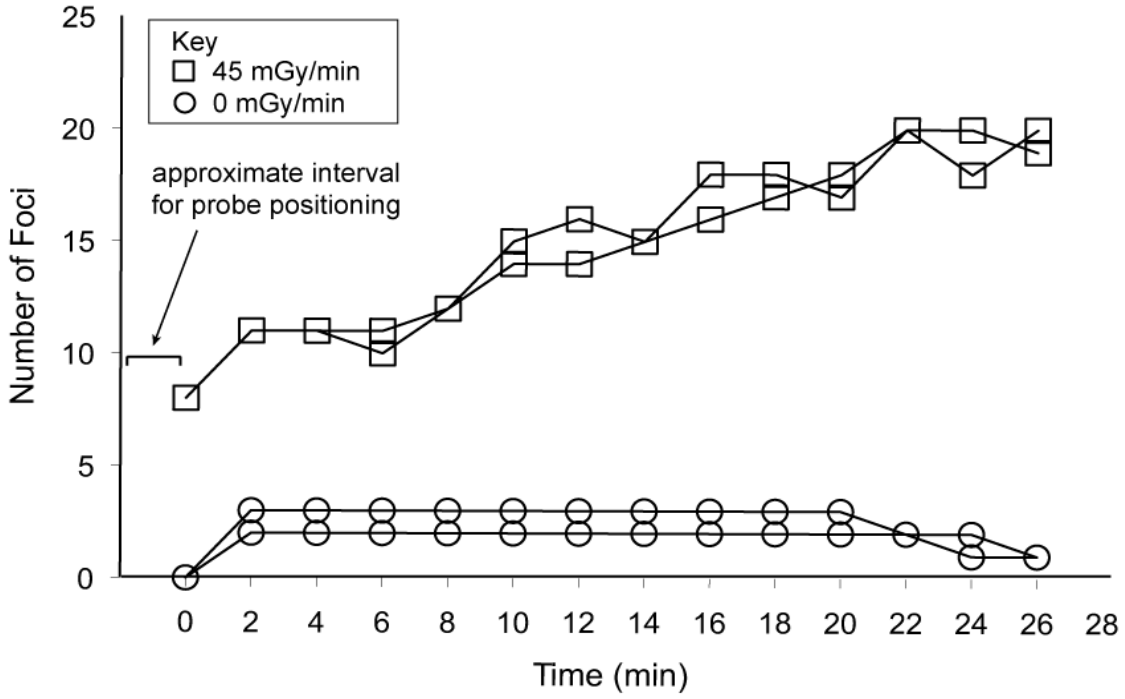

Figure 22. Graph in time of foci observed from 2 Bq irradiator vs. control.

These experiments were repeated twice, for the irradiator and the control, respectively. However, after this experiment the results could not be repeated again with the same and different recessed disk microirradiators. An additional experiment was conducted to ensure that Ni-63 was indeed causing dsDNA damage, and is shown below. A 10 uCi Ni-63 source was used on an osteosarcoma cell and observed for foci formation. In the timeframe shown in the picture, it is clear that the foci generated were indeed caused by the Ni-63 source. The channel is approximately 30 um in length from the tip of the Ni-63 deposit to the end of the irradiator. The energy of the beta particle of Ni-63 is approximately 5 cm in air, and 60 um in water. Because of the channel, it could be possibly filling with cellular medium, blocking the radiation received to the cell. Additionally, these experiments are manually done by inserting the irradiator into the

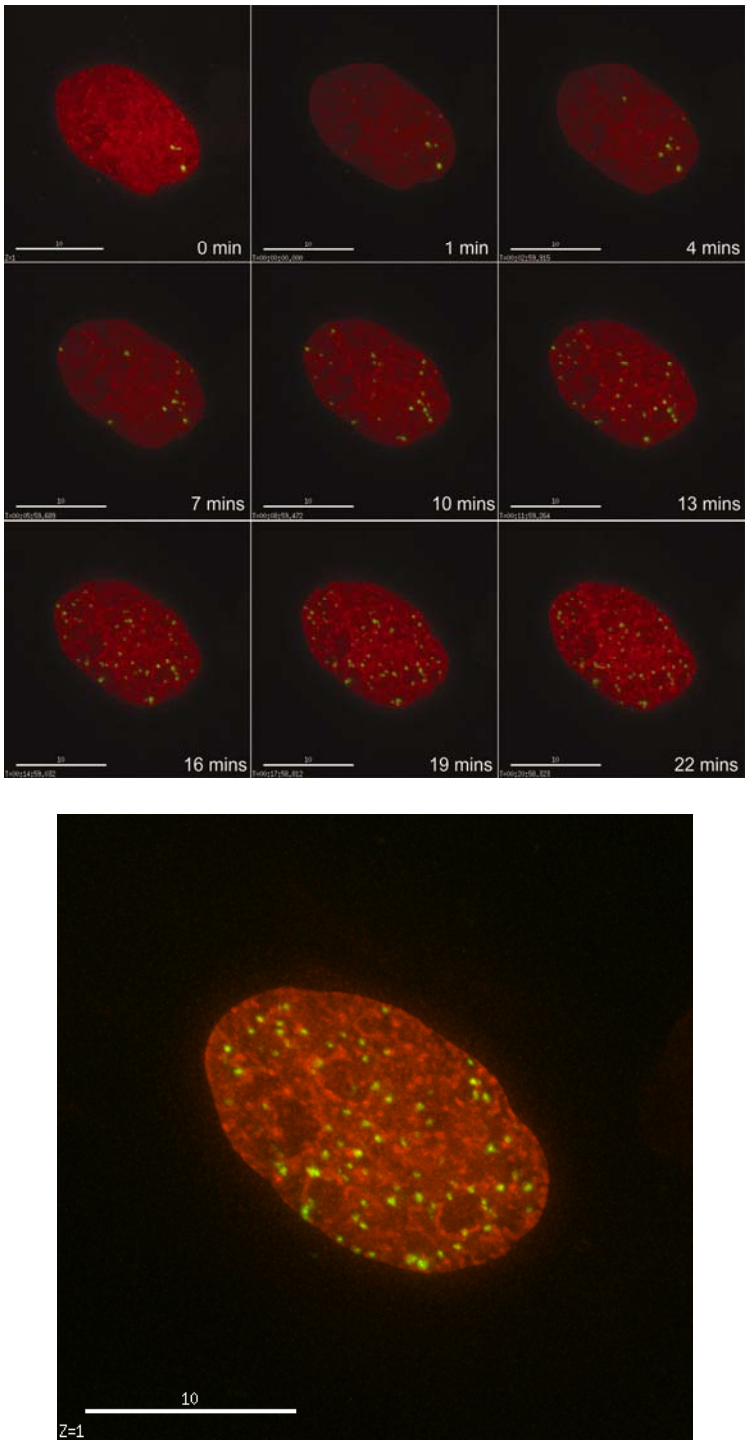

Figure 23. Time lapsed image of osteosarcoma nucleus undergoing irradiaton by 10 uCi Ni-63 source

cellular medium by a micromanipulator, and observing the tip of the microirradiator within the line of sight of the cell under a microscope. This leads to a tremendous amount of error in the positioning of the probe, and could be another source of why these experiments could not be repeated. Because of these concerns, a few design changes including removing the recessed disk from the microirradiator was achieved that saw multiple repetitions of data completed.

CHAPTER 5

PORTABLE SOLID STATE SCINTILLATION CALIBRATOR

5.1 Introduction

The previous chapters of this thesis discussed novel radiation devices involving electrodeposited beta-emitting Ni-63 (67 keV) used in several research projects [1, 5]. Two of the critical devices that have been made are a microirradiator, which is a modified microelectrode deposited with Ni-63, and an ambient ionization device, involving Ni-63 custom electrodeposited onto a copper device.

The main objective of these microirradiators areto bring low activity levels (1-1000 Bq) of radiation into a laboratory but providing a high flux (10^6 Bq/cm^2) to the irradiated sample.[1 5, 63] However, accurate activity measurements are required for determination of activity, flux, and dose rates for these microirradiators as needed for the application. Typically, Ni-63 is only measured through a Liquid Scintillation Counter (LSC). LSC are very useful and accurate for compounds with low energy particles such as Ni-63 [2]. Because they are expensive, often multiple users use the instrument. For more measurements of Ni-63 activity in a dry environment, in laboratory a new type of benchtop instrument was developed. Solid state scintillation runs on the same principle, but the solvent is a plastic instead of a liquid. A fluorescent compound, most commonly anthracene, is mixed into the plastic scintillator and the light emitted is detected by a photomultiplier tube.[27] The advantages of a solid state scintillator, especially in the case of custom Ni-63 sources, are that the liquid scintillation cocktail does not come into contact with the electrodeposited Ni-63. This ensures that residues are not present on the irradiator which can be detected through mass spectrometry.

A novel solid state bench-top instrument, consisting of a photomultiplier tube (PMT), plastic scintillation crystal, a high voltage power supply, and a computer were all used for calibration of Ni-63 microirradiator activity.

5.2 Experimental

5.2.1 Safety Considerations

Working with radioactive materials requires proper adherence to safety guidelines set by the user's workplace.

5.2.2 Chemicals

The liquid scintillation cocktail (LS-275) was purchased from National Diagnostics, Inc. A standard luria broth (Tryptone 10 g/L, yeast extract 5 g/L, NaCl 10 g/L) was used in all cell culture medium experiments.

5.2.3 Calibrator Set-up.

The calibrator composes of a power supply, a photomultiplier tube (PMT) with attached plastic scintillation, and data acquisition equipment (Fig 24a). A specialized photomultiplier tube (PMT) for plastic scintillation measurements, model H6410, was purchased from Hamamatsu Corporation. A Fluke 415B high voltage power supply was used in conjunction with the photomultiplier tube. A 2 in. diameter, 1 in. height plastic scintillation crystal, EJ-212, was custom made to cover the entire window of the PMT (Fig 24b). A 1 mm diameter, 20mm length hole was hand drilled into the center of the crystal to allow for an almost 4pi detection of the beta particles from the microirradiators. To prevent loss of light collection from the differing indices of refraction from the glass of the PMT and scintillation crystal, silicone grease was applied generously to the outer

glass before attachment of the crystal. An aluminum lined cup (not shown) was fitted over the scintillation crystal for additional reflection and enhancement of light collection. Data acquisition devices and software will be discussed in more detail below. The photomultiplier tube was housed in a custom built light-tight box, with black felt lining the entire interior (Fig. 24b). This enables the calibrator to be operated in room light without skewing data from inadvertent light pollution.

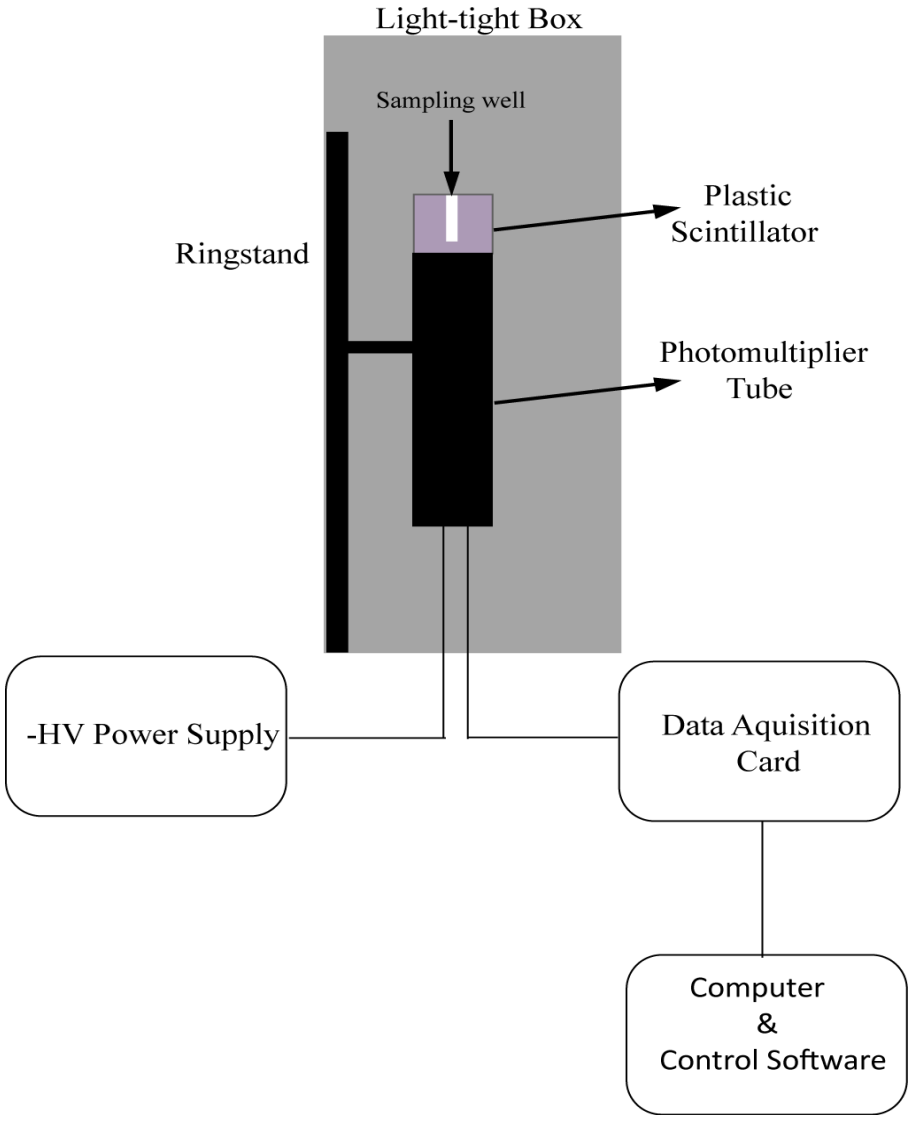

Figure 24 a. Schematic of calibrator, including external electronics.

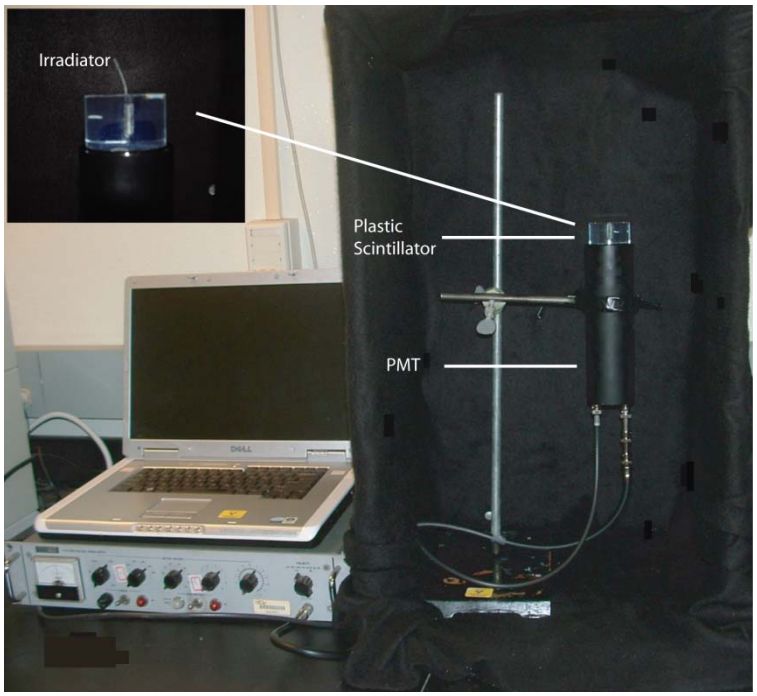

Figure 24 b. Picture of calibrator set-up.

5.2.4 Microirradiators

Five microirradiators of varying activity and one copper wire based Ni-63 source were used during experimentation. Methods of fabrication and electrochemical deposition of Ni-63 onto these devices can be found elsewhere [1]. For standardization, liquid scintillation measurements within the Office of Radiation Safety on the Georgia Institute of Technology campus were used to determine activity levels of each radioactive source prior to experimentation with the calibrator. For the five individual microirradiators labeled 1-5, activity levels of 27, 85, 134, 59 and 58 Bq were measured, respectively. For the Ni-63 plated source onto copper wire, an activity of 3766 Bq was measured

5.2.5 Data Acquisition and Processing.

The voltage output from the PMT is amplified and digitized using a National Instruments USB-4431 dynamic signal acquisition module. The signal is DC-coupled in pseudodifferential mode and sampled at a rate of 100kS/s and a vertical resolution of 24-bit. The chassis of the USB-4431 is grounded to suppress electromagnetic interference. LabVIEW 8.5 software was written to obtain and process data from the USB-4431. For each measurement time, Δt, 100kS/s$\times\Delta t$ data points are collected and the peaks are identified by fitting a quadratic polynomial to every three data points. Only peaks with heights greater than the threshold value are kept. The number of peaks is then divided by Δt to give the photon count per second. Additionally, a histogram is created of the peak heights. Operation of the calibrator remained at -1900 V for optimal gain(1×10^{-7}) for all trials.

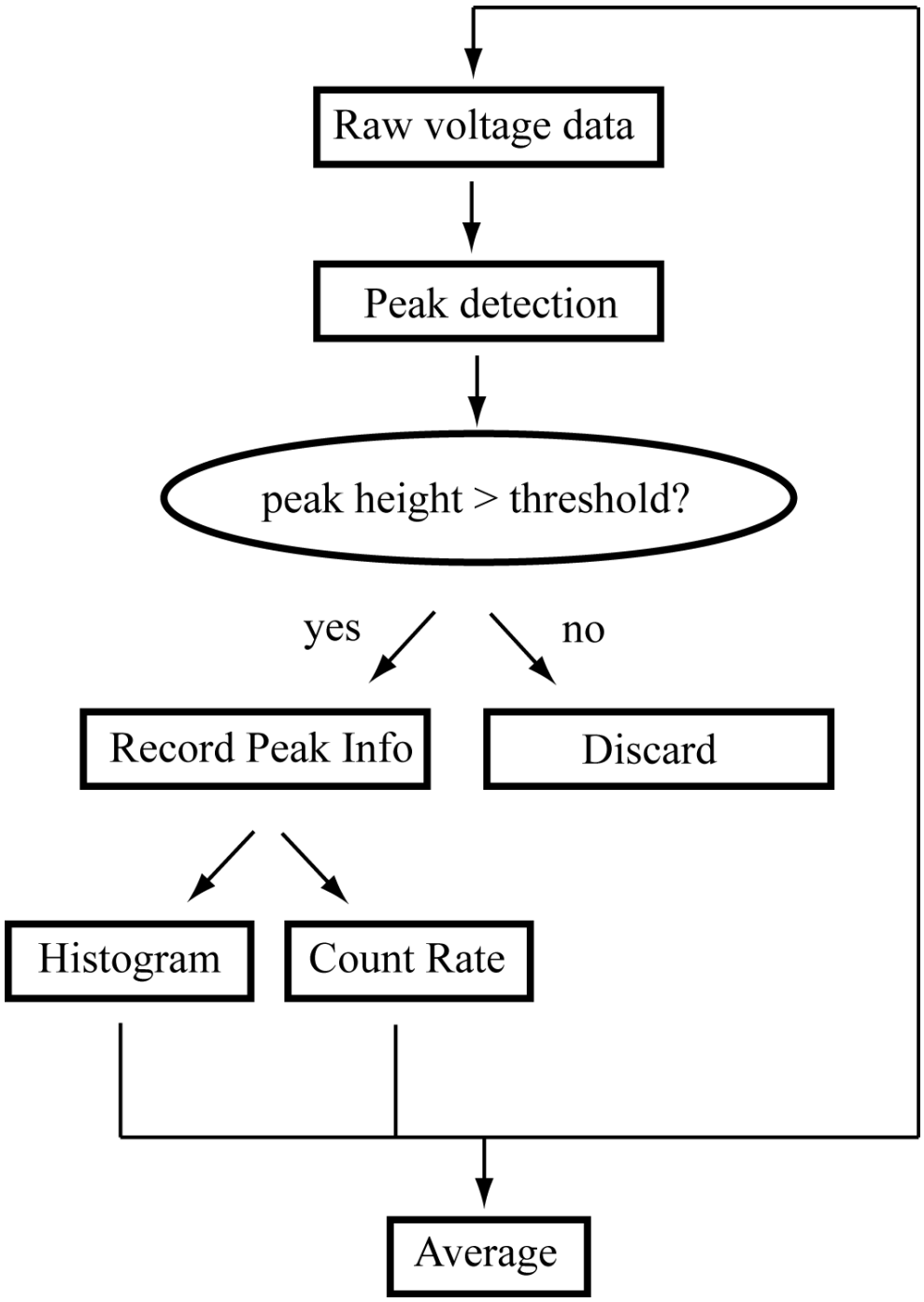

Figure 25. Data acquisition from photomultiplier to computer

5.3 Results

5.3.1 Timed Calibrations

To assess the accuracy and proper calibration of the setup, multiple trials were conducted at differing irradiation time lengths to determine accuracy and validity of counting statistics. Before each microirradiator was placed into the instrument, a background measurement of equal time length was recorded for each trial to ensure values were not skewed by fluctuating background values. Two different times of measurement, approximately 100 and 600 seconds of background and direct measurement were taken for each of the sources (200 and 1200) total. An example of the raw data produced from the background and irradiation measurements from a 134 Bq irradiator and 3766 Bq source are shown in Figure 25 and 26, respectively.

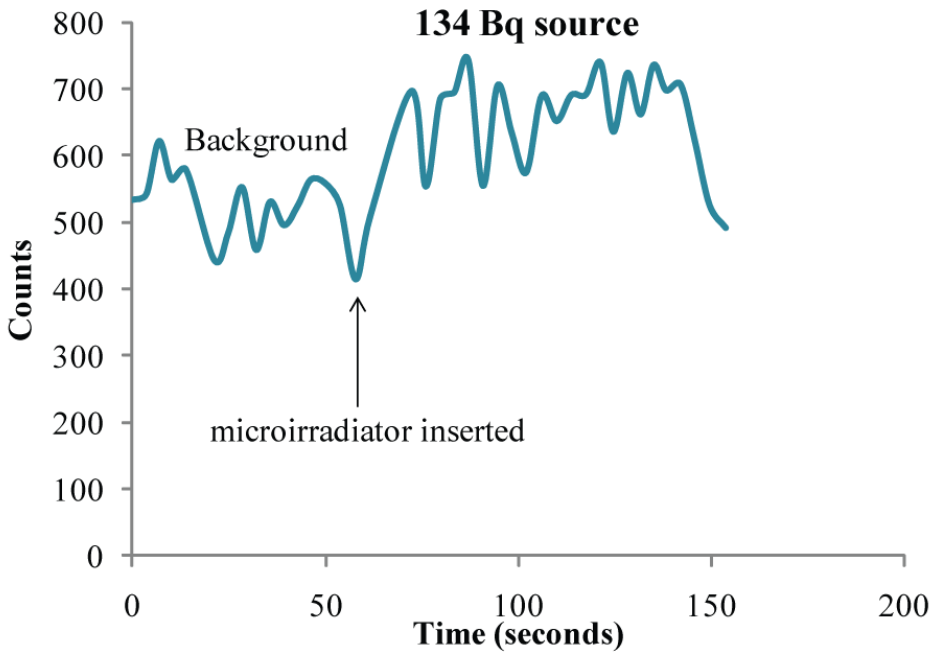

Figure 26. Graph of counts versus time of one individual trial of microirradiator 1 within the calibrator. The activity measurement of 134 Bq was determined by liquid scintillation. Measurement of background is taken before the measurement of the irradiator. Arrows indicate point of time in which the background and microirradiator have been inserted

into the calibrator. Activity determined by the calibrator is calculated by subtraction of the background from the microirradiator reading.

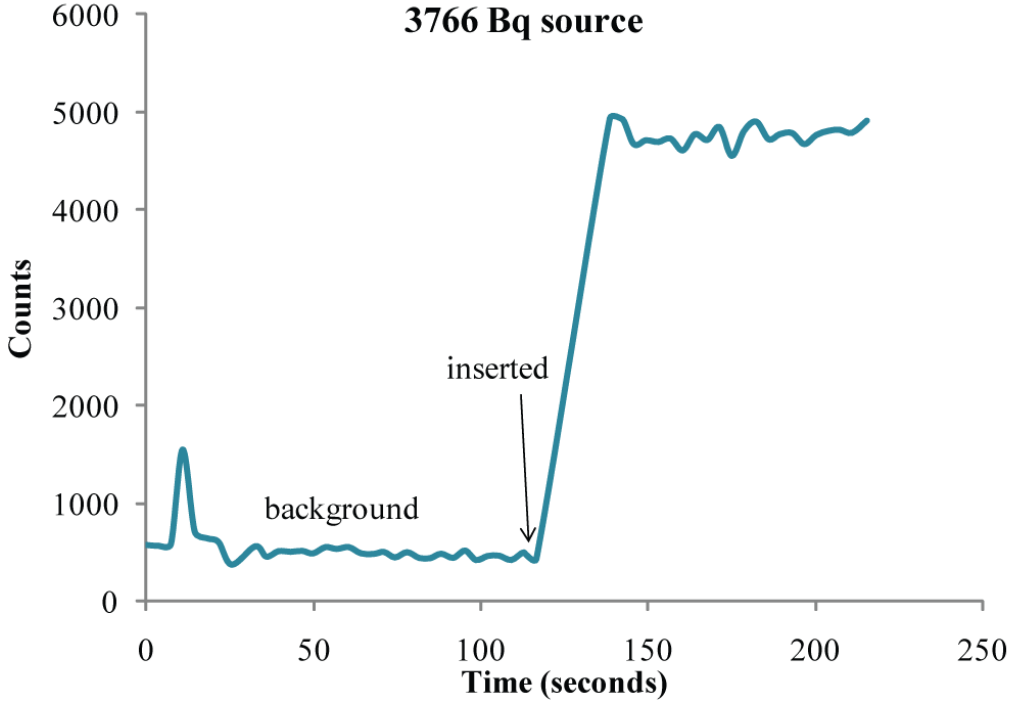

Figure 27. Graph of counts versus time of one individual trial of a Ni-63 electroplated wire source (2 cm length, 1 mm diameter Cu wire with microns thick Ni-63 deposit). Procedures to determine the activity of the wire from the calibrator are followed as explained in figure 2a.

In Fig. 26, the background is visibly fluctuating, with an abrupt rise in count rate occurring immediately after insertion of the microirradiator into the calibrator. These fluctuations are expected due to multiple factors, such as cosmic radiation, natural random fluctuations of the source, and external electrical noise. In Fig. 27, with larger source, larger count rates are visible as expected from the point of insertion of the source, due to the larger amounts of radioactivity present. To determine total levels of activity, count rates are averaged for both the background and source. With the background subtracted from the irradiated value, an activity measurement is reached for that trial.

Table 2: Averaged measured activity values in Bq for the short (100 seconds) and long (600 second) trials, degrees of freedom, chi squared values (X^2), and probability values for microirradiators 1-5, and the Ni-63 plated source.

Micro-irradiator	Ave. (95% CL)	X^2	Degree Freedom (N-1)	Prob (P)	Ave. long trial (95% CL)	X^2	Degree Freedom (N-1)	Prob. (P)
1 (26.67 Bq)	20.43 +/- 9.59	7.04	6	0.69	18.40 +/- 10.88	6.69	4	0.85
2 (85 Bq)	36.29 +/- 9.10	3.58	6	0.27	45.67 +/- 12.80	6.13 1387	5	0.71
3 (134 Bq)	63.29 +/- 17.92	7.97	6	0.76	71.83 +/- 34.00	8.61 7169	5	0.88
4 (59 Bq)	33.6 +/- 13.04	5.27	4	0.75	42.50 +/- 14.81	10.2 5	4	0.96
5 (58 Bq)	43	3.98	5	0.45	46.60 +/- 17.28	6.67	5	0.75
Plated source (3766 Bq)	3821 127.88	4.46	6	0.65	3731 +/- 175.1 7	10	5	0.93

Table 3: Averaged measured activity values in Bq for the liquid scintillation in the recess and cell culture medium trials, degrees of freedom, chi squared values (X^2), and probability values for microirradiators 1-5.

Micro-irradiator	Ave. (95% CL) scintillation	X^2	Degre Freedom (N-1)	Prob (P)	Ave. cell cult. (95% CL)	X^2	Degree Freedom (N-1)	Prob. P
1 (26.67 Bq)	19 +/- 10.26552	7.37	5	0.81	8.8 +/- 8.0	7.59	4	0.89
2 (85 Bq)	88.8 +/- 33.5289	13.46	5	0.98	52.4 +/- 17.4	6.16	4	0.81
3 (134 Bq)	131.6667 +/- 47.38792	22.67	5	0.99	17.4 +/- 8.38	4.20	4	0.62
4 (59 Bq)	81.4 +/- 11.40	3.09	4	0.46	33.4 +/- 20.30	12.85	4	0.99
5 (58 Bq)	51.3 +/- 16.96	4.39	5	0.51	36.30 +/- 23.00	19.65	5	0.99

Since radioactive decay events are a binomial distribution of randomized events, length of time is critical in making an accurate determination of the true mean of the amount of activity. The longer the record of measurement, the closer the experimental value ($\overline{x_e}$) approaches the true mean $\bar{x}$ [27]. Because of this, it is imperative to determine if the bench-top calibrator can provide accurate measurements within short and long time periods in comparison to liquid scintillation. To demonstrate, multiple trials of all sources

mentioned above at both 100 (short) and 600 (long) seconds were conducted. After each trial's activity was recorded, a total average was taken for each source to determine the experimental mean. As shown in table 2a and b, the experimental mean $\overline{x_e}$ within 95% confidence (+/- 1.96σ) for microirradiators 1 through 5 for the short measurements are 20.43 +/- 9.59, 36.29 +/- 9.10, 63.29 +/- 17.92, 33.60 +/- 13.04, and 43.0 +/- 3.98 Bq, respectively. For the plated Ni-63 source, its value was determined to be 3821 +/- 127.88 Bq. For the 600 second intervals, the experimental mean $\overline{x_e}$ within 95% confidence for microirradiators 1 through 5 are 18.40 +/-10.88, 45.67 +/- 12.80, 71.83 +/- 34.00, 42.50 +/-14.81, and 46.60 +/- 17.28 Bq, respectively. The plated source measured 3731+/- 175.17 Bq (Table 2). When evaluating a radiation detection instrument, counting statistics are crucial in determination if the system is working correctly. One of the prime statistical measurements in evaluating the instrument is the chi square test, defined as

$$X^2 = \frac{(N-1)s^2}{\overline{x_e}} \quad (13)$$

Where N is the sample size, s is the sample variance, and $\overline{x_e}$ is the experimental mean. Since the sample variance should not differ greatly from the experimental mean, $s^2 / \overline{x_e}$ is a direct measurement of the sample variance deviating from the predicted variance. The amount to which X^2 deviates from (N-1) is a measurement of the departure from the predicted Poisson distributions [27]. To determine the probability that each random sample would fit into a true Poisson distribution, the equation is defined as

$$\mathrm{P} = \frac{\bar{x}^x e^{-x}}{x!} \quad (14)$$

where $\bar{x}$ is defined as the true mean and x the trial size. If following the Poisson distribution, $s^2 \approx \sigma^2$ and the assumption that $\bar{x} = \overline{x_e}$, values of p that are not too high

(>.98) or low (<.02) are acceptable. Values of .98 and higher represent abnormally low fluctuations, where values of .02 and lower represent abnormally large fluctuations. Taking into consideration the degrees of freedom (N-1) for each trial, all chi squared and subsequent probability values fell into acceptable ranges for this detection device for both the short and long measurements. It is interesting to note that statistically the probability values for the longer measurements are moderately higher on a whole than the shorter measurements, indicating a smaller amount of fluctuations between measurements.

Statistics aside, the calibrator consistently measured lower values than presented by the liquid scintillation detector. However, the plated Ni-63 source was well within 100 Bq of its LSC value. This result was anticipated due to the shape of the Ni-63 source within each microirradiator. The recessed disk microirradiator before electrodeposition of Ni-63 has a recessed channel of approximately 30 microns. With deposition of Ni-63 onto the electrode surface, the channel still has a depth from 20-29 microns. This channel effectively shields the radioactive source to about 70% of the total activity deposited [1]. Within a liquid scintillation counter, it is plausible that cocktail can seep into this channel, skewing the shielding effects by allowing passage of each interacting photon through the glass of the microirradiator, whereas with plastic scintillation this would not be the case. However, the plated Ni-63 source was well within 100 Bq of its LSC value. Therefore, we speculate the lower results possibly due to the channel interference with liquid scintillation cocktails.

5.3.2 Liquid Scintillation

To prove that the lower results are due to channel interference with liquid scintillation cocktail, an experiment was conducted involving each microirradiator containing liquid scintillation cocktail within the recess and measured with the calibrator accordingly. Although the cocktail does react with the plastic scintillation material, the scintillation cocktail was carefully pumped into the recess under vacuum and all excess amounts were removed prior to measurements. Results indicated in green show that the cocktail significantly increased the activity measured by the calibrator (Fig. 28) and show an approximate 1:1 ratio with the pre-determined LSC values (Fig. 29). This result is significant because of the decrease in activity seen with the calibrator in general and the shielding effects of each microirradiator discussed in Timed Calibrations, showing that the recessed disk does indeed shield the beta radiation within the microirradiator significantly.

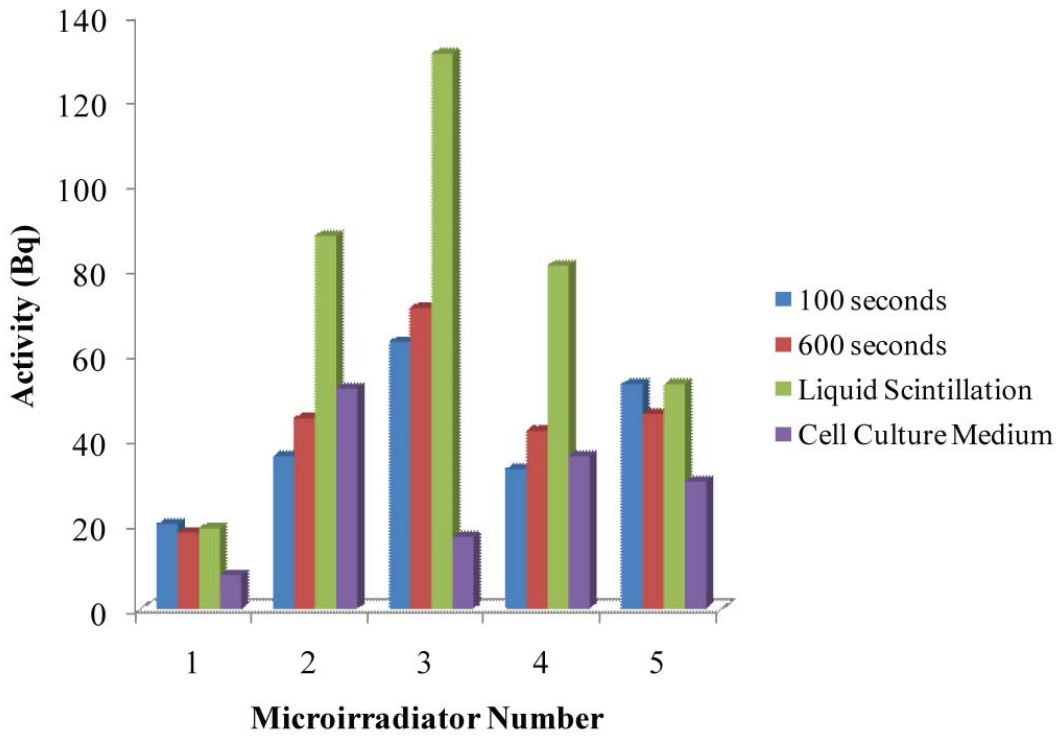

Figure 28. Comparison of short, long, liquid scintillation and cell culture medium measurements for the solid state scintillation calibrator. Graph corresponding to activities (x axis) versus microirradiators 1-5 (y axis). The colored bars are indicative of short (100 seconds, blue), long (600 seconds, red), liquid scintillation within recess (green) and cell culture medium experiments (purple).

5.3.3 Cell culture medium.

Since microirradiators are predominately used in in radiobiology, these devices are used as irradiation devices while in contact will cellular medium. Live cells are typically irradiated within 10-20 um with each microirradiator, with the fluid filling the gap between the cell and the radioactive Ni-63. It was important to ascertain whether or not cell culture medium would block the amount of radiation events penetrating to the cell, or whether this fluid would have no effect. To test this, approximately 1 mL was used to fill the entire channel of the hand-drilled scintillation crystal, and a

microirradiator pre-sonicated in said solution was measured following the procedures defined above. As indicated in Figure 27, microirradiators 1 and 3 were significantly lower than the other activity measurements, which microirradiators 2,4 and 5 were either slightly or approximately the same activity values as determined with the calibrator (Table 2, Fig. 27). Statistically, microirradiators 4 and 5 fell outside of the Poisson distribution probability as discussed in Timed Calibrations. Since each microirradiator is hand-made, many variations are present between microirradiators within a batch. The channels can range anywhere from 10-30 microns, and making the assumption that all channels are filled with liquid once submerged into a cellular experiment, the amount of water present in the channel is the limiting factor for shielding of the activity from Ni-63. Therefore, we theorize that the channel lengths are the factors behind the varying displays of activity in cell culture medium.

5.3.4 Comparison to LSC

Most importantly, the objective of this custom bench-top calibrator is to eliminate the need of liquid scintillation for determination of activity levels before experimentation. Despite the scarcity of the LSC instruments on campuses and the contamination issues with the cocktail itself, liquid scintillation is practically the only accurate detection method for Ni-63. With this being said, it is imperative to compare activity values obtained from the calibrator against the liquid scintillation values to ensure linearity between all measurements.

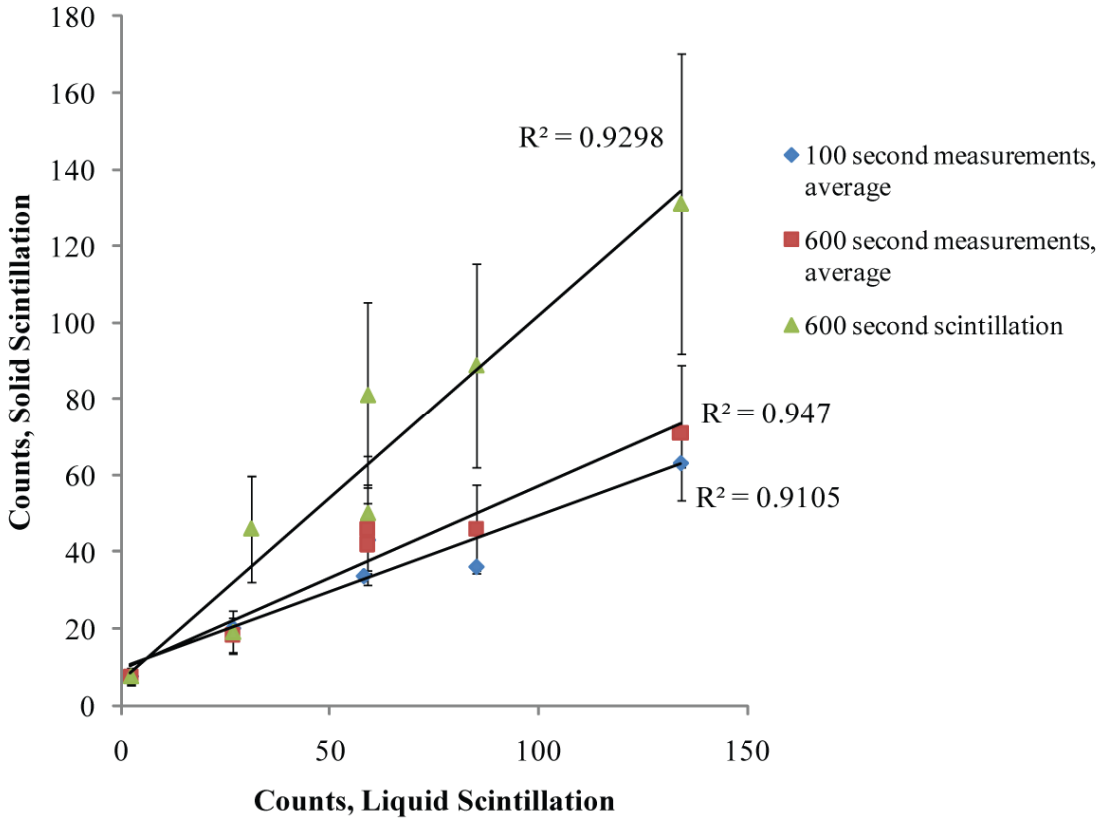

Figure 29. Comparison of the microirradiators' liquid scintillation measured activities versus solid state scintillation activities (in Bq). Short (100 seconds, red), long (600 seconds, blue) and Liquid scintillation within recess (green) trials are indicated. R^2 values indicative of the trend of linearity of each data set.

Linearity is a key to determine if the bench top calibrator is consistent in count rate values to ensure precision of measurements in compared to LSC. In Figure 29, averages for all trials of microirradiators 1-5 for the short, long and liquid scintillation in recess were compared to their corresponding liquid scintillation calibration value. As shown in the graph, the short and long measurements are below a 1:1 correlation with the calibrated liquid scintillation values, with the long measurements slightly more accurate than the short. However, it is clearly shown for the liquid scintillation in the recess

experiments that these values are the closest to a 1-1 ratio with the calibrated liquid scintillation values, and this is thought to be due to the cocktail interacting with the Ni-63, allowing light to pass through the glass of the microirradiator to the detector. It is to our knowledge that this is the first scintillation device specifically designed to measure varying Ni-63 sources.

5.3.5 Histogram

In addition to the software's ability to determine the count rate, histograms of the distribution of various amplitudes can be determined for each source, each radiation event that interacts with the scintillator produces photons, which in turn produces electrons within the photomultiplier tube and ultimately produces a voltage pulse of a specific amplitude displayed on the computer. Since each radiation event has a specific energy, and the scintillation crystal produces approximately 8-10 photons/keV, the height of each voltage pulse is directly proportional to the energy of the incident radiation [27].

In Figure 30 is an example of this histogram of counts per energy unit (keV) for a 10 second measurement of microirradiator 5 (59 Bq). The spectrum begins at 0 keV, and ends at 70 keV Ni-63 has a maximum beta electron of 67 keV, with an average $E_{1/3}$ value of 18 keV. Typically in radiation measurements, energy spectrums for alpha and gamma interactions are monoenergetic, meaning that with the right analysis system the peak will be very narrow and distinct. Graphs of this nature can be normalized and converted from bins of voltage amplitudes into the energy spectrum upon calibration of the instrument. With beta electrons, due to the interaction with the neutrino, beta spectrums are broad, as show in Figure 30. In the microirradiator energy spectrum, there is a sharp peak

corresponding at 1 keV not typically seen in a Ni-63 beta spectrum. This peak was also present in the calibration of the energy spectrum with a larger Ni-63 wire source (data not shown). This peak could be due to multiple factors, such as the data acquisition and the shape of the corresponding source.

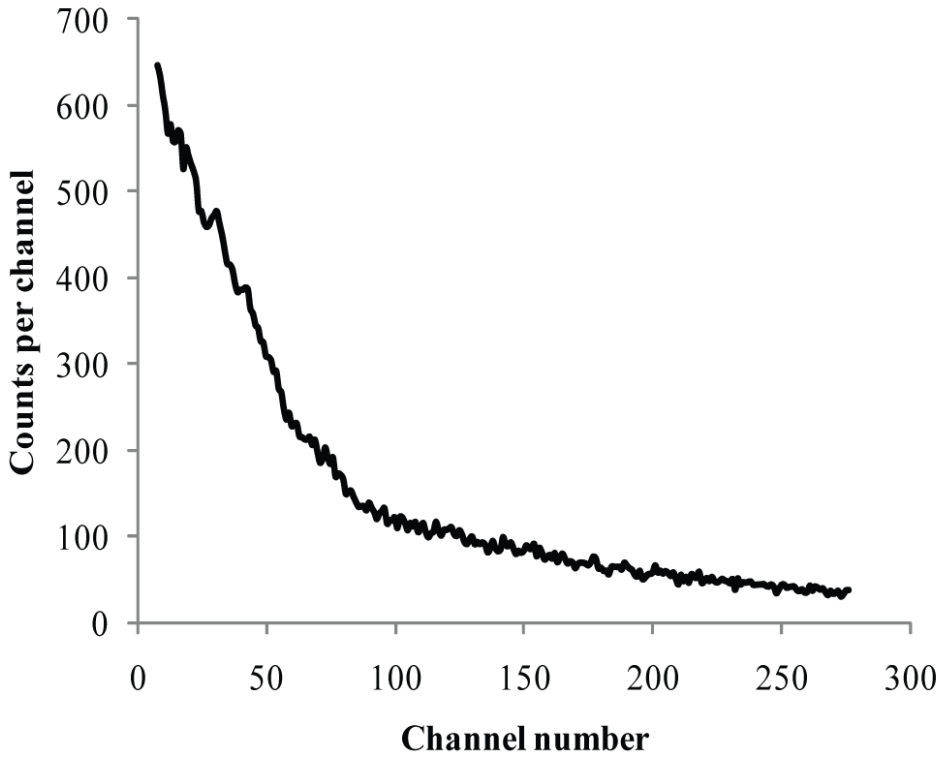

Figure 30. Energy spectrum of Ni-63 (3766 Bq) plated source. A typical shape of a beta spectrum is obtained as expected from a Ni-63 source, with an approximate $E_{1/3}$ value at 17 keV and a max energy of approximately 67 keV with bremsstrahlung radiation extending past the maximum energy. These energies correspond to the channel numbers presented.

5.4 Conclusions

A Ni-63 bench-top solid state calibrator for determination of activities of various custom-made sources has been successfully developed. Statistics on experimentally

obtained data confirms that measurements follow reasonable allowed fluctuations. It is planned to verify the performance of the calibrator with other elements of low activity alpha or gamma emitting isotopes and corroborate the data with already obtained beta results.

CHAPTER 6

BETA ASSISTED CHEMICAL DESORPTION IONIZATION

6.1 Introduction

Throughout this thesis, the microirradiator has been used as a tool for delivering radiation. In manufacturing the microirradiator, the electrochemical methods used to electrodeposit Ni-63 can be used on any shape of metallic source. Electrodepositing Ni-63 onto a copper wire source, 1-2 mm in diameter would create a stronger ionization up to 10 μCi for various applications. Other such applications are in mass spectrometry, manufacturing novel ambient ionization sources. Ambient Ionization (AI) is an emerging research technique in the field of mass spectrometry (MS). [64] In this chapter, we report a new ambient ionization technique, named beta-assisted direct chemical ionization (BADCI) comprising a simple low activity radioactive source, safe enough for direct open air ionization. This new probe utilizes an electroplated thin layer of ^{63}Ni, a low-energy β-emitting radionuclide. Previously, Horning *et al*. have incorporated a ^{63}Ni foil as part of an external ion source for MS operating at atmospheric pressure.[65] However, this type of ion source employed an activity of 15 mCi requiring it to be shielded from the operator. Additionally, Horning's source was strictly applied to electronegative compounds that are sensitive to electrons. Such configuration did not allow for "ambient air" operation, requiring sample dissolution prior to injection through a septum into a high purity nitrogen carrier. The main advantage of manufacturing smaller activity,

custom diameter radioactive sources is the safety of the lower amount of radioactivity deposited and various different shapes of the source for applications.

Ambient ionization eliminates the need for sample preparation procedures, thus providing a significant advantage for high throughput, real-time and *in situ* MS analysis. Since the introduction of desorption electrospray ionization (DESI),[66] and direct analysis in real time (DART),[67] a handful of ambient desorption/ionization methods have been reported.[68] Despite the analytical power of these techniques, a certain degree of instrumental complexity is still involved in their operation, mostly due to the use of high voltage for creating ionizing species and/or the use of solvent or lasers for analyte desorption. These requirements hinder the extent to which these techniques can be applied to field instrumentation.

Ion mobility (IM) spectrometers commonly employ 15 mCi radioactive ^{63}Ni foils as part of the ion source.[69, 70] However, due to the relatively high radioactivity dose delivered, there is a considerable administrative burden and cumbersome safety protocols associated with these types of devices, including contamination testing and special regulations regarding manufacturing, storage, disposal, and transportation. The BADCI probe proposed here uses a significantly lower amount of ^{63}Ni activity ($\sim$10 μCi), typically three orders of magnitude lower than in IM spectrometers. These radiation levels do not require shielding or radiation detection monitors, and result in zero-dose radiation exposure to the user, even in an unshielded configuration such as the one proposed here.

6.2 Experimental

The BADCI probe was constructed by electroplating a 10 μm thick, 1 cm long ^{63}Ni layer with a total activity of 10 μCi onto the end of a 1 mm diameter, 5 cm long copper wire (Figure X). ^{63}Ni was purchased from NRD, LLC (Grand Island, NY) in $NiCl_2$ form (50 mCi in 5 mL of .6 M HCl). Detailed procedures for the electrochemical deposition of the ^{63}Ni layer have been described elsewhere[1] (note: possessing and using radioactive materials must follow safety guidelines provided by the user's workspace). Shrink-wrap tubing around the bare Cu wire provided grip for the Swagelok® fitting that enables mounting of the probe in position. MS experiments were conducted using a LCQ Deca *XP* quadrupole ion trap mass spectrometer operated in positive and negative ion detection modes. Various over-the-counter (OTC) pharmaceuticals in tablet form, including Tylenol®, Claritin®, Excedrin®, generic ibuprofen, and a multivitamin tablet were analyzed.

The experimental setup is shown in Fig 31. The ionization probe was mounted at a 90° angle, ~5 mm away from the mass spectrometer capillary inlet, and ~4 mm above the sampled surface. Heated N_2 gas was placed approximately 1 cm directly behind the ionization probe at an angle of ~55°. Analytes thermally desorbed by a 2–4 L min^{-1} heated N_2 stream were ionized in their path towards the mass spectrometer inlet. The N_2 gas temperature was maintained between 70–75 °C. Samples were affixed directly underneath an extended capillary inlet (16 cm long, 381 μm i.d. and 1588 μm o.d.) on an *x*, *y*, *z* stage as previously described,[64] allowing the user to control sample position with respect to the probe and heated gas flow.

The ^{63}Ni probe emits beta particles with average energy of 17 keV.[2] In air, each beta particle reacts with nitrogen to generate N_2^+, which subsequently reacts with atmospheric traces of water through a series of ion–molecule reactions, generating a series of charged clusters such as $(H_2O)_nNH_4^+$, $(H_2O)_nNO^+$ and $(H_2O)_nH^+$ (equations in Fig. 30) These clusters in turn ionize analytes thermally desorbed by the gas stream.[69, 71]

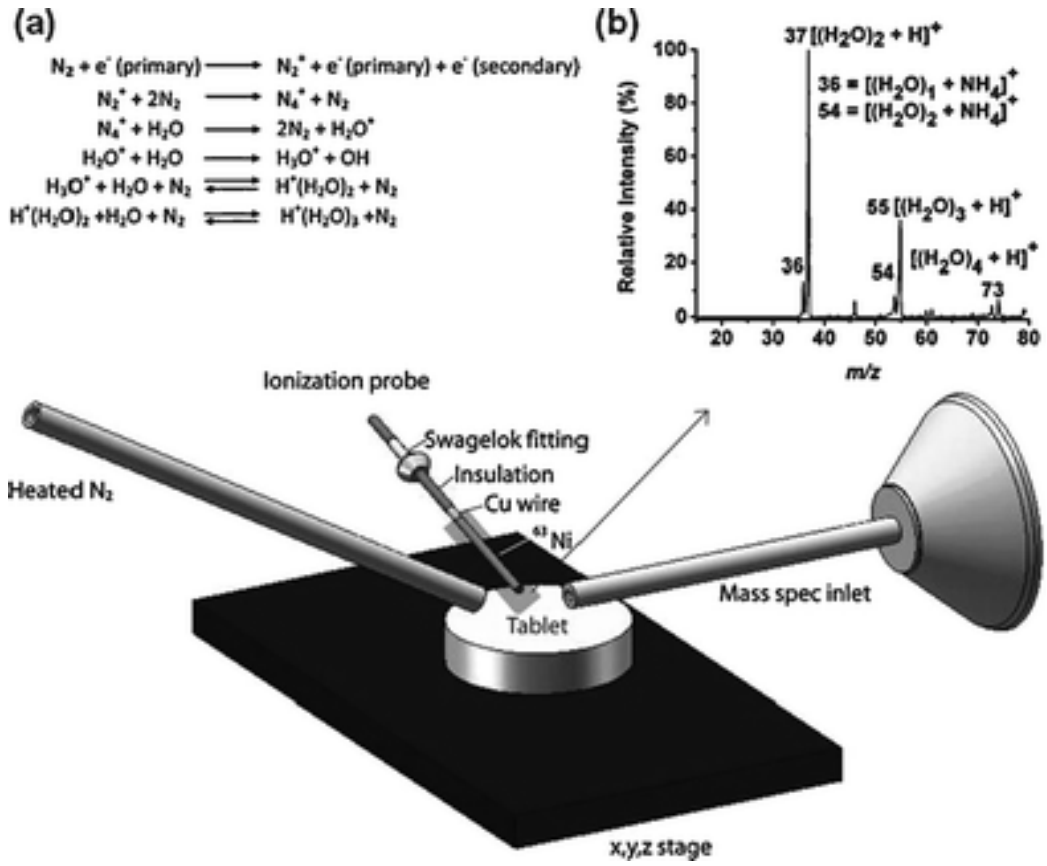

Figure 31 (a) Schematic of the beta electron-assisted direct chemical ionization (BADCI) ion source coupled to a quadrupole ion trap mass spectrometer, and (b) mass spectrum showing the typical reactant ion background produced by the ionization probe held ~1 cm away form the capillary inlet.

The two most salient differences of the ^{63}Ni source used in BADCI and traditional ^{63}Ni sources are that (a) it is used as part of a direct open-air ionization probe outside of the

spectrometer and that (b) the ^{63}Ni activity used is in μCi levels. At these levels, dose to the user is negligible since the emitted beta particles are absorbed within 30 μm of tissue (equivalent to the dead outer layer of skin). Low energy beta electrons produced by the BADCI probe cannot be detected with a Geiger–Müller counter. Typical beta electrons at the energy levels used in BADCI have a 5% efficiency of traversing such a detector, meaning that if the Geiger–Müller counter reading is less than twice the background radiation level, such radiation source is considered non-contaminating. No external shielding is required because absorption of beta electrons occurs within a few centimeters of air. In summary, the ^{63}Ni probe used in BADCI, while handled following simple radiation safety procedures, is not an external radiation hazard, causing a negligible dose to users.

6.3 Results

The position of the beta emitter, the direction of the heated gas flow and the sample position were optimized for the highest sensitivity. The maximum signal was obtained in an arrangement where the radioactive tip of the probe was held perpendicular with respect to the capillary inlet, held parallel to the sample surface with the gas flow directly behind the source (Fig. 31). In this configuration, more abundant protonated water clusters are formed, also increasing the resulting analyte signal.

Fig 1b shows a typical reactant ion mass spectrum generated by the BADCI probe in positive ion mode. Peaks at *m*/*z* 37, 55 and 73 were observed corresponding to water clusters ($(H_2O)_nH^+$, n = 2–4) with n = 2 dominating the spectrum. Kawai *et al.*[72] have shown that clusters with n = 2 have the largest reaction cross-section and the second

lowest proton affinity in the series, thus being most effective in proton transfer reactions. Being the most dominant species in the spectrum, $(H_2O)_2H^+$ is thus expected to effectively ionize analytes with a variety of chemistries.[72] Concurrent to the observation of protonated water clusters, mixed ammonium/water clusters $[(H_2O)_1NH_4]^+$ and $[(H_2O)_2NH_4]^+$ with *m*/*z* 36 and 54, arising as a result of ligand exchange of $[(H_2O)_nH]^+$ species with ammonia present in the lab atmosphere were also observed.[73] Minute peaks at *m*/*z* 46, 74 and 79 corresponding to protonated formamide, dimethyl formamide (DMF) and dimethyl sulfoxide (DMSO), were also detected in the background spectrum.

6.3.1 Pharmaceutical Tablets

To provide a first illustration of the analytical performance of the BADCI technique, several intact pharmaceutical tablets were examined as test samples. An optimum flow rate and temperature of 4 L min^{-1} and 75 ° C were respectively used for these experiments. Fig 32 shows the positive-ion mode BADCI mass spectrum of regular strength Tylenol® tablet. The base peak in the spectrum corresponded to the protonated acetaminophen monomer (*m*/*z* 152), the active ingredient in Tylenol®. The acetaminophen dimer ion was also observed, but to a lesser extent. No significant fragmentation was observed in the spectrum, suggesting that this ionization technique is quite soft in nature.

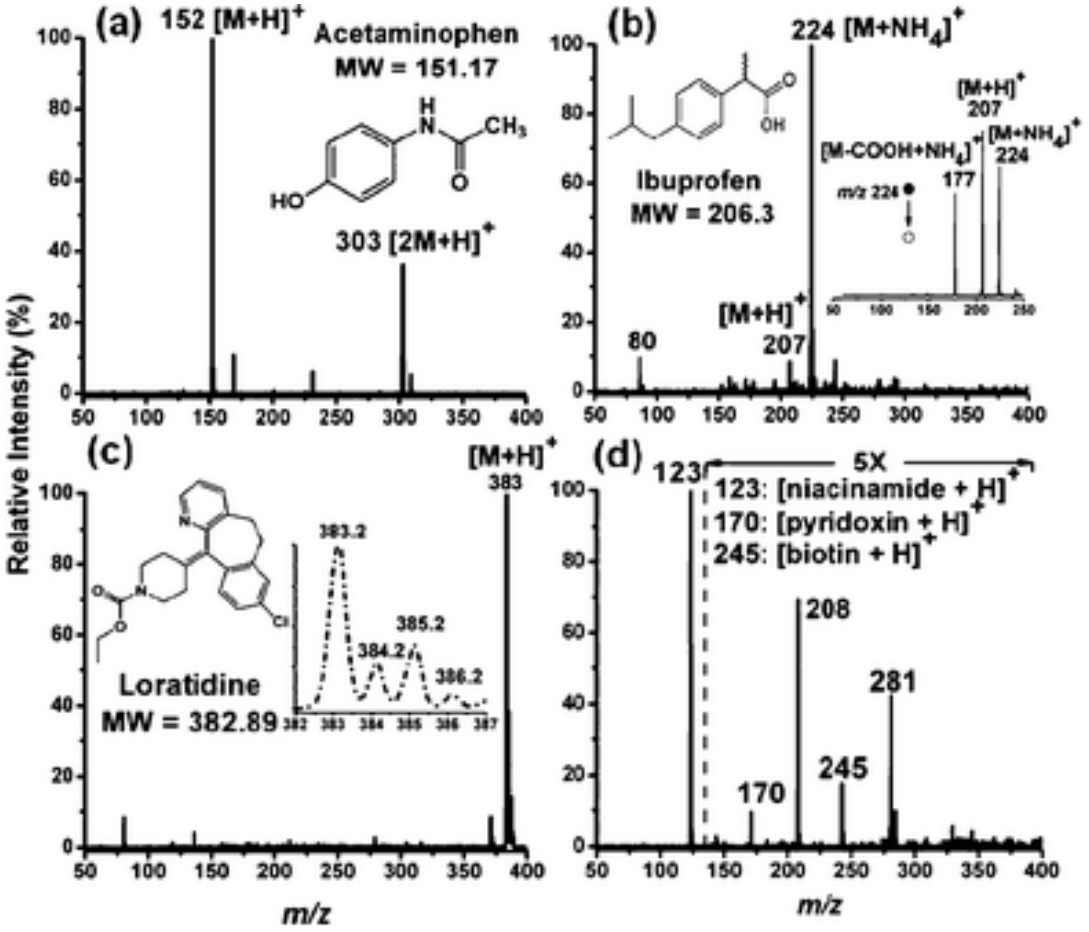

Figure 32. Analysis of various pharmaceutical tablets *via* BADCI: **(a)** a Tylenol® tablet containing 325 mg of acetaminophen, **(b)** a generic ibuprofen tablet (200 mg), **(c)** a Claritin® tablet containing 10 mg of loratadine, and **(d)** a generic multivitamin tablet. Insets show the **(b)** product ion spectrum of ibuprofen and **(c)** base peak region of loratadine.

The nonsteroidal anti-inflammatory drug ibuprofen was detected as the ammonium adduct (*m*/*z* 224) (Fig. 31b). The source of NH_4^+ was presumed to be background $[(H_2O)_nNH_4]^+$ species. In order to further confirm the identity of this peak, a tandem MS/MS experiment on the precursor ion at *m*/*z* 224 was performed (inset in Fig 31b). The most intense peak at *m*/*z* 207 corresponded to protonated ibuprofen, due to loss of NH_3, with the species at *m*/*z* 177 assigned to the formaldehyde loss from the protonated

molecule. The active ingredient loratadine was detected as the protonated molecule during analysis of Claritin® tablets (Fig. 31 c). The inset shows its characteristic chlorine isotopic signature.[15] Analysis of a generic multivitamin tablet showed predominantly one peak corresponding to protonated niacinamide (Fig. 31 d). However, weak signals attributed to pyridoxine, biotin and two other unknown species were detected. The unknown signals may have originated from the tablet coating.

A multi-component migraine relief medicine, Excedrin®, containing acetylsalicylic acid (250 mg), acetaminophen (250 mg) and caffeine (65 mg) was analyzed in both positive and negative ion modes. In the positive ion mode, all three active ingredients, acetaminophen, acetylsalicylic acid and caffeine, were detected, as shown in Fig 32.

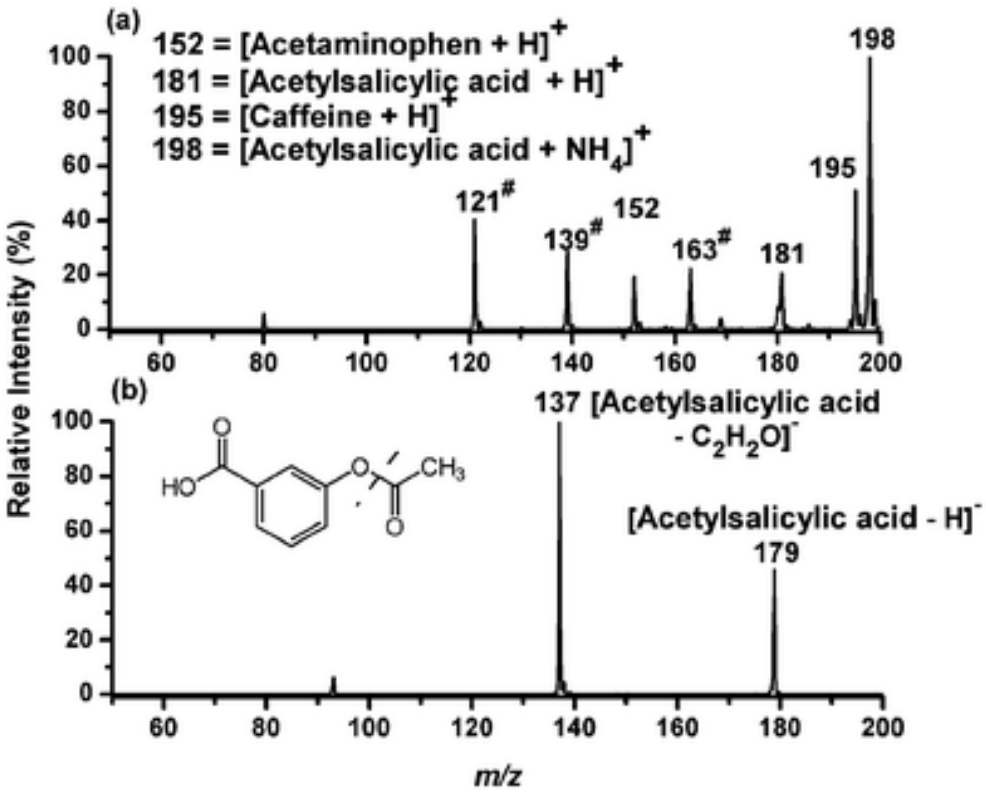

Figure 33. Mass spectra of a multicomponent pharmaceutical tablet Excedrin® interrogated with the BADCI probe: (a) positive ion mode, (b) negative ion mode. The peaks annotated with "#" are fragment ions from acetylsalicylic acid.

The protonated molecule signals are expected at *m*/*z* 152, 181 and 195.[74] However, presence of $[(H_2O)_nNH_4]^+$ in the background readily allows the formation of the complementary NH_4^+ adduct of acetylsalicylic acid. Although the proposed BADCI probe appears to be soft in ionizing many pharmaceuticals, several fragment ions were observed in the case of acetylsalicylic acid. The peak at *m*/*z* 121 corresponds to acetic acid loss from the protonated molecule. Peaks at *m*/*z* 139 and 163 derive from losses of CH_2CO and water, respectively. The negative ion mode mass spectrum of the same tablet revealed the formation of the deprotonated acetylsalicylic acid, along with a fragment ion due to loss of CH_2CO Fig. 31b. The mechanism of negative ion formation has been well documented, involving electron transfer reaction(s) to molecules with high electron affinity.[65] No other active ingredients were detected in negative ion mode.

6.3.2 Limit of Detection

Table 3 summarizes the calculated limits of detection (LODs) for several active pharmaceutical ingredients (APIs) analyzed by BADCI-MS. It is apparent from these results that the presence of multiple active ingredients or differences in tablet formulation can have a strong effect in the detection of some APIs. For example, the detection limit for acetaminophen in Excedrin® was 4.41 mg per tablet, whereas the LOD for the same API in Tylenol® was 0.20 mg per tablet. This effect can be attributed to either differences in thermal desorption rates of the analyte from different matrices, or competition for reactant ions when multiple species are desorbed.

Table 4. LODs of different APIs using the BADCI probe

Drug	API	Ion mode	LOD (per tablet weight)
Excedrin®	Caffeine	+	1.22 mg (680 mg)
	Acetaminophen	+	4.41 mg (680 mg)
	Acetylsalicylic acid	+	0.68 mg (680 mg)
		−	0.08 mg (680 mg)
Tylenol®	Acetaminophen	+	0.20 mg (432 mg)
Ibuprofen (generic)	Ibuprofen	+	3.52 mg (336 mg)
Claritin®	Loratadine	+	0.55 mg (130 mg)

6.4 Conclusions

In conclusion, the initial proof-of-principle performance of a new low-dose ambient ionization technique named BADCI is presented here. Additionally, this was the first experiment using a custom Ni-63 electrodeposited source that was not a microirradiator. In general BADCI is soft in nature, simple and safe to handle, with no external detectable radiation hazard for the user because of the low energy Ni-63 beta particles (67 keV). It has been shown to be effective in probing pharmaceuticals in solid form. The major ionic species generated by BADCI were protonated molecules. However, formation of ammonium adducts were also evident for some chemical compounds. Efforts towards more in depth characterization of this ionization technique are currently underway.

CHAPTER 7

Te-125 MICROIRRADIATOR

7.1 Introduction

Originally, this thesis project was developed to study the low dose, low linear energy transfer radioactive materials upon cells. There is a debate within the scientific community, commonly referred to the linear no-dose threshold, whether or not low doses of radiation scales linearly from previous data collected, or there is a non linear response to low doses. The ultimate results of this debate would be whether or not low amounts of radiation are harmful, or actually helpful in cellular repair. To achieve this, a microirradiator would be used to study the effects of low dose low energy radiation delivered to cells.

As discussed in chapter one, the basis of this thesis derived from the original microirradiator, a tritium saturated polyaniline film deposited onto a 25 um platinum wire.[10] It was determined from these experiments that metallic depositions of radioactive metals would be best for further development of this project because of its stability and the elimination of volatile tritium. One of the first projects to demonstrate the feasibility of electrodepositing a metal onto a platinum microelectrode involved the use of Te-125m. Te-125m is involved in an isomeric transition, defined as the decay of a nucleus in a meta, or metastable state.[2] To reach the ground state, a gamma ray is released. For Te-125m, 144.8 keV gamma ray with two auger x-rays at 109.3 and 35.5 keV are emitted.[9] In conjunction with Oak Ridge National laboratory, Te-125m was established as the metal of choice because of its low energy x-ray and abundance of supply available.

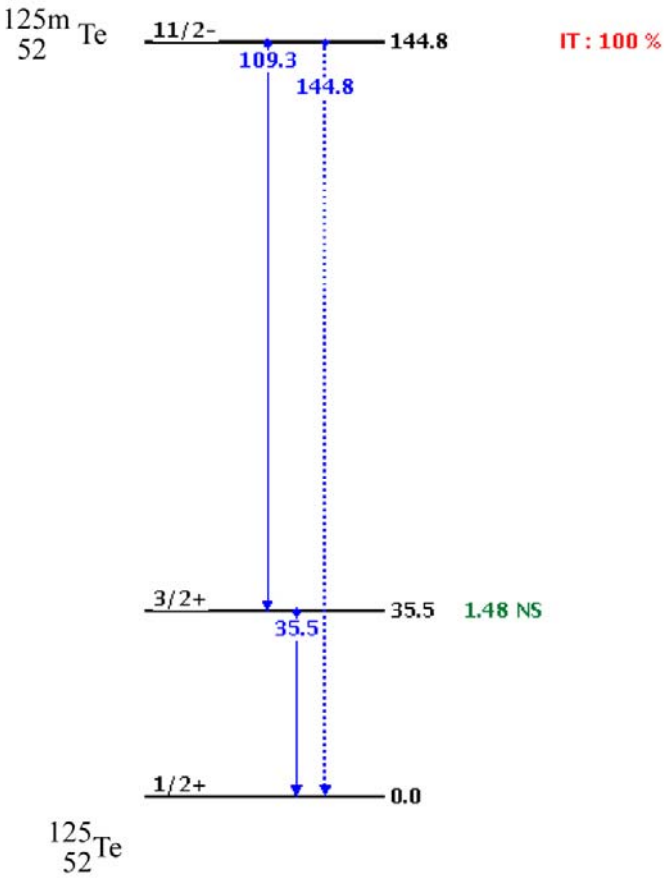

Figure 34. Decay Scheme of Te-125m to Te-125. In red, IT represenets isomeric transition. In blue, 144.8 keV 109.3 keV, and 35.5 keV photons are emitted.[75]

7.2 Experimental

Te-125m was electroplated onto 5 platinum microelectrodes following procedures discussed elsewhere.[76] Because Te-125 was irradiated on site at the High Flux Isotope Reactor at Oak Ridge National Laboratory, the Te was dissolved in aqua regia, evaporated, and dissolved in 5 mL 1 M HCl. A transfer of 40 µL of .28 µM Te-125 solution was added to 3 mL of our background electrolyte .5 M K_2SO_4. The radioactive solution was bubbled under argon for 30 min prior to and during deposition to purge

oxygen from solution, and deposition of Te-125 occurred at -.765 V for 75 minutes. Each electrode post-deposition was washed thoroughly with methanol and water, and placed into a scintillation vial for activity determination by gamma spectroscopy. A control electrode was also placed in identical conditions to the Te-125m plated electrodes to determine background adsorption onto the microelectrode. Each electrode was then stripped for determination of activity on each electrode. The stripping solution was also analyzed by gamma spectroscopy.

In the first trial of 3 electrodes, each electrode after deposition and washing was measured by gamma spectroscopy and activity on each probe measured 49.72, 58.05, and 47.56 nCi respectively. After total activity was measured, the electrode after stripping and the stripped solution were measured for activity. As you can see in yellow, there is a great amount of radiation attributed to glass adsorption onto the probe, with little attributed to the deposition itself. However, if these two are superimposed as in Figure 35, they both equal approximately the total amount of radiation measured. It can be deduced that glass adsorption while depositing and after thorough rinsing is a significant problem in development of the Te-125m microirradiator.

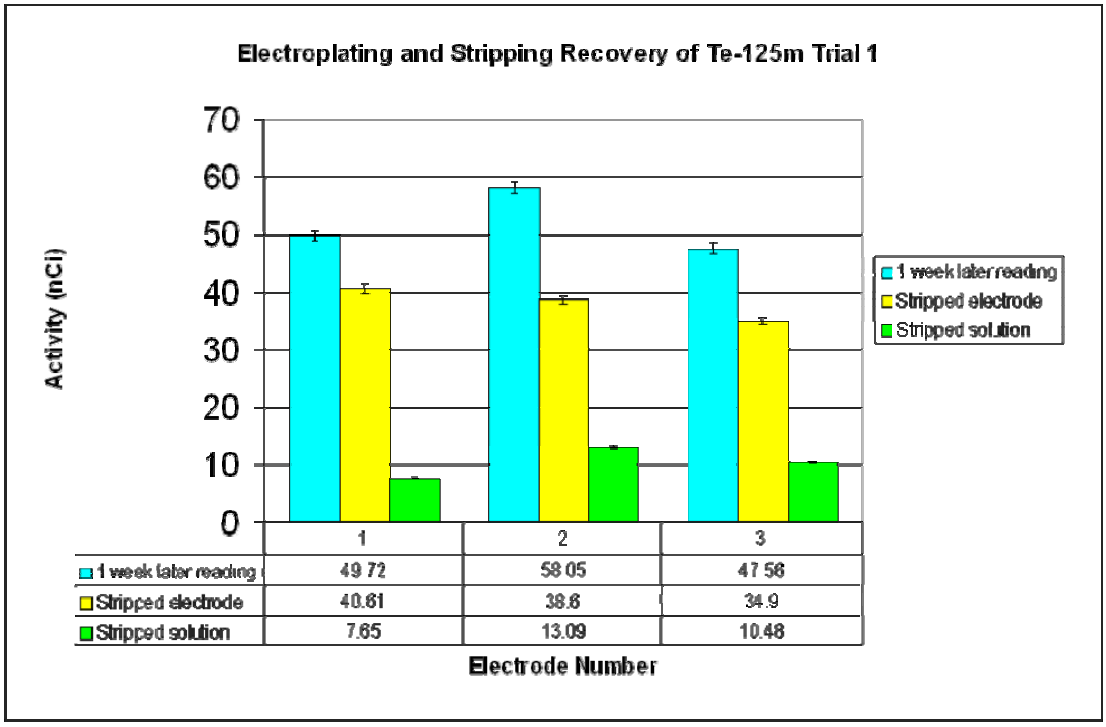

Figure 35. Bar graph of 3 of the 5 Te-125 microirradiators tested. Gamma spectroscopy measurements to indicate activity (in nCi) were measured with blue representing the activity of the electroplated probe 1 week after deposition, yellow the activity of the electrochemically stripped electrode, and green the activity of the stripped solution, respectively

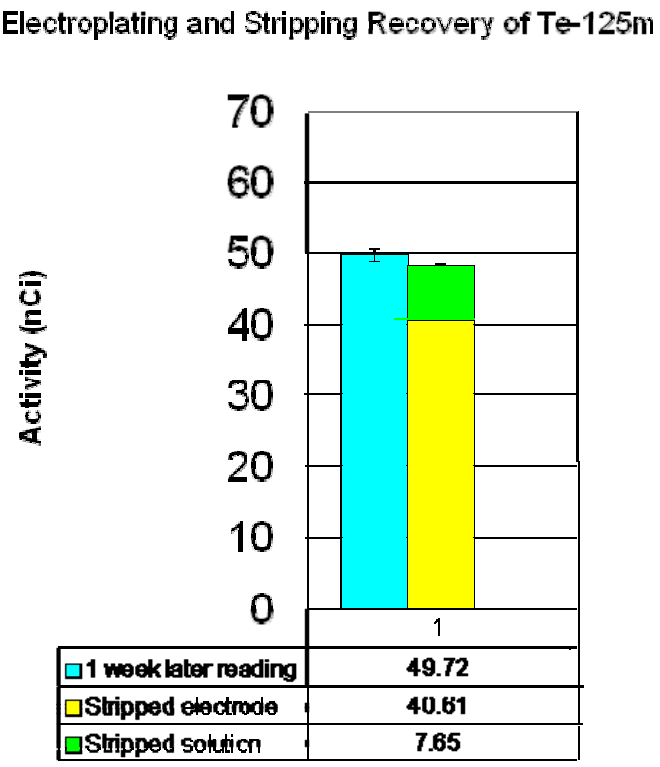

Figure 36. Superimposed graph of the stripped (yellow) and stripped solution (green) from electrode 1 in Figure 33.

Because of the limited time frame at the laboratory while performing this work, lower sophisticated equipment, and lack of a recorder to determine the charge applied, we were unable to compare the amount of Te-125m deposited to the activity data obtained. To try to make a connection between the two, work was then done in a cold setting at Georgia Tech trying to obtain electrochemical data to compare to the activity data obtained at ORNL.

To begin, we wanted a relation of the activity after stripping to the amount electrodeposited. Below is a calibration curve of stripping following the same procedure to plate Te-125m done at ORNL using cold Te, but varying the deposition times. In ascending order, depositions occured at 100, 250, 500, 1000 and 2000 seconds of

deposition and cycling at 10 mV/s from .1 to .8 V. With increasing deposition times, each stripping peak height increased in magnitude, therefore proving that increased deposition times indeed produced more Te on the electrode surface.

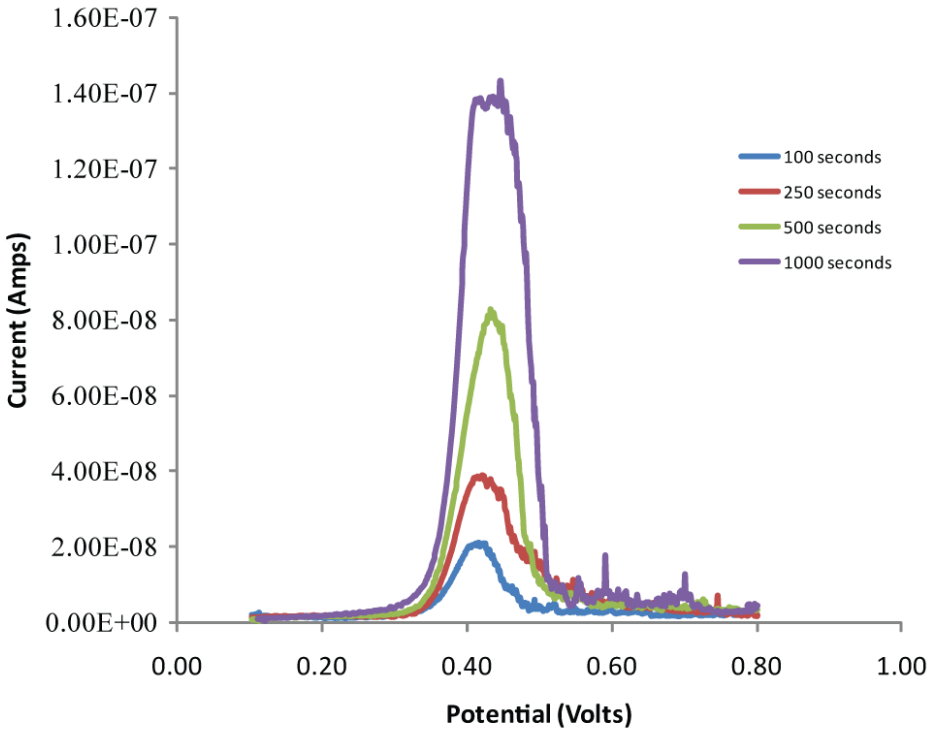

Figure 37. Linear Stripping Voltammetry in 5 mL solution of 3 nM TeO_2, .5 M K2SO4 vs. Ag/AgCl. Colors indicate amounts of Te deposited by time of voltage applied of non radiological Te.

However, these results could not be reproduced unless the electrode with Te electrodeposited remained in the same deposition solution for stripping. Once the electrode after deposition was removed and/or moved to a different solution, a stripping peak was not observed.

To test this theory, each electrode was deposited with cold Te, under the same time conditions. Figure 38 was stripped in the same deposition solution, and Figure 39

mimicked the same conditions followed at ORNL by taking the electrode out of solution, switching to a different deposition solution, and stripping.

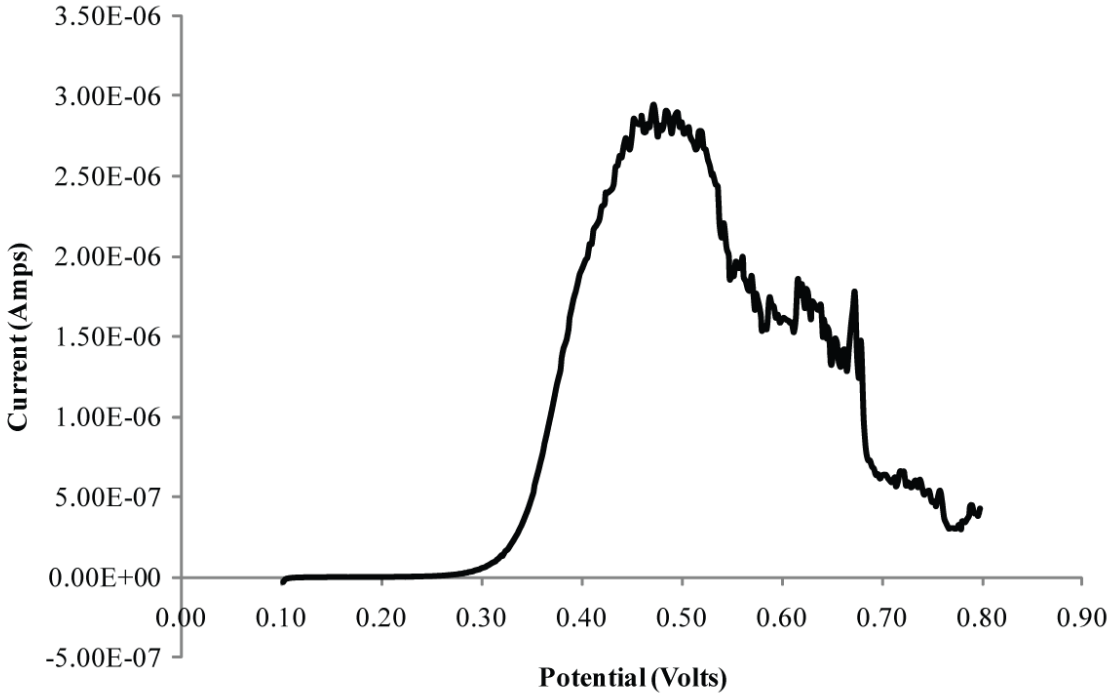

Figure 38. Linear Stripping Voltametry of Te in 5 mL 3 nM TeO_2, .5 M K_2SO_4 vs Ag/AgCl. without removal of electrode from solution.

By moving the electrode, it was observed that the current decreased by two orders of magnitude, leading to a significant drop in peak height. This drop in magnitude of peak height indicates less Te is on the electrode, leading to the conclusion that Te must flake off the electrode after handling. Because of this, we concluded the deposited metal was likely falling off the electrode under cold radiological conditions and after initial activity calculations at ORNL. Ultimately, we could not correlate the amount of Te to its activity because of the instability of the film adhesion to the electrode.

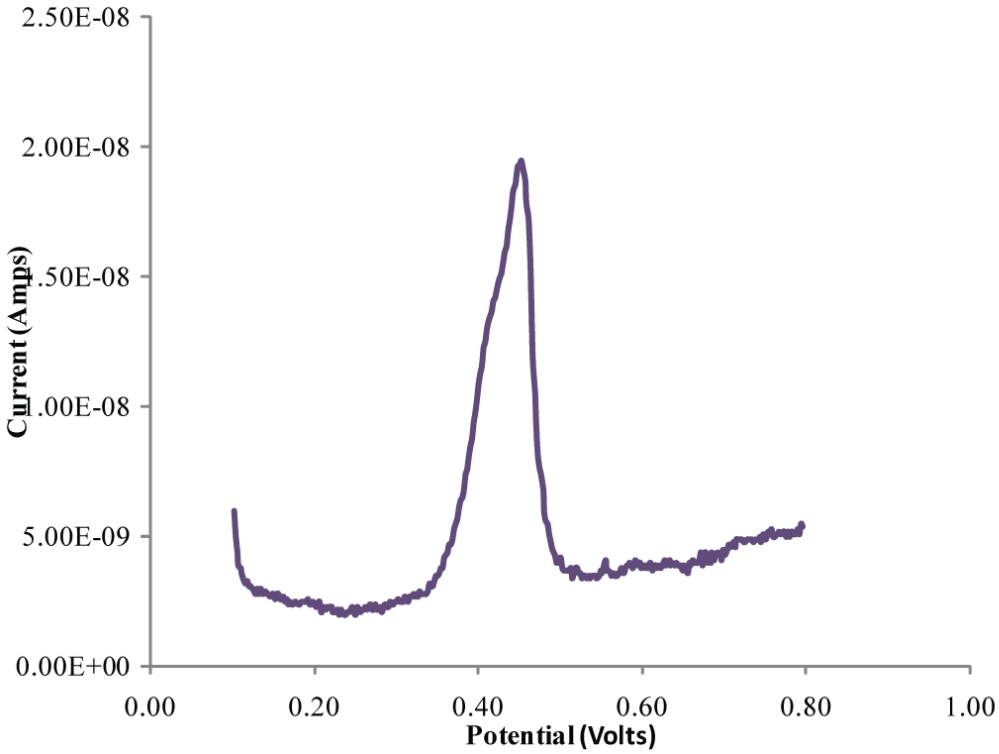

Figure 39. Linear Stripping Voltametry of Te in 5 mL of 3 nM TeO_2, .5 M K_2SO_4 vs. Ag/AgCl. Electrode was lightly tapped after electrodeposition of Te, and electrochemically stripped in the same solution.

Additionally, Monte Carlo approximations (MCNP) were calculated to estimate the penetration depth of the gamma and x-ray photons emitted from Te-125m. Below in the figure, red through blue is the highest through the lowest dose received for a 2mm x 1 mm slice of water, respectively. From this calculation it was determined that the low energy gamma and x-ray photons emitted were extending well past the 20 x 5 micron cell to be used during experimentation, and due to these findings plus the instability of the Te film, this specific element was abandoned. However, from these findings it was determined that lower energy and a more stable electrochemical deposit were needed, and with this Ni-63 was chosen as the new element for experimentation.

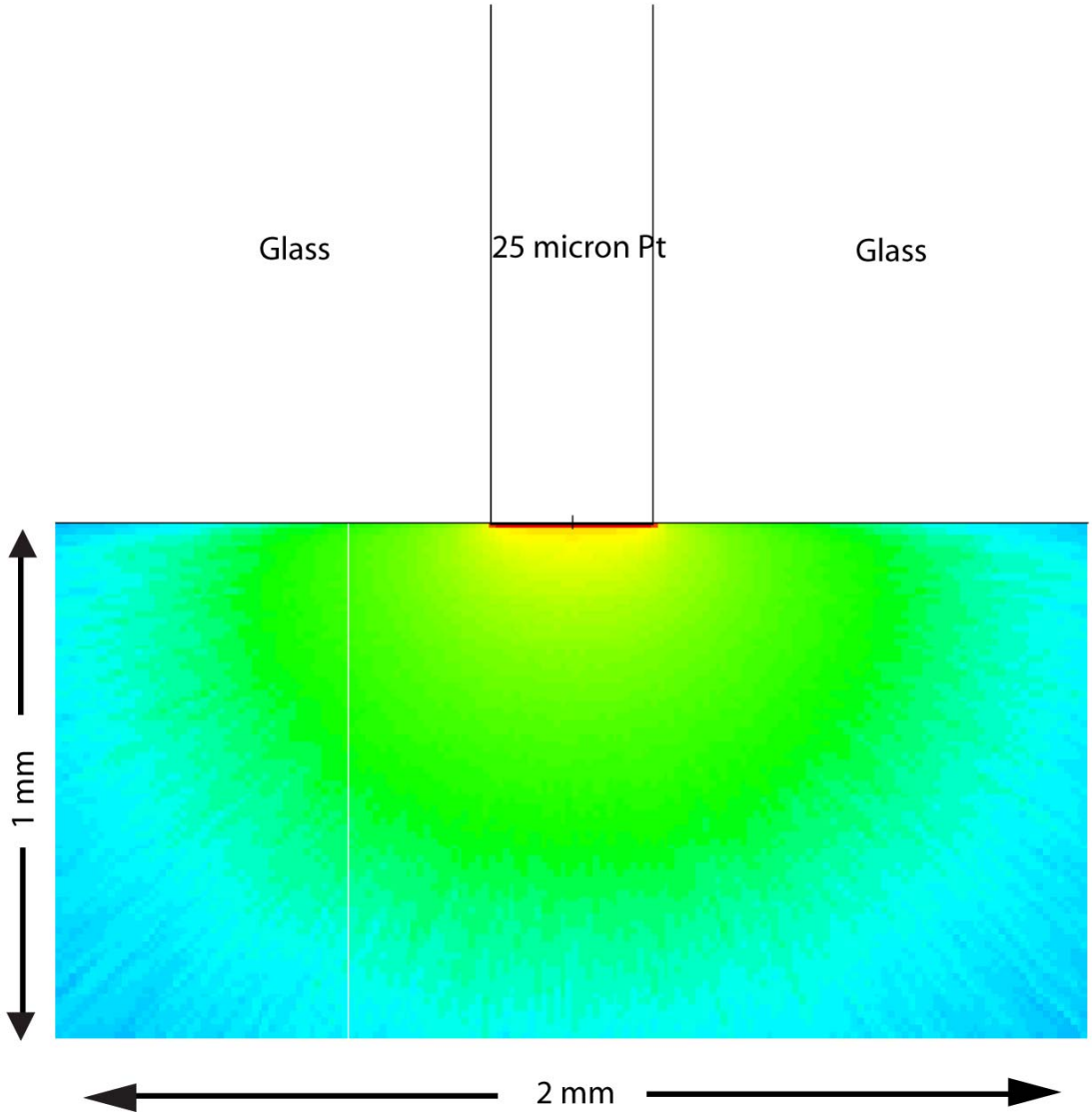

Figure 40. MCNP dose profile of 25 micron Te-25 deposit onto microelectrode. Colors from Red-Blue represent highest-lowest dose from the irradiator.

7.3 Conclusions

To conclude, Te-125m was a good initial experiment to determine whether or not a metal electrodeposited onto a microelectrode would be feasible for a microirradiator. Lessons were learned in electrodeposition, deposition quality, and the type of radiation

used for the microirradiator. Regardless whether or not the experiments worked, Te-125m ultimately lead to Ni-63 as the metal of choice, with great success.[1]

CHAPTER 8

FUTURE WORK

8.1 Table of Radioisotopes

With the success using Ni-63, there are various other isotopes that can be convenient for microirradiators. Any element that can be electrochemically electrodeposited onto an electrically conducting surface can be used on a microirradiator. It is important to note that this thesis has only explored the low dose capabilities of beta radiation. It is equally if not more interesting to explore the use of alpha and gamma radiation with microirradiators and compare their effects to the ones demonstrated within this thesis. To begin, a table of the most commonly used radioisotopes of interest to health physicists is presented in Table 5.

There is vast information in the literature of different electrodeposition methods for metallic and non-metallic elements. Since these isotopes described in the table have the same general properties as their cold non-radioactive counterparts, using electrodeposition procedures found in the literature and formulating it to the radioactive source is the ideal starting point for depositing a new material. Optimizing new deposition potentials and maximizing the current efficiency is also key in creating a quality and stable electrochemical deposit onto a microirradiator. With various different elements that can be plated, other future application for the microirradiator and Ni-63 microirradiators are as follows.

Table 5. Radiosotopes of general interest to health physists. Symbols for decay mode: β – is beta electron, β+ is positron, γ is gamma radiation, α is alpha radiation, n for neutron radiation, and x is x-ray radiation. Half life symbols: h is hour, d is day, y is year.

Radionuclide	Decay Mode	Half Life	Energy (MeV)
Ag-110m	β - ,γ	249 d	0.116
Am-241	α , γ	432.2 y	5.6, 1.2
Bi-210	β -	5 d	1.2
C-14	β -	5730 y	0.156
Cf-252	α, n	2.63 y	6.2
Cm-242	α	160 d	6.1
Co-60	β -, γ	5.26 y	2.8, 1.2
Cs-137	β - ,γ	30 y	1.2
Cu-64	β -, β+, γ	12 h	0.58, 1.7, 1.34
Cr-51	γ	27 d	0.76
Fe-55	γ	2.7 y	0.23
I-125	γ	59.6 d	0.18
I-131	β -	8 d	0.97
Ir-192	γ	74 d	1.5
Mo-99	β -, γ	66 h	1.4
Ni-63	β -	100 y	0.067
Pb-210	β -	22.3 y	0.063
Pd-103	β -, x	17 d	0.549, 0.081
Pm-147	β -	2.62 y	0.22
Po-210	α	138 d	5.4
Pu-239	α, γ	24065 y	5.2, 0.41
Ra-228	β -	5.75 y	.046
Ru-103	β -, x	39 d	.763, .059
Sn-123	β -	129 d	1.4
Sr-90	β -	29.12 y	0.55
Tc-99m	γ	6.02 h	0.14
Te-125m	γ	58 d	0.15
U-232	α	72 y	4.0
U-238	α, γ	4E9 y	5.4, 0.23
Y-90	β -	64 h	2.3
93-Zr	β -, x	1,530,000 y	0.091, 0.031

8.2 Brachytherapy

Brachytherapy is most commonly known as a type of radiation therapy in which the radiation source is adjacent internally or externally to the targeted area of therapy, most often cancer.[34] It is most commonly used in prostate cancer, with additional uses in breast and skin cancers. Palladium-103 seeds are the preferred treatment for prostate cancer, allowing the patient to not have radical surgery or common side effects such as impotence and incontinence as seen after surgical removal of the tumors.[77] [78]

The most important aspects of brachytherapy are the source placement (or location), the dose rate, and the total dose received.[34] [28] The radiation source can be placed in various locations such as implantations adjacent to the targeted source, or intravascular in combination with a heart stent to prevent macrophage buildup. Secondly, the dose rate is an indication of the intensity of the radiation applied, with low doses typically reserved for oral cancers and higher dose rates for prostate and other internal cancers. The overall dose applied is dependent upon how long the radiation source is applied in conjuction with the dose rate. Brachytherapy sources, such as prostate cancer, are most commonly permanently implanted within the body, allowing the source, Pd-103, to completely decay for the prescribed treatment period.

The role in which microirradiators, with various radioisotopes of interest, can be used as a brachytherapy treatment is on skin cancer, which is a promising technique to replace surgery.[79] [80] Basal Cell Carcinoma (BCC) and Squamous Cell Carcinoma (SCC) are the most common types of nonmelanoma skin cancer seen in patients. These types of skin cancers found on the face, nose, and ears usually require excisions, disfigurement of

the affected skin, and extensive reconstructive surgery. For cosmetic reasons, brachytherapy has been used with Ir-192 or an external beam to irradiate the tumors and avoid surgical removal.[79] However, the brachytherapy treatments involve patients with masks or mold-fitting devices with the radiation implant covering the tumor externally. A more graceful approach to this would be using a microirradiator on smaller BCC and SCC tumors, with Ra-228. The microirradiator with a controller could precisely target each of the tumors and deliver the needed dose of 2-4 Gy/session due to its high flux density.[79-81] For larger tumors, microirradiators could be custom manufactured to the size of the tumor, allowing the radiation dose profile to be exposed to the entire tumor. This approach would be simpler and easier for the patient versus masks and molds placed on the face. Additionally, health technicians would be exposed to a significantly smaller dose than larger brachytherapy seeds or external beams, significantly reducing the risk of second hand exposure.

8.3 Bystander Effect

The bystander effect is defined as non-irradiated cells adjacent to irradiated cells exhibiting radiation induced effects.[81] It has been hypothesized that either radiation induced chemical damage or cellular signaling is the main cause of the bystander effect, but the origins remain unknown.[82, 83 84] Typical bystander experiments involve cell cultures prepared next to an adjacent lab within a microbeam facility. Microbeam facilities are multi-user instruments in which allotted time is given to researchers to irradiate cells and other biological materials.[85] Cell cultures and other necessities must be prepared next to the microbeam facility to ensure a healthy cell culture and adequate time

to transfer the cells to and from the microbeam. Additionally, real time information and information after irradiation is lost due to time constraints and limited facilities while conducting experiments.

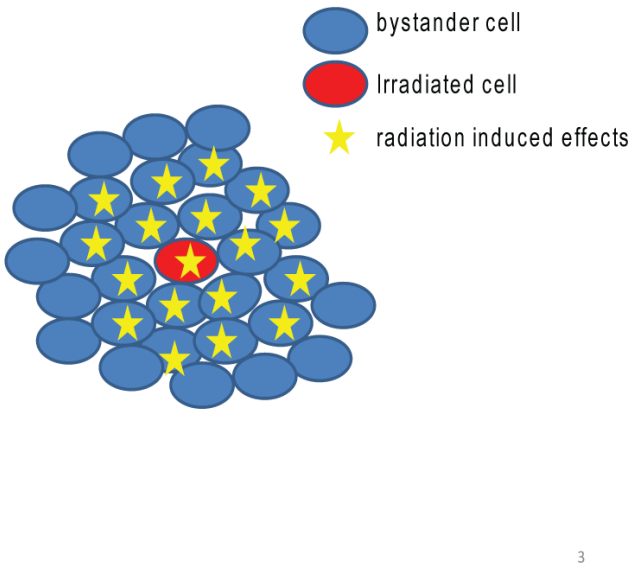

Figure 41. Illustration of the bystander effect from ionizing radiation.

To continue this project, it would be advantageous to use the microirradiator with Ni-63 and ultimately an alpha emitter, such as U-238, U-232, Am-141, Po-210, and others. The first feasible new radioisotope would be Co-60, a gamma emitting radioisotope with similar electrodeposition techniques to Ni-63.[86] Radiation involving low LET beta particles is an area that has not been fully explored, and to our knowledge H-3 has been used in solution to demonstrate cellular damage effects.[87] Any radioactive element that can be electroplated onto the surface can be used in conjunction with the

microirradiator. Studying the dose rate effects on cells with either alpha or beta radiation, and the adjacent cellular death in time is a starting experiment for preliminary results.

Additionally, studying the effect of radiation induced damage on embryos would be equally promising in conjunction with the microirradiator. Embryos are a field of interest because of their susceptibility to ionizing radiation because of their high cell division rate. There is a large area of radiation biology that involves the use of embryos, most commonly zebrafish and japanese medaka fish, and their affects of ionizing radiation.[88] [89]

Figure 42. Image of Japanese medaka fish

Most commonly, radiation is targeted to one area of the embryo using a microbeam or a collimated source and DNA damage proliferation is observed in time after radiation. However, with use of a microbeam facility is it an enormous task to keep the embryos alive after irradiation for long periods of time due to the travel to and from

the facility. The microirradiator can pinpoint the radiation to the targeted area of the embryo under a microscope, as proven in DNA double strand damage in individual cells. The target can then be irradiated by the microirradiator in real time under a microscope, and then allowed to grow to adult size to see the damage proliferate within the same facility.

Additionally, high LET radioisotopes such as alpha and neutron emitters have been used in conjuction with the fish embryos because of the accessibility to those two sources.[91 3] The microirradiator is advantageous in this scenario because it can be used to study the effects of low LET low dose ionizing radiation with embryos. In conjunction with the linear no dose threshold debate, it is virtually unknown whether low doses of ionizing radiation is harmful, or helpful to the human body.[87] Using the microirradiatiors, with Ni-63 or another low LET element in conjuction with the medaka or zebrafish embryo would add addition significant data to this debate.

8.4 Ni-63 Batteries

The betavoltaic effect is defined as harvesting beta electrons for electrical energy. There has been a strong push in battery research for a long life battery, especially in space applications.[92] The requirements for such a long-life battery has led into exploration of radioactive materials in conjunction with diodes for batteries. Elements such as Ni-63 and Pm-147 have already been demonstrated as viable radioisotopes due to their pure beta emission and long half lives.[93 94] Ni-63 as well has also been modeled to have a thickness saturation at approximately 3 μm, which fits well with other studies.[95] Using the techniques described in Chapter 2, beta voltaic batteries are constructed by

electrochemical deposition of Ni-63 onto the substrate of choice. Ni is usually the element of choice, because of its ease in electrochemical deposition and general availability. However, the source is typically purchased in its chloride form in acidic medium, and used without additional additives and pH adjustments. The advantage of using the technique as described in Chapter 2, is that additives are added to the $^{63}NiCl_2$ source, enabling a stronger Ni deposit with a high reproducible current efficiency.

CHAPTER 9

CONCLUSIONS

This thesis research with microirradiators and electrochemically deposited radioactive sources has hopefully opened the door to more benchtop radiation research without extensive safety shielding. One of the main drawbacks of conducting radiation research is that large radiation sources are housed in separate facilities. By introducing the microirradiator, a radioisotope can be deposited onto the small surface area of a microelectrode and be used as a tool for safely delivering radiation. The largest application of the microirradiator is in radiobiology. Images of cells being irradiated in real time by ionizing radiation is now possible due to the microirradiator. The information that can be obtained by this method is of great interest to the radiation community, due to other methods such as multiple-user radiation sources/instruments incapable of real time information and inability to transport a microscope to where the radiation source is located.

By manufacturing the microirradiator, this thesis project evolved to making custom, low activity radioactive sources for other applications such as ionization sources for mass spectrometry and a prototype miniature ECD detector for gas chromatography. By using electrochemical techniques to modify and enhance liquid radioactive sources available, unique sources can be made into any shape as long as the surface is electrically conducting. These sources can be miniaturized, and in return have a lower activity than typical radiation sources (e.g. ECD). Miniaturization has the potential of developing field

portable detectors, while lowering the activity lowers the fear in using such a radioactive source.

It is the hopes of this author that this thesis has opened the door to future works not only with Ni-63, but combining chemical methods with radioisotopes to manufacture novel radioactive sources for benchtop and other critical applications.

APPENDIX A

SUPPLEMENTAL INFORMATION FOR CHAPTER 4

A.1 Terminology and Definitions

Chapter four of this thesis delves into the topic of radiobiology in conjunction with the Ni-63 microirradiators. Multiple terms discussed in the chapter are familiar to the radiobiologist community, but not necessarily to the general scientific reader. In this appendix, multiple terms are defined to enable a fuller understanding of research and information in chapter four.

A.1.1 Double Strand DNA Break

A double strand DNA break (dsDNA) is defined as break of the chromatin strand into two separate pieces. Double strand DNA breaks are such a heavily researched field in radiobiology due to the risk of cell death and mutations. A single strand DNA break (ssDNA) involes a break in the chromatin, but not resulting in the separation of the strand into two separate pieces. Single strand DNA breaks are not of utmost concern due to the ability of copying the other unbroken strand. Double strand DNA breaks scale linearly with dose, with approximately 40 double strand breaks per Gy of deposited radiation.[28]

A.1.2 Mechanism of dsDNA

The formation of a dsDNA break is caused by either free radicals generated from the ionizing radiation, or direct ionizations. The average energy needed to break a strand of DNA is approximately 100 eV, well below low energy radioisotopes such as tritium

(17 keV) and Ni-63 used in this thesis (67 keV).[96] The energy from the ionizing radiation, is not uniformly deposited across the material being ionized. Rather, it is deposited in tracks, where the ionizing radiation have interacted with the material, creating a cascading event of radiation events along the aforementioned track. Along these tracks are events referred to as spurs and blobs. These are clusters of hydroxyl, peroxyl, and other radicals along each track. They are typically the equivalent to the diameter of DNA, and in effect cause the most damage seen in a double strand DNA break. A track is dependent upon the range of the energy of the particle within a specific medium. For example, Ni-63 has a maximum range of 5 cm in air and 60 μm in water, leading to tracks of radiation events along this range equaling 1 keV/μm.[28] This value is commonly referred to as its Linear energy transfer (LET), defined as the average energy (dE) deposited into a medium traveling along a distance l (dl). The importance of LET in radiobiology research is that it is an indication of the relative biologic effectiveness (RBE). Relative biologic effectiveness is a term describing the absorbed dose in units Grey (Gy = J/kg). However, equal doses of 1 Gy from a beta emitting source and a gamma emitting source are not equivalent, and this is due to the LET.

A.1.3 Foci Formation

Once a dsDNA break occurs, various enzymes, genes and repair proteins begin the DNA repair process. To visualize the double strand DNA break, compounds that participate in the dsDNA event are labeled with a fluorescent labeled protein. Once the dsDNA break occurs, these fluorescently labeled repair proteins migrate to the break site, and the multiple fluorescent-labeled proteins are then visualized as a small focal point of

light under a microscope, commonly referred to as foci. Each foci has been calibrated to represent one dsDNA break.[52]

The fluorescent compounds that are synthesized onto the repair proteins are fluorophores. Each fluorophore absorbs at a specific wavelength, and emits light at a different wavelength during de-excitation. The most commonly known fluorophore is the green fluorescent protein, GFP.[97] The discovery of this protein has lead to many other variations as well, suitable to each specific experiment. In these experiments, a Halo-TMR specialized fluorophore is made, by Promega. Within this fluor, instead of GFP tetramethyl rhodamine dextran is used. The advantages of using the Halo-TMR fluor is that it can be rapidly introduced and reproduced by the cell, enabling experiments to commence within 72 hrs of introduction.[98]

A.2 Supplemental Information for Chapter Four

A.2.1 DNA sequence of pcDNA-DEST40-EYFP-53BP1 WT

GACGGATCGGGAGATCTCCCGATCCCCTATGGTGCACTCTCAGTACAATCTG

CTCTGATGCCGCATAGTTAAGCCAGTATCTGCTCCCTGCTTGTGTGTTGGAGG

TCGCTGAGTAGTGCGCGAGCAAAATTTAAGCTACAACAAGGCAAGGCTTGAC

CGACAATTGCATGAAGAATCTGCTTAGGGTTAGGCGTTTTGCGCTGCTTCGCG

ATGTACGGGCCAGATATACGCGTTGACATTGATTATTGACTAGTTATTAATAG

TAATCAATTACGGGGTCATTAGTTCATAGCCCATATATGGAGTTCCGCGTTAC

ATAACTTACGGTAAATGGCCCGCCTGGCTGACCGCCCAACGACCCCCGCCCA

TTGACGTCAATAATGACGTATGTTCCCATAGTAACGCCAATAGGGACTTTCCA

TTGACGTCAATGGGTGGAGTATTTACGGTAAACTGCCCACTTGGCAGTACATC

AAGTGTATCATATGCCAAGTACGCCCCCTATTGACGTCAATGACGGTAAATG

GCCCGCCTGGCATTATGCCCAGTACATGACCTTATGGGACTTTCCTACTTGGC

AGTACATCTACGTATTAGTCATCGCTATTACCATGGTGATGCGGTTTTGGCAG

TACATCAATGGGCGTGGATAGCGGTTTGACTCACGGGGATTTCCAAGTCTCC

ACCCCATTGACGTCAATGGGAGTTTGTTTTGGCACCAAAATCAACGGGACTTT

CCAAAATGTCGTAACAACTCCGCCCCATTGACGCAAATGGGCGGTAGGCGTG

TACGGTGGGAGGTCTATATAAGCAGAGCTCTCTGGCTAACTAGAGAACCCAC

TGCTTACTGGCTTATCGAAATTAATACGACTCACTATAGGGAGACCCAAGCT

GGCTAGTTAAGCTATCAACAAGTTTGTACAAAAAAGCAGGCTCCGCGGCCGC

GCCACCATGGTGAGCAAGGGCGAGGAGCTGTTCACCGGGGTGGTGCCCATCC

TGGTCGAGCTGGACGGCGACGTAAACGGCCACAAGTTCAGCGTGTCCGGCGA

GGGCGAGGGCGATGCCACCTACGGCAAGCTGACCCTGAAGTTCATCTGCACC

ACCGGCAAGCTGCCCGTGCCCTGGCCCACCCTCGTGACCACCTTCGGCTACG

GCCTGCAGTGCTTCGCCCGCTACCCCGACCACATGAAGCAGCACGACTTCTTC

AAGTCCGCCATGCCCGAAGGCTACGTCCAGGAGCGCACCATCTTCTTCAAGG

ACGACGGCAACTACAAGACCCGCGCCGAGGTGAAGTTCGAGGGCGACACCC

TGGTGAACCGCATCGAGCTGAAGGGCATCGACTTCAAGGAGGACGGCAACAT

CCTGGGGCACAAGCTGGAGTACAACTACAACAGCCACAACGTCTATATCATG

GCCGACAAGCAGAAGAACGGCATCAAGGTGAACTTCAAGATCCGCCACAAC

ATCGAGGACGGCAGCGTGCAGCTCGCCGACCACTACCAGCAGAACACCCCCA

TCGGCGACGGCCCCGTGCTGCTGCCCGACAACCACTACCTGAGCTACCAGTC

CGCCCTGAGCAAAGACCCCAACGAGAAGCGCGATCACATGGTCCTGCTGGAG

TTCGTGACCGCCGCCGGGATCACTCTCGGCATGGACGAGCTGTACAAGCTCG

AGATGGACCCTACTGGAAGTCAGTTGGATTCAGATTTCTCTCAGCAAGATACT

CCTTGCCTGATAATTGAAGATTCTCAGCCTGAAAGCCAGGTTCTAGAGGATG

ATTCTGGTTCTCACTTCAGTATGCTATCTCGACACCTTCCTAATCTCCAGACGC

ACAAAGAAAATCCTGTGTTGGATGTTGTGTCCAATCCTGAACAAACAGCTGG

AGAAGAACGAGGAGACGGTAATAGTGGGTTCAATGAACATTTGAAAGAAAA

CAAGGTTGCAGACCCTGTGGATTCTTCTAACTTGGACACATGTGGTTCCATCA

GTCAGGTCATTGAGCAGTTACCTCAGCCAAACAGGACAAGCAGTGTTCTGGG

AATGTCAGTGGAATCTGCTCCTGCTGTGGAGGAAGAGAAGGGAGAAGAGTTG

GAACAGAAGGAGAAAGAGAAGGAAGAAGATACTTCAGGCAATACTACACAT

TCCCTTGGTGCTGAAGATACTGCCTCATCACAGTTGGGTTTTGGGGTTCTGGA

ACTCTCCCAGAGCCAGGATGTTGAGGAAAATACTGTGCCATATGAAGTGGAC

AAAGAGCAGCTACAATCAGTAACCACCAACTCTGGTTATACCAGGCTGTCTG

ATGTGGATGCTAATACTGCAATTAAGCATGAAGAACAGTCCAACGAAGATAT

CCCCATAGCAGAACAGTCCAGCAAGGACATCCCTGTGACAGCACAGCCCAGT

AAGGATGTACATGTTGTAAAAGAGCAAAATCCACCACCTGCAAGGTCAGAGG

ACATGCCTTTTAGCCCCAAAGCATCTGTTGCTGCTATGGAAGCAAAAGAACA

GTTGTCTGCACAAGAACTTATGGAAAGTGGACTGCAGATTCAGAAGTCACCA

GAGCCTGAGGTTTTGTCAACTCAGGAAGACTTGTTTGACCAGAGCAATAAAA

CAGTATCTTCTGATGGTTGCTCTACTCCTTCAAGGGAGGAAGGTGGGTGTTCT

TTGGCTTCCACTCCTGCCACCACTCTGCATCTCCTGCAGCTCTCTGGTCAGAG

GTCCCTTGTTCAGGACAGTCTTTCCACGAATTCTTCAGATCTTGTTGCTCCTTC

TCCTGATGCTTTCCGATCTACTCCTTTTATCGTTCCTAGCAGTCCCACAGAGCA

AGAAGGGAGACAAGATAAGCCAATGGACACGTCAGTGTTATCTGAAGAAGG

AGGAGAGCCTTTTCAGAAGAAACTTCAAAGTGGTGAACCAGTGGAGTTAGAA

AACCCCCCTCTCCTGCCTGAGTCCACTGTATCACCACAAGCCTCAACACCAAT

ATCTCAGAGCACACCAGTCTTCCCTCCTGGGTCACTTCCTATCCCATCCCAGC

CTCAGTTTTCTCATGACATTTTTATTCCTTCCCCAAGTCTGGAAGAACAATCA

AATGATGGGAAGAAAGATGGAGATATGCATAGTTCATCTTTGACAGTTGAGT

GTTCTAAAACTTCAGAGATTGAACCAAAGAATTCCCCTGAGGATCTTGGGCT

ATCTTTGACAGGGGATTCTTGCAAGTTGATGCTTTCTACAAGTGAATATAGTC

AGTCCCCAAAGATGGAGAGCTTGAGTTCTCACAGAATTGATGAAGATGGAGA

AAACACACAGATTGAGGATACGGAACCCATGTCTCCAGTTCTCAATTCTAAA

TTTGTTCCTGCTGAAAATGATAGTATCCTGATGAATCCAGCACAGGATGGTGA

AGTACAACTGAGTCAGAATGATGACAAAACAAAGGGAGATGATACAGACAC

CAGGGATGACATTAGTATTTTAGCCACTGGTTGCAAGGGCAGAGAAGAAACG

GTAGCAGAAGATGTTTGTATTGATCTCACTTGTGATTCGGGGAGTCAGGCAGT

TCCGTCACCAGCTACTCGATCTGAGGCACTTTCTAGTGTGTTAGATCAGGAGG

AAGCTATGGAAATTAAAGAACACCATCCAGAGGAGGGGTCTTCAGGGTCTGA

GGTGGAAGAAATCCCTGAGACACCTTGTGAAAGTCAAGGAGAGGAACTCAA

AGAAGAAAATATGGAGAGTGTTCCGTTGCACCTTTCTCTGACTGAAACTCAG

TCCCAAGGGTTGTGTCTTCAAAAGGAAATGCCAAAAAAAGAATGCTCAGAAG

CTATGGAAGTTGAAACCAGTGTGATTAGTATTGATTCCCCTCAAAAGTTGGCA

ATACTTGACCAAGAATTGGAACATAAGGAACAGGAAGCTTGGGAAGAAGCT

ACTTCAGAGGACTCCAGTGTTGTCATTGTAGATGTGAAAGAGCCATCTCCCA

GAGTTGATGTTTCTTGTGAACCTTTGGAGGGAGTGGAGAAGTGCTCAGATTCC

CAGTCATGGGAGGATATTGCTCCAGAAATAGAACCATGTGCTGAGAATAGAT

TAGACACCAAGGAAGAAAAGAGTGTAGAATATGAAGGAGATCTGAAATCAG

GGACTGCAGAAACAGAACCTGTAGAGCAAGATTCTTCACAGCCTTCCTTACC

TTTAGTGAGAGCAGATGATCCTTTAAGACTTGACCAGGAGTTGCAGCAGCCC

CAAACTCAGGAGAAAACAAGTAATTCATTAACAGAAGACTCAAAAATGGCT

AATGCAAAGCAGCTAAGCTCAGATGCAGAGGCCCAGAAGCTGGGGAAGCCC

TCTGCCCATGCCTCACAAAGCTTCTGTGAAAGTTCTAGTGAAACCCCATTTCA

TTTCACTTTGCCTAAAGAAGGTGATATCATCCCACCATTGACTGGTGCAACCC

CACCTCTTATTGGGCACCTAAAATTGGAGCCCAAGAGACACAGTACTCCTATT

GGTATTAGCAACTATCCAGAAAGCACCATAGCAACCAGTGATGTCATGTCTG

AAAGCATGGTGGAGACCCATGATCCCATACTTGGGAGTGGAAAAGGGGATTC

TGGGGCTGCCCCAGACGTGGATGATAAATTATGTCTAAGAATGAAACTGGTT

AGTCCTGAGACTGAGGCGAGTGAAGAGTCTTTGCAGTTCAACCTGGAAAAGC

CTGCAACTGGTGAAAGAAAAAATGGATCTACTGCTGTTGCTGAGTCTGTTGC

CAGTCCCCAGAAGACCATGTCTGTGTTGAGCTGTATCTGTGAAGCCAGGCAA

GAGAATGAGGCTCGAAGTGAGGATCCCCCCACCACACCCATCAGGGGGAAC

TTGCTCCACTTTCCAAGTTCTCAAGGAGAAGAGGAGAAAGAAAAATTGGAGG

GTGACCATACAATCAGGCAGAGTCAACAGCCTATGAAGCCCATTAGTCCTGT

CAAGGACCCTGTTTCTCCTGCTTCCCAGAAGATGGTCATACAAGGGCCATCC

AGTCCTCAAGGAGAGGCAATGGTGACAGATGTGCTAGAAGACCAGAAAGAA

GGACGGAGTACTAATAAGGAAAATCCTAGTAAGGCCTTGATTGAAAGGCCCA

GCCAAAATAACATAGGAATCCAAACCATGGAGTGTTCCTTGAGGGTCCCAGA

AACTGTTTCAGCAGCAACCCAGACTATAAAGAATGTGTGTGAGCAGGGGACC

AGTACAGTGGACCAGAACTTTGGAAAGCAAGATGCCACAGTTCAGACTGAGA

GGGGGAGTGGTGAGAAACCAGTCAGTGCTCCTGGGGATGATACAGAGTCGCT

CCATAGCCAGGGAGAAGAAGAGTTTGATATGCCTCAGCCTCCACATGGCCAT

GTCTTACATCGTCACATGAGAACAATCCGGGAAGTACGCACACTTGTCACTC

GTGTCATTACAGATGTGTATTATGTGGATGGAACAGAAGTAGAAAGAAAAGT

AACTGAGGAGACTGAAGAGCCAATTGTAGAGTGTCAGGAGTGTGAAACTGA

AGTTTCCCCTTCACAGACTGGGGGCTCCTCAGGTGACCTGGGGGATATCAGCT

CCTTCTCCTCCAAGGCATCCAGCTTACACCGCACATCAAGTGGGACAAGTCTC

TCAGCTATGCACAGCAGTGGAAGCTCAGGGAAAGGAGCCGGACCACTCAGA

GGGAAAACCAGCGGGACAGAACCCGCAGATTTTGCCTTACCCAGCTCCCGAG

GAGGCCCAGGAAAACTGAGTCCTAGAAAAGGGGTCAGTCAGACAGGGACGC

CAGTGTGTGAGGAGGATGGTGATGCAGGCCTTGGCATCAGACAGGGAGGGA

AGGCTCCAGTCACGCCTCGTGGGCGTGGGCGAAGGGGCCGCCCACCTTCTCG

GACCACTGGAACCAGAGAAACAGCTGTGCCTGGCCCCTTGGGCATAGAGGAC

ATTTCACCTAACTTGTCACCAGATGATAAATCCTTCAGCCGTGTCGTGCCCCG

AGTGCCAGACTCCACCAGACGAACAGATGTGGGTGCTGGTGCTTTGCGTCGT

AGTGACTCTCCAGAAATTCCTTTCCAGGCTGCTGCTGGCCCTTCTGATGGCTT

AGATGCCTCCTCTCCAGGAAATAGCTTTGTAGGGCTCCGTGTTGTAGCCAAGT

GGTCATCCAATGGCTACTTTTACTCTGGGAAAATCACACGAGATGTCGGAGC

TGGGAAGTATAAATTGCTCTTTGATGATGGGTACGAATGTGATGTGTTGGGC

AAAGACATTCTGTTATGTGACCCCATCCCGCTGGACACTGAAGTGACGGCCC

TCTCGGAGGATGAGTATTTCAGTGCAGGAGTGGTGAAAGGACATAGGAAGG

AGTCTGGGGAACTGTACTACAGCATTGAAAAAGAAGGCCAAAGAAAGTGGT

ATAAGCGAATGGCTGTCATCCTGTCCTTGGAGCAAGGAAACAGACTGAGAGA

GCAGTATGGGCTTGGCCCCTATGAAGCAGTAACACCTCTTACAAAGGCAGCA

GATATCAGCTTAGACAATTTGGTGGAAGGGAAGCGGAAACGGCGCAGTAAC

GTCAGCTCCCCAGCCACCCCTACTGCCTCCAGTAGCAGCAGCACAACCCCTA

CCCGAAAGATCACAGAAAGTCCTCGTGCCTCCATGGGAGTTCTCTCAGGCAA

AAGAAAACTTATCACTTCTGAAGAGGAACGGTCCCCTGCCAAGCGAGGTCGC

AAGTCTGCCACAGTAAAACCTGGTGCAGTAGGGGCAGGAGAGTTTGTGAGCC

CCTGTGAGAGTGGAGACAACACCGGTGAACCCTCTGCCCTGGAAGAGCAGA

GAGGGCCTTTGCCTCTCAACAAGACCTTGTTTCTGGGCTACGCATTTCTCCTT

ACCATGGCCACAACCAGTGACAAGTTGGCCAGCCGCTCCAAACTGCCAGATG

GTCCTACAGGAAGCAGTGAAGAAGAGGAGGAATTTTTGGAAATTCCTCCTTT

CAACAAGCAGTATACAGAATCCCAGCTTCGAGCAGGAGCTGGCTATATCCTT

GAAGATTTCAATGAAGCCCAGTGTAACACAGCTTACCAGTGTCTTCTAATTGC

GGATCAGCATTGTCGAACCCGGAAGTACTTCCTGTGCCTTGCCAGTGGGATTC

CTTGTGTGTCTCATGTCTGGGTCCATGATAGTTGCCATGCCAACCAGCTCCAG

AACTACCGTAATTATCTGTTGCCAGCTGGGTACAGCCTTGAGGAGCAAAGAA

TTCTGGACTGGCAACCCCGTGAAAATCCTTTCCAGAATCTGAAGGTACTCTTG

GTATCAGACCAACAGCAGAACTTCCTGGAGCTCTGGTCTGAGATCCTCATGA

CTGGTGGTGCAGCCTCTGTGAAGCAGCACCATTCAAGTGCCCATAACAAAGA

TATTGCTTTAGGGGTATTTGATGTGGTGGTGACGGACCCCTCATGCCCAGCCT

CGGTGCTGAAGTGTGCTGAAGCATTGCAGCTGCCTGTGGTGTCACAAGAGTG

GGTGATCCAGTGCCTCATTGTTGGGGAGAGAATTGGATTCAAGCAGCATCCA

AAATATAAACACGATTATGTTTCTCACTAAAGATACTTGGTCTTACTGGTTTT

ATTCCCTGCTATCGTGGAGATTGTGTTAAGGGCGAATTCCAGCACACTGGCG

GCCGTTACTAGTGGATCCGAGCTCGGTACCGCGGGCCCGGGATCCACCGGAT

CTAGATAACTGATCAGCAAGGGTGGGCGCGCCGACCCAGCTTTCTTGTACAA

AGTGGTTGATCTAGAGGGCCCGCGGTTCGAAGGTAAGCCTATCCCTAACCCT

CTCCTCGGTCTCGATTCTACGCGTACCGGTCATCATCACCATCACCATTGAGT

TTAAACCCGCTGATCAGCCTCGACTGTGCCTTCTAGTTGCCAGCCATCTGTTG

TTTGCCCCTCCCCCGTGCCTTCCTTGACCCTGGAAGGTGCCACTCCCACTGTC

CTTTCCTAATAAAATGAGGAAATTGCATCGCATTGTCTGAGTAGGTGTCATTC

TATTCTGGGGGGTGGGGTGGGGCAGGACAGCAAGGGGGAGGATTGGGAAGA

CAATAGCAGGCATGCTGGGGATGCGGTGGGCTCTATGGCTTCTGAGGCGGAA

AGAACCAGCTGGGGCTCTAGGGGGTATCCCCACGCGCCCTGTAGCGGCGCAT

TAAGCGCGGCGGGTGTGGTGGTTACGCGCAGCGTGACCGCTACACTTGCCAG

CGCCCTAGCGCCCGCTCCTTTCGCTTTCTTCCCTTCCTTTCTCGCCACGTTCGC

CGGCTTTCCCCGTCAAGCTCTAAATCGGGGGCTCCCTTTAGGGTTCCGATTTA

GTGCTTTACGGCACCTCGACCCCAAAAAACTTGATTAGGGTGATGGTTCACGT

AGTGGGCCATCGCCCTGATAGACGGTTTTTCGCCCTTTGACGTTGGAGTCCAC

GTTCTTTAATAGTGGACTCTTGTTCCAAACTGGAACAACACTCAACCCTATCT

CGGTCTATTCTTTTGATTTATAAGGGATTTTGCCGATTTCGGCCTATTGGTTAA

AAAATGAGCTGATTTAACAAAAATTTAACGCGAATTAATTCTGTGGAATGTG

TGTCAGTTAGGGTGTGGAAAGTCCCCAGGCTCCCCAGCAGGCAGAAGTATGC

AAAGCATGCATCTCAATTAGTCAGCAACCAGGTGTGGAAAGTCCCCAGGCTC

CCCAGCAGGCAGAAGTATGCAAAGCATGCATCTCAATTAGTCAGCAACCATA

GTCCCGCCCCTAACTCCGCCCATCCCGCCCCTAACTCCGCCCAGTTCCGCCCA

TTCTCCGCCCCATGGCTGACTAATTTTTTTTATTTATGCAGAGGCCGAGGCCG

CCTCTGCCTCTGAGCTATTCCAGAAGTAGTGAGGAGGCTTTTTTGGAGGCCTA

GGCTTTTGCAAAAAGCTCCCGGGAGCTTGTATATCCATTTTCGGATCTGATCA

AGAGACAGGATGAGGATCGTTTCGCATGATTGAACAAGATGGATTGCACGCA

GGTTCTCCGGCCGCTTGGGTGGAGAGGCTATTCGGCTATGACTGGGCACAAC

AGACAATCGGCTGCTCTGATGCCGCCGTGTTCCGGCTGTCAGCGCAGGGGCG

CCCGGTTCTTTTTGTCAAGACCGACCTGTCCGGTGCCCTGAATGAACTGCAGG

ACGAGGCAGCGCGGCTATCGTGGCTGGCCACGACGGGCGTTCCTTGCGCAGC

TGTGCTCGACGTTGTCACTGAAGCGGGAAGGGACTGGCTGCTATTGGGCGAA

GTGCCGGGGCAGGATCTCCTGTCATCTCACCTTGCTCCTGCCGAGAAAGTATC

CATCATGGCTGATGCAATGCGGCGGCTGCATACGCTTGATCCGGCTACCTGC

CCATTCGACCACCAAGCGAAACATCGCATCGAGCGAGCACGTACTCGGATGG

AAGCCGGTCTTGTCGATCAGGATGATCTGGACGAAGAGCATCAGGGGCTCGC

GCCAGCCGAACTGTTCGCCAGGCTCAAGGCGCGCATGCCCGACGGCGAGGAT

CTCGTCGTGACCCATGGCGATGCCTGCTTGCCGAATATCATGGTGGAAAATG

GCCGCTTTTCTGGATTCATCGACTGTGGCCGGCTGGGTGTGGCGGACCGCTAT

CAGGACATAGCGTTGGCTACCCGTGATATTGCTGAAGAGCTTGGCGGCGAAT

GGGCTGACCGCTTCCTCGTGCTTTACGGTATCGCCGCTCCCGATTCGCAGCGC

ATCGCCTTCTATCGCCTTCTTGACGAGTTCTTCTGAGCGGGACTCTGGGGTTC

GCGAAATGACCGACCAAGCGACGCCCAACCTGCCATCACGAGATTTCGATTC

CACCGCCGCCTTCTATGAAAGGTTGGGCTTCGGAATCGTTTTCCGGGACGCCG

GCTGGATGATCCTCCAGCGCGGGGATCTCATGCTGGAGTTCTTCGCCCACCCC

AACTTGTTTATTGCAGCTTATAATGGTTACAAATAAAGCAATAGCATCACAA

ATTTCACAAATAAAGCATTTTTTTCACTGCATTCTAGTTGTGGTTTGTCCAAAC

TCATCAATGTATCTTATCATGTCTGTATACCGTCGACCTCTAGCTAGAGCTTG

GCGTAATCATGGTCATAGCTGTTTCCTGTGTGAAATTGTTATCCGCTCACAAT

TCCACACAACATACGAGCCGGAAGCATAAAGTGTAAAGCCTGGGGTGCCTAA

TGAGTGAGCTAACTCACATTAATTGCGTTGCGCTCACTGCCCGCTTTCCAGTC

GGGAAACCTGTCGTGCCAGCTGCATTAATGAATCGGCCAACGCGCGGGGAGA

GGCGGTTTGCGTATTGGGCGCTCTTCCGCTTCCTCGCTCACTGACTCGCTGCG

CTCGGTCGTTCGGCTGCGGCGAGCGGTATCAGCTCACTCAAAGGCGGTAATA

CGGTTATCCACAGAATCAGGGGATAACGCAGGAAAGAACATGTGAGCAAAA

GGCCAGCAAAAGGCCAGGAACCGTAAAAAGGCCGCGTTGCTGGCGTTTTTCC

ATAGGCTCCGCCCCCCTGACGAGCATCACAAAAATCGACGCTCAAGTCAGAG

GTGGCGAAACCCGACAGGACTATAAAGATACCAGGCGTTTCCCCCTGGAAGC

TCCCTCGTGCGCTCTCCTGTTCCGACCCTGCCGCTTACCGGATACCTGTCCGC

CTTTCTCCCTTCGGGAAGCGTGGCGCTTTCTCATAGCTCACGCTGTAGGTATC

TCAGTTCGGTGTAGGTCGTTCGCTCCAAGCTGGGCTGTGTGCACGAACCCCCC

GTTCAGCCCGACCGCTGCGCCTTATCCGGTAACTATCGTCTTGAGTCCAACCC

GGTAAGACACGACTTATCGCCACTGGCAGCAGCCACTGGTAACAGGATTAGC

AGAGCGAGGTATGTAGGCGGTGCTACAGAGTTCTTGAAGTGGTGGCCTAACT

ACGGCTACACTAGAAGAACAGTATTTGGTATCTGCGCTCTGCTGAAGCCAGT

TACCTTCGGAAAAAGAGTTGGTAGCTCTTGATCCGGCAAACAAACCACCGCT

GGTAGCGGTGGTTTTTTTGTTTGCAAGCAGCAGATTACGCGCAGAAAAAAAG

GATCTCAAGAAGATCCTTTGATCTTTTCTACGGGGTCTGACGCTCAGTGGAAC

GAAAACTCACGTTAAGGGATTTTGGTCATGAGATTATCAAAAAGGATCTTCA

CCTAGATCCTTTTAAATTAAAAATGAAGTTTTAAATCAATCTAAAGTATATAT

GAGTAAACTTGGTCTGACAGTTACCAATGCTTAATCAGTGAGGCACCTATCTC

AGCGATCTGTCTATTTCGTTCATCCATAGTTGCCTGACTCCCCGTCGTGTAGA

TAACTACGATACGGGAGGGCTTACCATCTGGCCCCAGTGCTGCAATGATACC

GCGAGACCCACGCTCACCGGCTCCAGATTTATCAGCAATAAACCAGCCAGCC

GGAAGGGCCGAGCGCAGAAGTGGTCCTGCAACTTTATCCGCCTCCATCCAGT

CTATTAATTGTTGCCGGGAAGCTAGAGTAAGTAGTTCGCCAGTTAATAGTTTG

CGCAACGTTGTTGCCATTGCTACAGGCATCGTGGTGTCACGCTCGTCGTTTGG

TATGGCTTCATTCAGCTCCGGTTCCCAACGATCAAGGCGAGTTACATGATCCC

CCATGTTGTGCAAAAAAGCGGTTAGCTCCTTCGGTCCTCCGATCGTTGTCAGA

AGTAAGTTGGCCGCAGTGTTATCACTCATGGTTATGGCAGCACTGCATAATTC

TCTTACTGTCATGCCATCCGTAAGATGCTTTTCTGTGACTGGTGAGTACTCAA

CCAAGTCATTCTGAGAATAGTGTATGCGGCGACCGAGTTGCTCTTGCCCGGC

GTCAATACGGGATAATACCGCGCCACATAGCAGAACTTTAAAAGTGCTCATC

ATTGGAAAACGTTCTTCGGGGCGAAAACTCTCAAGGATCTTACCGCTGTTGA

GATCCAGTTCGATGTAACCCACTCGTGCACCCAACTGATCTTCAGCATCTTTT

ACTTTCACCAGCGTTTCTGGGTGAGCAAAAACAGGAAGGCAAAATGCCGCAA

AAAAGGGAATAAGGGCGACACGGAAATGTTGAATACTCATACTCTTCCTTTT

TCAATATTATTGAAGCATTTATCAGGGTTATTGTCTCATGAGCGGATACATAT

TTGAATGTATTTAGAAAAATAAACAAATAGGGGTTCCGCGCACATTTCCCCG

AAAAGTGCCACCTGACGTC

A.2.2 Dose estimate for hemispherical microirradiator

One of the most important characteristics of chapter four was estimating the dose each cell received from the microirradiator used. The dose that was estimated from the 2000 Bq flush-deposited microirradiator followed the equation

$$D_{\beta} = (5.678\ x\ 10^{-5})\Phi_{\beta}\mu_{\beta}\bar{E}[e^{\rho_a x_a \mu}][e^{\rho_b x_b \mu}](0.5) \quad (15)$$

Where D_β is the dose rate in Rad/hr, Φ_β is the flux of beta particles in Bq/cm^2, $\bar{E}$ is average energy of the beta particles, μ is the absorption coefficient of beta particles in deposition material (370 cm^2/g), ρ_a is density of the PEDOT coating in g/cm^3, x_a is thickness of the PEDOT in cm, ρ_b is the density of water in g/cm^3, x_b is the working distance between the microirradiator and the target DNA, and 0.5 is the geometric factor for a hemispherical emitter. The flux density, Φ_β was calculated by dividing the total activity (2000 Bq) by the surface area of the plated electrode in cm^2. The nominal diameter of the microirradiator itself is 25 μm and the area is $3\pi r^2$, equating Φ_β equal to 1.35 10^8.The average energy $\bar{E}$ is assumed to be 1/3 of the maximum energy, or 0.017 MeV. The PEDOT density ρ_a is 0.87 g/cm^3 and the PEDOT thickness x_a is 0.0001 cm (10 μm). The water density ρ_b is 1.0 g/cm^3 and the working distance x_a is 0.001 cm. However, the working distance within the water can be varied to show an estimation of where the exact location of the microirradiator was placed in relation to the cell. Due to this, estimated dose rates decline to 1.88 Gy/min at 20 μm and 1.30 Gy/min at 30 μm.

APPENDIX B

INCOMPLETE WORK: MINIATURE NICKEL-63 ELECTRON CAPTURE DETECTOR

B.1 Introduction

The electron capture detector was first invented in the 1950's by J.E. Lovelock.[99] The principle behind the electron capture detector is that a radioactive source ionizes the carrier gas (N, He, Ar) within a chamber forming a stable cloud of free electrons. This cloud will generate a current, around 1-10 nA. When electronegative compounds are introduced into the chamber, the compounds absorb electrons, causing a decrease in current. Originally, the idea behind this steady ionization cloud within a chamber came from an anemometer that had contained Radium painted dials.[99] Observations were made but never fully understood that when cigarette smoke passed through the anemometer, the signal would be quenched. From this observation, J.E. Lovelock tweaked this idea using Tritium painted silver foils, Sr-90 foils, and eventually Ni-63.[100, 101]

Today, virtually all ECD are composed of Ni-63 metal foils, ranging from 10-15 mCi. This foil is located within a stainless steel chamber, in which electrodes placed within the chamber with a few volts applied generates a standing current in the nA region. With this being said, the shape and activity of the Ni-63 foil has not changed since its invention. Micro-ECDs have been invented, but this is the inlets and outlets being scaled down to the micron size, improving detection limits due to volume constrictions.[102 103] With using the experimental procedure for plating Ni-63 discussed in

Chapter 2, a miniature Ni-63 ECD detector has been built in the first step in creating a micro-ECD-GC system on a chip that is field portable.

B.2 Experimental

The design of the ECD consists of a stainless steel tube (23 mm length, 7.9 mm width, 500 um cavitiy) with a .02 inch hole drilled into the center of the tube. A more detailed description of the ECD housing can be seen in Figure 39. An acetal screw .08 in diameter, .125 in. length is placed into this hole, with an additional .02 in. hole drilled into the center of the screw. A 28 μCi Ni-63 source following procedures outlined in Chapter 2 was plated on the

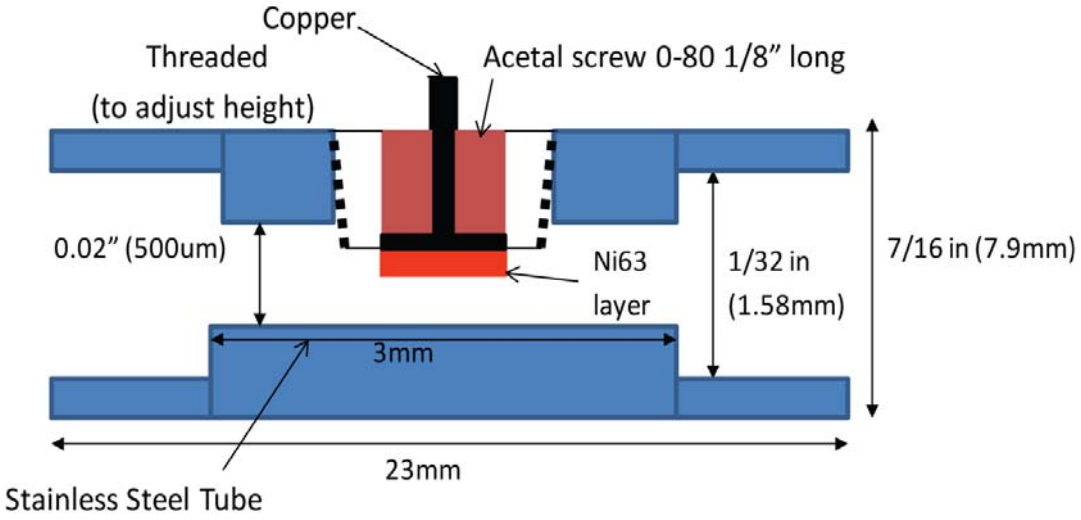

Figure 43. Diagram of ECD housing with Ni-63 source inside.

distal end of a 1mm diameter, 2 cm in length copper wire. The Ni-63 plated copper wire was inserted into the .02 in. drilled hole of the acetal screw, and sealed with epoxy. The Ni-63 source was unscrewed slightly out of the stainless steel tube to ensure no unintentional contact between the two, confirmed by monitoring the current passed

between the tube and the wire source. A micro Agilent column was inserted into both ends of the electron capture detector. Helium gas was chosen as the carrier gas for all experiments. The first set of calibration curves involves solutions of simple chloroalkanes of various chain lengths including 1-chlorodecane, 1-chloroctane, and 1-chlorononane in hexane.

The purpose of the development of this prototype of a miniature ECD is to eventually fabricate a device composed of silicon, that can be housed onto a chip for a low cost, field portable GC system. These initial tests involve the miniature Ni-63 ECD prototype used in conjunction with an He carrier Aglient 6850 fast GC system in tandem with flame ionization source (FID), confirmating of the analytes elution from the column. Aglient 6850 computer software will record data from the FID detector, in tandem with manual recording of the current from a princeton applied research (PAR) pico-ammeter.

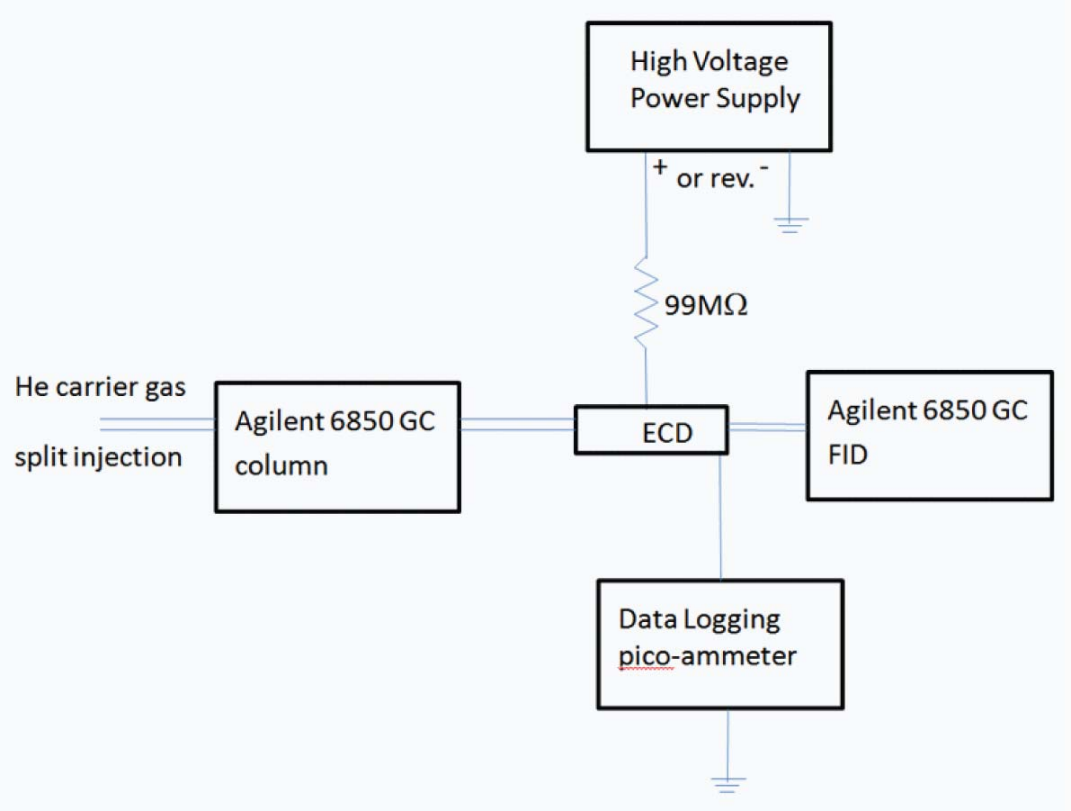

Figure 44. Gas Chromatography setup with Ni-63 miniature ECD.

B.3 Initial Results and Future Work

Initial results from the gas chromatography setup indicate a significant gas leak throughout the system, rendering zero signal from either the FID or the ECD detectors. At this time, investigation of the gas leak must be done in order to achieve positive results from either detector. In the future, the optimization of either constant voltage or constant current has not been achieved. Constant current applied to the electron capture detector has been known to stabilize the baseline of the signal.[104] In constant voltage applications, baseline drift is a common problem, and this is what has been observed in the initial trials of the miniature ECD.

Besides the gas leak, the current configuration has the Ni-63 wire source orgthogonal to the anode, making it difficult to know the distance from the tip of the wire to the anode. To solve this, a new configuration involving the Ni-63 wire parallel to the anode will be developed. This allows a definitive calculation of the electric field and confident the Ni-63 is not in contact with the anode.

APPENDIX C

INCOMPLETE WORK: POLYANILINE REVERSIBLE RADIATION SENSOR

C.1 Introduction

Polyaniline (PANI) is an electrically conducting polymer composing of three main oxidation states: leucoemeraldine, emeraldine, and pernigraniline. Leucoemeraldine is the fully reduced state, with an appearance of a white to yellow-green state. Emeraldine, a forest green color, is the neutral state and the most common form of polyaniline, due to its ability to be doped and stability.[105] Pernigraniline, the most oxidized state, has an appearance of blue to violet in color. The ability to visualize these color changes leads to the potential of polyaniline used as a reversible radiation sensor.

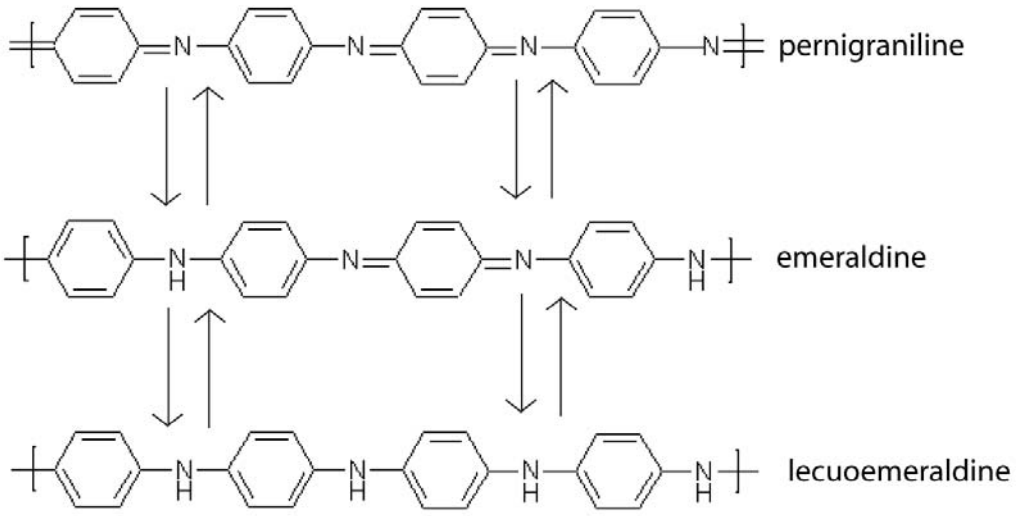

Figure 45. Structure of PANI in different redox states

C.2 Results

Within the literature, PANI has been shown to increase in conductivity linearly to radiation dose. The majority of this research however has dealt with interaction of gamma rays from Co-60 rather than any other types of radiation.[106, 107] As a preliminary experiment, we chose to test PANI synthesized onto a 1.8 mm diameter Pt electrode (BAS, Inc.) from .1M aniline in 1 M HCl held at .9 V vs Ag/AgCl for 100 seconds. The color of the PANI film was dark green, indicating the polymer was in its emeraldine state. After deposition, the PANI film was cycled in 1 M HCl from -.1 to .85 V and stopped at -.1V. The color of the PANI film at this stage was yellow-green, indicative of the leucoemeraldine state. After cycling, each film without drying was exposed to a custom made 100 μCi Ni-63 source, which instantaneously changed the color of the PANI film from yellow-green to dark green, indicating an oxidation of the PANI from leucoemeraldine to emeraldine. After exposure to beta radiation, a CV of the electrode with the PANI film was taken in 1 M HCl, and the results compared against each other. In Figure 41, a graph of the initial cycle of PANI without radiation, 1 hr exposure of radiation to PANI, and 50 min of relaxation post irradiation. After irradiation of the polymer, the voltammogram's area increases, indicating a radiation induced change within the polymer. However, after allowing the irradiation PANI to relax for 50 minutes, the polymer relaxed back to its original conformation. Based on these results, manufacturing a reversible PANI radiation sensor for Ni-63 seemed achievable.

PANI doped with Cl- has been shown under exposure to gamma irradiation to increase conductivity within the polymer film.[108, 109] Experiments without additional doping compounds were performed, and no observable difference we shown. From this

observation, incorporating more electronegative compounds that are sensitive in electron capture detection was the next plausible step in converting PANI into a reversible Ni-63 radiation sensor. Electron capture detectors, as discussed in Appendix A, are extremely sensitive detection methods for electronegative compounds.

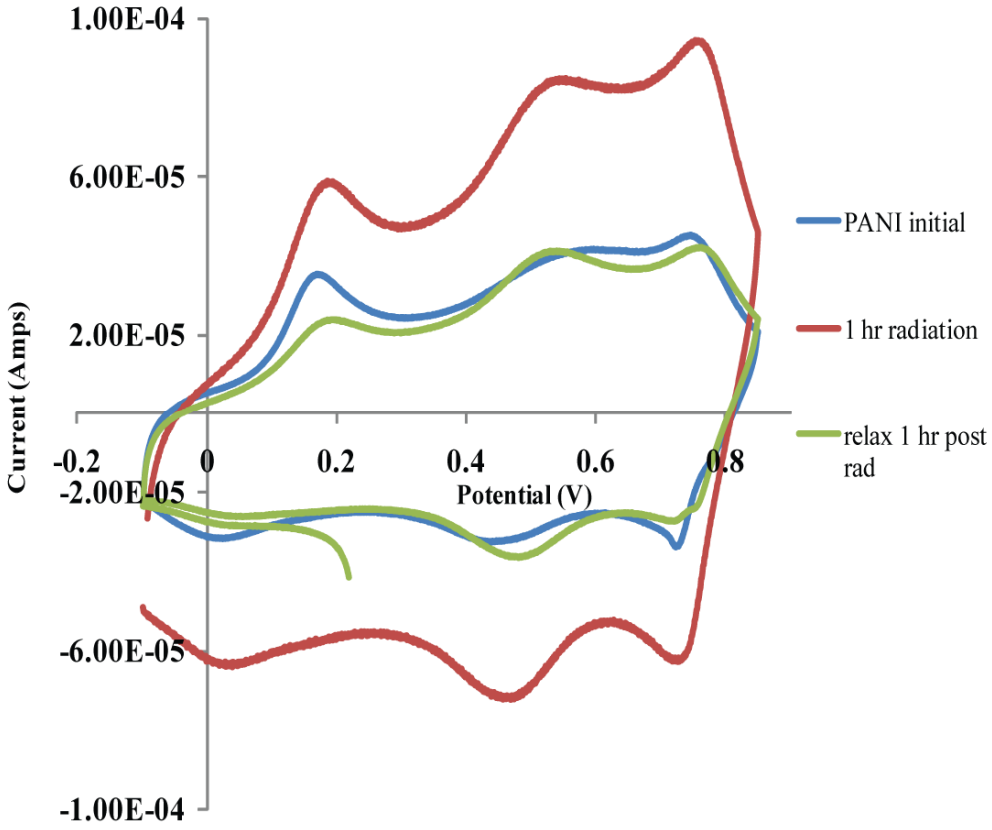

Figure 46. Cyclic voltammograms of polyaniline film in .1 M HCl cycled from -0.1 to 0.85 V vs. Ag/AgCl. Comparison of polyaniline before irradiation (blue), after 1 hr of radiation (red), and a relaxation period of 50 minutes post irradiation (green) are indicated.

Compounds such as chloranil, with an electron affinity of 2.67 eV, can be incorporated into the PANI film or doped directly, in hopes of its interaction with radiation significantly changing the conductivity of the polymer film.

Emeraldine base (MW 5000 g/mol, Alfa Aesar) was added in a ration of 5 mg of base per 1 mL formic acid (Fischer, ACS reagent grade). The PANI solution was sonicated for 10 min and drop cast onto quartz slides (2 mm dia.) and dried at room temperature. After drying, a 10% w/w solution of chloranil in chloroform was dropped over each dried film. The 100 µCi Ni-63 source irradiated each film for 24 hrs, and UV-vis spectrum was taken of each chloranil-PANI film pre and post-irradiation.

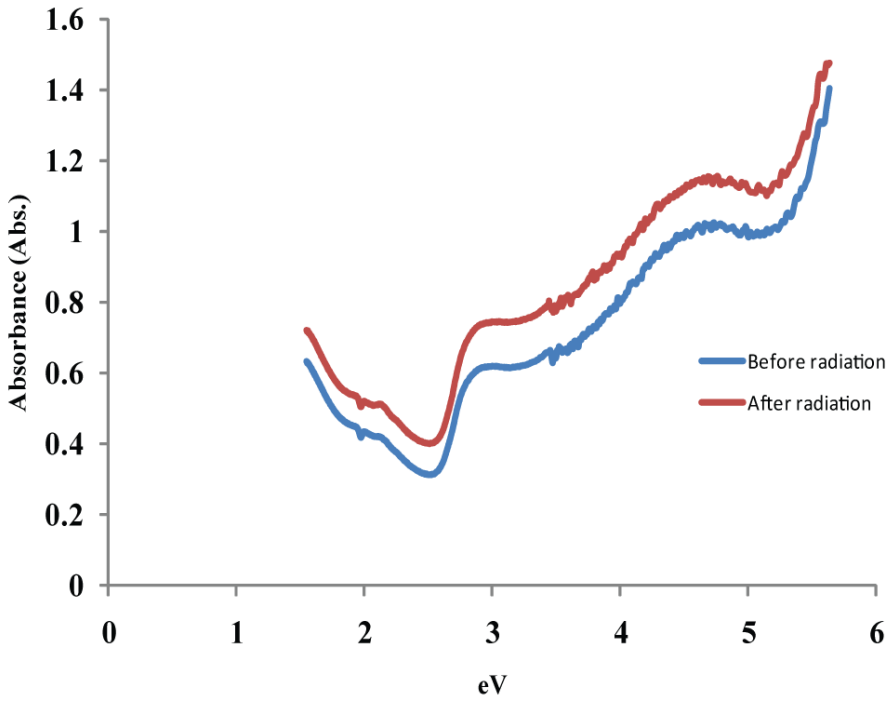

Figure 47. UV-vis spectrum of PANI with chloranil before and after irradiation

Fig. 42 shows that there is an absorbance change between the pre and post irradiated PANI films, however there is no significant change besides absorbance intensity within the spectrum. While there are many theories that could explain this change in absorbance, such as the chloranil donating an electron to PANI itself, oxidation of PANI from sitting in the atmosphere, it is still unknown the cause of the change.

In Fig. 43, polyaniline with no additives is shown before and after irradiation. The spectrum of PANI without chloranil, stopped at -.1 V fits well with previous research.[110] Although the thickness of the film is larger than the film in Fig. 42, in comparison there is an obvious change to the PANI spectrum between figs 42. and 43 due to the donacity of chloranil itself. The same procedure was applied to PANI bare (Fig. 43) as was to PANI with chloranil. After applying radiation for 24 hours, no significant absorbance change was seen. However, since the thickness of the films were not equivalent it cannot be ruled out that the beta irradiation could not fully penetrate the film. Although the mechanism behind this is still unknown, it is worth further investigation into developing a radiation sensor.

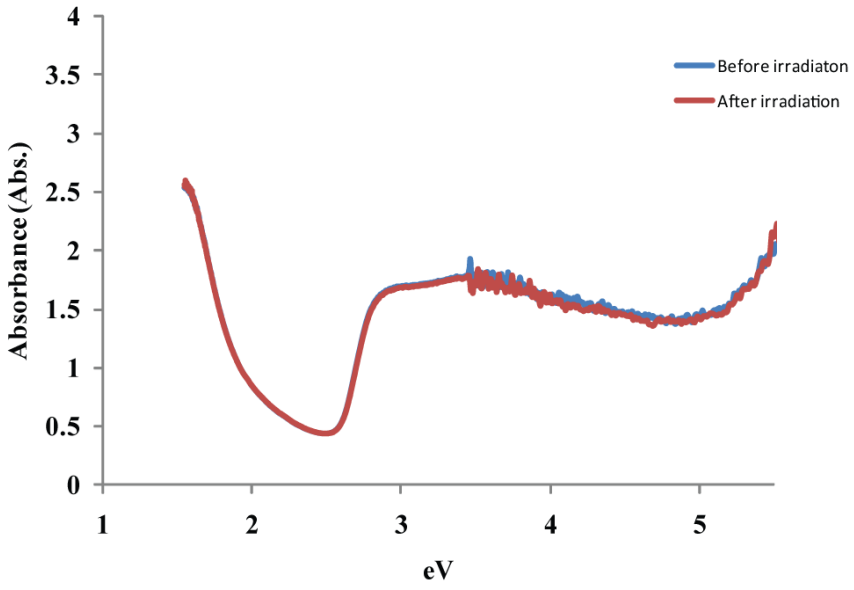

Figure 48. Polyaniline with no additives before (blue) and after (red) irradiation.

In conclusion, there is much to be continued in this research project to achieve a reversible PANI radiation sensor. The problems with the first experiment conducted with

CVs of PANI before and after irradiation is that they were wet films. It is plausible that the water within the polymer layer was hydrolyzed through radiolysis from the Ni-63, causing hydroxyl radicals to oxidize the polymer film. Future experiments should include PANI films dry while irradiating. Additionally, PANI in the atmosphere changes oxidation states slowly due to the oxygen in the atmosphere. All experiments should be conducted under nitrogen or argon to eliminate this possibility.

Besides the use of chloranil in combination with PANI, there are numerous other electronegative compounds that could be used in conjunction with the polymer. Chloranil was originally chosen because it was readily available; however there are other compounds that can be used. Chloranil is difficult to dissolve with the PANI before drop casting, because of its insolubility with formic acid, and being only slightly soluble in methanol and chloroform. Using the methods described previously in which chloranil was drop cast after PANI, the compound was not completed intertwined within the polymer. In the future, experiments need to be conducted using an electronegative compound that can dissolve in formic acid, the solvent used to dissolve the emeraldine base of polyaniline. This would lead to a more uniform deposition of the polymer onto the quartz slides.

Lastly, other forms of radiation must be applied, such as stronger beta emitting radioisotopes such as P-32 or Cs-137 to test the PANI as a reversible radiation sensor. Ni-63 has a beta electron of maximum energy of 67 keV, with an average of approximately 17 keV. The weak beta particles emitted from this radioisotope might not be strong enough to interact and cause a change within the polymer film. All in all, the use of radiation in conjunction with PANI has demonstrated and increase in conductivity within

the film. Because of this, we have presented the incorporation of electronegative compounds sensitive to beta irradiation in hopes of creating a radiation sensor.

REFERENCES

[1] Steeb, J.; Josowicz, M.; Janata, J., Analytical Chemistry 2009, 81 (5), 1976-1981.

[2] Martin, J. E., Physics for Radiation Protection. 2000.

[3] Randers-Pehrson, G., Radiation Research 2001, 156 (4), 435-435.

[4] Hala, J., Radioactivity, Ionizing Radiation, and Nuclear Energy. 2003; p 467.

[5] Steeb, J.; Galhena, A. S.; Nyadong, L.; Facundo, J. J.; Fernandez, M., Chemical Communications 2009, (31), 4699-4701.

[6] Hu, Z. W.; Wu, L. J.; Yu, Z. L., Plasma Science & Technology 2005, 7 (2), 2789-2796.

[7] Garty, G.; Ross, G. J.; Bigelow, A.; Randers-Pehrson, G.; Brenner, D. J., Nuclear Instruments & Methods in Physics Research Section B-Beam Interactions with Materials and Atoms 2005, 241 (1-4), 392-396.

[8] Cooper, S. D.; Moseley, M. A.; Pellizzari, E. D., Analytical Chemistry 1985, 57 (13), 2469-2473.

[9] CRC Handbook of Chemistry and Physics. 80th ed.; CRC Press: 2000.

[10] Summerour, J.; Chen, Y. F.; Josowicz, M.; Orlando, T. M.; Janata, J.; Paulenova, A., Radiation Physics and Chemistry 2006, 75 (3), 369-374.

[11] Bard, A. J.; Faulkner, L. R., Electrochemical Methods. In Fundamentals and Applications, 2nd Edition ed.; John Wiley and Sons, Inc.: 2001.

[12] Janata, J., Chemical Sensors. 2008.

[13] Vavra, K. C. Ni and Cu depositions on a Quartz Crystal Microbalance. Georgia Institute of Technology, Atlanta.

[14] Amatore, C. A.; Fosset, B.; Deakin, M. R.; Wightman, R. M., Journal of Electroanalytical Chemistry 1987, 225 (1-2), 33-48.

[15] Wightman, R. M.; Wipf, D. O., Electroanalytical Chemistry 1989, 15, 267-353.

[16] Zhang, B.; Zhang, Y. H.; White, H. S., Analytical Chemistry 2006, 78 (2), 477-483.

[17] Amatore, C.; Oleinick, A. I.; Svir, I., Journal of Electroanalytical Chemistry 2006, 597 (1), 77-85.

[18] Zhang, B.; Galusha, J.; Shiozawa, P. G.; Wang, G. L.; Bergren, A. J.; Jones, R. M.; White, R. J.; Ervin, E. N.; Cauley, C. C.; White, H. S., Analytical Chemistry 2007, 79 (13), 4778-4787.

[19] Hoare, J. P., Journal of the Electrochemical Society 1986, 133 (12), 2491-2494.

[20] Elsherik, A. M.; Erb, U., Journal of Materials Science 1995, 30 (22), 5743-5749.

[21] Ferkel, H.; Muller, B.; Riehemann, W. In Electrodeposition of particle-strengthened nickel films, 1997; pp 474-476.

[22] Ibrahim, M. A. M., Journal of Applied Electrochemistry 2006, 36 (3), 295-301.

[23] Mohan, S.; Venkatachalam, R.; Renganathan, N. G.; Rajeswari, C., Transactions of the Institute of Metal Finishing 2001, 79, 73-76.

[24] Motoyama, M.; Fukunaka, Y.; Sakka, T.; Ogata, Y. H., Journal of the Electrochemical Society 2006, 153 (7), C502-C508.

[25] Lister, D. H.; Cook, W. G. Reactor Chemistry and Corrosion, Section 12: Aqueous Corrosion Thermodynamics. (accessed February).

[26] Buchheit, T. E.; LaVan, D. A.; Michael, J. R.; Christenson, T. R.; Leith, S. D., Metallurgical and Materials Transactions a-Physical Metallurgy and Materials Science 2002, 33 (3), 539-554.

[27] Knoll, G. F., Radiation Detection and Measurement. 3rd ed.; John Wiley & Sons, Inc.: 2000.

[28] Hall, E. J.; Biaccia, A. J., Radiobiology for the Radiologist. Lippincott Williams & Wilkins: 2006.

[29] Kahn, B., Radioanalytical Chemistry. Springer: New York, 2007; p 473.

[30] Energy, U. S. D. o. Low Dose Radiation Research. http://www.lowdose.energy.gov/. Date Accessed: June 2008.

[31] Hakanen, A.; Siiskonen, T.; Pollanen, R.; Kosunen, A.; Turunen, A.; Belyakov, O., Applied Radiation and Isotopes 2006, 64 (8), 864-867.

[32] Schettino, G.; Folkard, M.; Michette, A. G.; Vojnovic, B.; Pfauntsch, S. J.; Prise, K. M.; Atkinson, K. D.; Holroyd, J.; Michael, B. D., Journal De Physique Iv 2003, 104, 301-304.

[33] Hall, E. J.; Hei, T. K., Oncogene 2003, 22 (45), 7034-7042.

[34] Shleien, B.; Slaback, L. A.; Birky, B. K., Handbook of Health Physics and Radiological Health. Lippincott Williams & Wilkins: 1998.

[35] Gonzalez, P.; Cortinez, V. A.; Fontan, C. A., Talanta 2002, 58 (4), 679-690.

[36] Gelsema, W. J.; Donk, L.; Vonencke.Jh; Blijleve.Ha, Journal of Chemical Education 1969, 46 (8), 528-&.

[37] Schweitzer, G. K.; Stein, B. R.; Nehls, J. W., Journal of Physical Chemistry 1952, 56 (6), 692-693.

[38] Sims, G. H. E.; Juhnke, D. G., International Journal of Applied Radiation and Isotopes 1967, 18 (10), 727-&.

[39] Wieckowski, A.; Kolics, A., Journal of Electroanalytical Chemistry 1999, 464 (1), 118-122.

[40] Kinner, A.; Wu, W.; Staudt, C.; Iliakis, G., Nucleic Acids Res 2008, 36 (17), 5678-94.

[41] Pandita, T. K.; Richardson, C., Nucleic Acids Res 2009, 37 (5), 1363-77.

[42] Radiation Source Use and Replacement: Abbreviated Version. National Academies Press: Washington, D.C., 2008.

[43] Munro, T. R., Exp Cell Res 1958, 15 (3), 529-50.

[44] Steeb, J.; Josowicz, M.; Janata, J., Anal Chem 2009, 81 (5), 1976-81.

[45] Costes, S. V.; Chiolo, I.; Pluth, J. M.; Barcellos-Hoff, M. H.; Jakob, B., Mutat Res 2010.

[46] FitzGerald, J. E.; Grenon, M.; Lowndes, N. F., Biochem Soc Trans 2009, 37 (Pt 4), 897-904.

[47] Kumaran, R. I.; Spector, D. L., J Cell Biol 2008, 180 (1), 51-65.

[48] Gerlich, D.; Beaudouin, J.; Kalbfuss, B.; Daigle, N.; Eils, R.; Ellenberg, J., Cell 2003, 112 (6), 751-64.

[49] Pryde, F.; Khalili, S.; Robertson, K.; Selfridge, J.; Ritchie, A. M.; Melton, D. W.; Jullien, D.; Adachi, Y., J Cell Sci 2005, 118 (Pt 9), 2043-55.

[50] Jakob, B.; Splinter, J.; Durante, M.; Taucher-Scholz, G., Proc Natl Acad Sci U S A 2009, 106 (9), 3172-7.

[51] Asaithamby, A.; Chen, D. J., Nucleic Acids Res 2009, 37 (12), 3912-23.

[52] Schultz, L. B.; Chehab, N. H.; Malikzay, A.; Halazonetis, T. D., J Cell Biol 2000, 151 (7), 1381-90.

[53] Rabut, G.; Ellenberg, J., J Microsc 2004, 216 (Pt 2), 131-7.

[54] Ruiz de Almodovar, J. M.; Steel, G. G.; Whitaker, S. J.; McMillan, T. J., Int J Radiat Biol 1994, 65 (6), 641-649.

[55] Iliakis, G. E.; Cicilioni, O.; Metzger, L., Int J Radiat Biol 1991, 59 (2), 343-357.

[56] Zirkle, R. E.; Bloom, W., Science 1953, 117 (3045), 487-93.

[57] Gerardi, S., J Radiat Res (Tokyo) 2009, 50 Suppl A, A13-20.

[58] Randers-Pehrson, G.; Geard, C. R.; Johnson, G.; Elliston, C. D.; Brenner, D. J., Radiat Res 2001, 156 (2), 210-4.

[59] Gerardi, S., Radiat Prot Dosimetry 2006, 122 (1-4), 285-91.

[60] Folkard, M.; Schettino, G.; Vojnovic, B.; Gilchrist, S.; Michette, A. G.; Pfauntsch, S. J.; Prise, K. M.; Michael, B. D., Radiat Res 2001, 156 (6), 796-804.

[61] Kim, E. H.; Sun, G. M.; Jang, M., Radiat Prot Dosimetry 2006, 122 (1-4), 297-300.

[62] Sowa, M. B.; Murphy, M. K.; Miller, J. H.; McDonald, J. C.; Strom, D. J.; Kimmel, G. A., Radiat Res 2005, 164 (5), 695-700.

[63] Cao, Z.; Kuhne, W. W.; Steeb, J.; Merkley, M. A.; Zhou, Y.; Dynan, W. S. Use of a microscope stage-mounted Nickel-63 microirradiator for real-time observation of the DNA double-strand break response. Nucleic Acids Research [Online], 2010.

[64] Harris, G. A.; Nyadong, L.; Fernandez, F. M., Analyst 2008, 133 (10), 1297-1301.

[65] Horning, E. C.; Horning, M. G.; Carroll, D. I.; Dzidic, I.; Stillwel.Rn, Analytical Chemistry 1973, 45 (6), 936-943.

[66] Takats, Z.; Wiseman, J. M.; Gologan, B.; Cooks, R. G., Science 2004, 306 (5695), 471-473.

[67] Cody, R. B.; Laramee, J. A.; Durst, H. D., Analytical Chemistry 2005, 77 (8), 2297-2302.

[68] Venter, A.; Nefliu, M.; Cooks, R. G., Trac-Trends in Analytical Chemistry 2008, 27 (4), 284-290.

[69] Hill, H. H.; Siems, W. F.; Stlouis, R. H.; McMinn, D. G., Analytical Chemistry 1990, 62 (23), A1201-A1209.

[70] Ewing, R. G.; Atkinson, D. A.; Eiceman, G. A.; Ewing, G. J., Talanta 2001, 54 (3), 515-529.

[71] Creaser, C. S.; Griffiths, J. R.; Bramwell, C. J.; Noreen, S.; Hill, C. A.; Thomas, C. L. P., Analyst 2004, 129 (11), 984-994.

[72] Kawai, Y.; Yamaguchi, S.; Okada, Y.; Takeuchi, K.; Yamauchi, Y.; Ozawa, S.; Nakai, H., Chemical Physics Letters 2003, 377 (1-2), 69-73.

[73] Karasek, F. W.; Kim, S. H.; Rokushika, S., Analytical Chemistry 1978, 50 (14), 2013-2016.

[74] Chen, H. W.; Talaty, N. N.; Takats, Z.; Cooks, R. G., Analytical Chemistry 2005, 77 (21), 6915-6927.

[75] http://www.nndc.bnl.gov/nudat2/getdecayscheme.jsp?nucleus=125TE&dsid=125te it decay&unc=nds. Date Accessed: May, 2010.

[76] Montiel-Santillan, T.; Solorza, O.; Sanchez, H., Journal of Solid State Electrochemistry 2002, 6 (7), 433-442.

[77] Blasko, J. C.; Grimm, P. D.; Sylvester, J. E.; Badiozamani, K. R.; Hoak, D.; Cavanagh, W., International Journal of Radiation Oncology Biology Physics 2000, 46 (4), 839-850.

[78] Fuks, Z.; Leibel, S. A.; Wallner, K. E.; Begg, C. B.; Fair, W. R.; Anderson, L. L.; Hilaris, B. S.; Whitmore, W. F., International Journal of Radiation Oncology Biology Physics 1991, 21 (3), 537-547.

[79] Montero, A.; Hernanz, R.; Capuz, A. B.; Fernandez, E.; Hervas, A.; Colmenares, R.; Polo, A.; Sancho, S.; Moleron, R.; Vallejo, C.; Ramos, A., Clinical & Translational Oncology 2009, 11 (11), 760-764.

[80] Yeung, W. K.; Luk, N. M.; Yu, K. H., Hong Kong Journal of Dermatology & Venereology 2009, 17 (2), 79-86.

[81] Mothersill, C.; Seymour, C., Radiation Research 2001, 155 (6), 759-767.

[82] Morgan, W. F., Radiation Research 2003, 159 (5), 581-596.

[83] Prise, K. M.; O'Sullivan, J. M., Nature Reviews Cancer 2009, 9 (5), 351-360.

[84] Shao, C.; Stewart, V.; Folkard, M.; Michael, B. A.; Prise, K. M., Cancer Research 2003, 63 (23), 8437-8442.

[85] Gault, N.; Rigaud, O.; Poncy, J. L.; Lefaix, J. L., Radiation Research 2007, 167 (5), 551-562.

[86] Barrera, E.; Pardave, M. P.; Batina, N.; Gonzalez, I., Journal of the Electrochemical Society 2000, 147 (5), 1787-1796.

[87] Prise, K. M.; Folkard, M.; Michael, B. D., Oncogene 2003, 22 (45), 7043-7049.

[88] Kubota, Y.; Shimada, A.; Shima, A., Mutation Research 1992, 283 (4), 263-270.

[89] Kudoh, T.; Tsang, M.; Hukriede, N. A.; Chen, X. F.; Dedekian, M.; Clarke, C. J.; Kiang, A.; Schultz, S.; Epstein, J. A.; Toyama, R.; Dawid, I. B., Genome Research 2001, 11 (12), 1979-1987.

[90] Japanese Medaka Fish in Space 2009.

[91] Mason, T. E.; Abernathy, D.; Anderson, I.; Ankner, J.; Egami, T.; Ehlers, G.; Ekkebus, A.; Granroth, G.; Hagen, M.; Herwig, K.; Hodges, J.; Hoffmann, C.; Horak, C.; Horton, L.; Klose, F.; Larese, J.; Mesecar, A.; Myles, D.; Neuefeind, J.; Ohl, M.; Tulk, C.; Wang, X. L.; Zhao, J., Physica B-Condensed Matter 2006, 385-86, 955-960.

[92] Honsberg, C.; Doolittle, W.; Allen, M.; Wang, C., GaC Betavoltaic Energy Converters. In 31st IEEE Photovoltaics Specialties Conference, `: Orlando, Fl, 2005.

[93] Pustovalov, A. A.; Gusev, V. V.; Zadde, V. V.; Petrenko, N. S.; Tsvetkov, L. A.; Tikhomirov, A. V., Atomic Energy 2007, 103 (6), 939-945.

[94] Ulmen, B.; Desai, P. D.; Moghaddam, S.; Miley, G. H.; Masel, R. I., Journal of Radioanalytical and Nuclear Chemistry 2009, 282 (2), 601-604.

[95] Wang, T. S.; Qiang, L.; Zhang, B. G.; Wang, Z. S.; Cao, Z. Y.; Zhang, P. X., Journal of Radioanalytical and Nuclear Chemistry-Articles 1996, 205 (1), 141-145.

[96] Nickoloff, J. A.; Hoekstra, M. F., DNA Damage and Repair Volume I: DNA Repair in Prokaryotes and Lower Eukaryotes. Humana Press, Inc.: 1998.

[97] Chalfie, M.; Tu, Y.; Euskirchen, G.; Ward, W. W.; Prasher, D. C., Science 1994, 263 (5148), 802-805.

[98] Los, G. V.; Encell, L. P.; McDougall, M. G.; Hartzell, D. D.; Karassina, N.; Zimprich, C.; Wood, M. G.; Learish, R.; Ohane, R. F.; Urh, M.; Simpson, D.; Mendez, J.; Zimmerman, K.; Otto, P.; Vidugiris, G.; Zhu, J.; Darzins, A.; Klaubert, D. H.; Bulleit, R. F.; Wood, K. V., Acs Chemical Biology 2008, 3 (6), 373-382.

[99] Chen, E. C. M.; Chen, E. S., The Electron Capture Etector and The Study of Reactions with Thermal Electrons. John Wiley & Sons, Inc.: Hoboken, New Jersey, 2004.

[100] Lovelock, J. E., Journal of Chromatography 1958, 1 (1), 35-46.

[101] Lovelock, J. E., Nature 1961, 189 (476), 729-&.

[102] Muscalu, A. M.; Reiner, E. J.; Liss, S. N.; Chen, T., International Journal of Environmental Analytical Chemistry 2010, 90 (1), 1-13.

[103] Quan, X.; Chen, S.; Platzer, B.; Chen, J. W.; Gfrerer, M., Spectrochimica Acta Part B-Atomic Spectroscopy 2002, 57 (1), 189-199.

[104] Lovelock, J. E., Journal of Chromatography 1974, 99 (NOV6), 3-12.

[105] Oki, Y.; Suzuki, T.; Miura, T.; Numajiri, M.; Kondo, K., APPLICATION OF POLYANILINE FILMS TO RADIATION-DOSIMETRY. In Polymeric Materials for Microelectronic Applications - Science and Technology, Ito, H.; Tagawa, S.; Horie, K., Eds. Amer Chemical Soc: Washington, 1994; Vol. 579, pp 336-342.

[106] Malmonge, J. A.; Mattoso, L. H. C. In Doping of polyaniline and derivatives induced by X-ray radiation, Elsevier Science Sa Lausanne: 1997; pp 779-780.

[107] Sevil, U. A.; Guven, O.; Kovacs, A.; Slezsak, I. In Gamma and electron dose response of the electrical conductivity of polyaniline based polymer composites, Pergamon-Elsevier Science Ltd: 2003; pp 575-580.

[108] Bhat, N. V.; Nate, M. M.; Gore, A. V.; Bhat, R. M., Journal of Applied Polymer Science 2008, 110 (4), 2243-2252.

[109] Bodugoz, H.; Guven, G. In Radiation induced dehydrochlorination as an in-situ doping technique for enhancement of the conductivity of polyaniline blends, Elsevier Science Bv: 2005; pp 153-159.

[110] Li, Y. F.; Yan, B. Z.; Yang, J.; Cao, Y.; Qian, R. Y., Synthetic Metals 1988, 25 (1), 79-88.

VITA

JENNIFER L. STEEB

Jennifer Steeb was born in Stuart, Fl to Susan and Fred Steeb. Jennifer attended the University of Miami and graduated with a B.S. in Chemistry, minor in Mathematics in 2006. After graduation, Jennifer attented the Georgia Institute of Technology, in which she is expected to graduate with a Ph.D. in Chemistry in 2010.

PUBLICATIONS

Steeb, J.; West, R.; Janata, J.; "Ni-63 Bench-top Solid State Scintillation Calibrator." Radiation Physics and Chemistry, 2010 (in preparation).

Cao, Z.; Kuhne, W.W.; Steeb,J.; Merkley, M.A.; Zhou,Y.; Janata,J.; Dynan,W.S. Use of a microscope stage-mounted Nickel-63 microirradiator for real-time observation of the DNA double-strand break response. Nucleic Acids Research, Accepted May 19th, 2010.

Steeb, J.; Josowicz, M.; Janata, J.; "Electrochemically Prepared Beta Microirradiator." ECS Transactions, 19(6) 305-313 (2009).

Steeb, J.; Galhena, A.S.; Nyadong, L; Janata, J.; Fernandez, F.M.; "Beta-Assisted Direct Chemical Ionization (BADCI) Probe for Ambient Mass Spectrometry." Chem. Comm., 31, 4699-4701. 2009.

Steeb, J.; Josowicz, M.; Janata, J. "Nickel-63 Microirradiators." Analytical Chemistry, vol. 81, p 1976-1981, 2009.

Hao, S.; Steeb, J.; Kaifer, A. "Efficient Electronic Communication between Two Identical Ferrocene Centers in a Hydrogen-Bonded Dimer." JACS. Volume 129, Issue 9, 2280-2281. 2006.